FIBER REINFORCED 3D PRINTABLE CEMENTITIOUS COMPOSITES

by

Nilhan Andiç

B.S, Civil Engineering, Boğaziçi University, 2021

Submitted to the Institute for Graduate Studies in

Science and Engineering in partial fulfillment of

the requirements for the degree of

Master of Science

Graduate Program in Civil Engineering

Boğaziçi University

2021

ACKNOWLEDGEMENTS

First of all, I would like to thank Prof. Dr. Nesrin Yardımcı Tiryakioğlu and Dr. Özgür Sümer Köylüoğlu, who helped me all the way through my studies in Turkey, guided me and never let me feel alone due to their vision and support.

Secondly, I thank Prof. Dr. Nilüfer Özyurt Zihnioğlu and Dr. Zeynep Başaran Bundur for giving me a chance to be a part of a visionary project on 3D printable cementitious composites. I am thankful to Dr. Zeynep Yıldırım, Prof. Dr. Turan Özturan and Şevket Tekin for their guidance and help.

I also would like to thank my lovely and sympathetic team Can Gürer Yücel, Gazican Özcan and Nur Hande Turan for their assistance and patience. They are my greatest supporters and strength. I value their support greatly. Besides my team, I would also like to thank lovely undergraduate students Erkam Portakal, Alphan Dilber and Melike Bilge Polatkan for their help and support.

I would like to thank my friends Ceren Yaylı, Onur Bilgin and İlayda Çinik for their support and love.

I am greatly thankful to my dear friend Eyüp Can Kökan, who made it possible in Covid-19 pandemic time to finish my laboratory tests. His patience and support made this study possible.

I, also, would like to thank my family and Dr.-Ing. Onur Güvenç, who supported, assisted, and guided me throughout my master studies. Their motivation and belief in me made me stronger. Last, but not least, I would like to thank my little friend *Lea*, whose presence is my greatest strength and light in life.

I should also thank the Scientific and Technical Research Council (TÜBİTAK) of Turkey (Project: MAG-119M520). I am thankful for their financial support due to this project.

ABSTRACT

FIBER REINFORCED 3D PRINTABLE CEMENTITIOUS COMPOSITES

Layer-by-layer extrusion of cementitious composites is a production method proposed for the 3D printing of concrete structures. Clay-based modifiers are commonly added to the cementitious mixture to adapt it to the extrusion process. However, these modifiers affect the mechanical properties as well. Therefore, it is essential to evaluate the buildability of the proposed composites mixtures. Hence the intended layer stability can be achieved during the extrusion process.

This thesis investigates the early age mechanical behavior of twelve 3D printable cementitious composite mixtures. It links the early age mechanical behavior to the hardened state of the 3D printable cementitious composite alternatives. The effects of varying percentages of two clay types on the buildability, the early-age strength development, and the load-bearing capacity of 3D printable cementitious composites are in focus. For this purpose, twelve mix designs were proposed with varying combinations of two clay types and a viscosity modifying agent (VMA). Combinations of two clay alternatives and VMA with/without fly ash content were compared to predetermined test cases. In total, two control mixtures, four mixtures with nano-montmorillonite, four mixtures with sepiolite, and two mixtures with VMA were produced and characterized. To evaluate the fresh state properties, the green strength, and to evaluate the hardened state properties, the 3-point bending tests, and the compression test, were performed at 28 days.

Furthermore, to improve mechanical properties and crack control of the predetermined mixes, 12 mm carbon fibers were included. Among twelve mixtures four representative mixtures were selected to include soft carbon fibers. All fresh and hardened state tests applied to fiber-reinforced cementitious composite mixtures.

ÖZET

FİBERLE GÜÇLENDİRİLMİŞ 3B YAZDIRILABİLEN ÇİMENTO ESASLI KOMPOZİTLER

Bu çalışmanın amacı, miktarı değişen iki farklı kil içeren, 3 boyutlu yazıcılarda yazdırılabilen çimento esaslı kompozitlerin inşa edilebilme, erken dönem güç kazanma ve yük kaldırabilme özelliklerinin incelenmesidir. Katmanlar halinde yazdırılan çimento esaslı malzemelerin inşa edilebilme özelliği çok kritiktir. İnşa edilebilme özelliğinin killerin reoloji düzenleyici olarak kullanılmasıyla mekanik performansa sağladığı katkı çok önemlidir. Bu sayede istenilen katman dengesine ulaşılabilir. Bu çalışmada iki farklı kil çeşidi ve viskozite düzenleyici katkı maddesi kullanılarak on iki adet karışım hazırlanmıştır. İki kil çeşidi ve viskozite düzenleyici katkı maddesi ile uçucu kül kombinasyonları önceden belirlenmiş testler sayesinde karşılaştırılmıştır. 2 kontrol karışımı, 4 nano montmorillonite kili içeren karışım, 4 lületaşı (sepiolite) içeren karışım ve 2 tane viskozite düzenleyici katkı içeren karışım karşılaştırılmak üzere hazırlanmıştır. Taze hal dayanımını karşılaştırmak için yeşil dayanım (green strength) testi, sertleşmiş hal dayanımı için 28 günlük numunelerde 3 noktalı eğilme testi ve basınç testi uygulanmıştır. Bu çalışmanın amacı 3 boyutlu yazıcıda yazdırılabilir çimento esaslı 12 tane karışımın erken dönem mekanik özelliklerini belirlemektir. Çalışmanın bir amacı da taze hal dayanımı ile sertlemiş hal dayanımını ilişkilendirmektir.

Ayrıca mekanik özellikleri iyileştirmek ve çatlak kontrolü sağlamak için belirlenmiş karışımlara 12 mm'lik karbon lifler katılmıştır. Üretilen 12 karışımdan, mekanik özellikler esas alınarak 4 temsili karışım seçilmiş ve yumuşak lifler katılmıştır. Yukarıda bahsi geçen taze ve sertleşmiş hal testlerinin tamamı lif katkılı çimento esaslı kompozit karışımlara da uygulanmıştır.

TABLE OF CONTENTS

LIST OF FIGURES

LIST OF TABLES

LIST OF ACRONYMS/ABBREVIATIONS

CO_2	Carbon dioxide
E	Elastic modulus of the material
G	Shear modulus
FA	Fly ash
NM	Nano-montmorillonite
SEP	Sepiolite
VMA	Viscosity Modifying Agent
OPC	Ordinary Portland Cement
GS	Green Strength
PCE	Polycarboxylate Ether
ASTM	American Society for Testing and Materials
SCC	Self-Compacting Concrete
SP	Superplasticizer

1. INTRODUCTION

In today's world, additive manufacturing is widely used in many sectors. Following this trend, the construction sector invests in more environment-friendly, fast-to-build, not labor-intensive, free from formwork, and architecturally free methods. These methods give both constructor and the client freedom in many areas.

Cementitious composites are highly preferred in the construction industry due to their high compressive strength, ability to bond with reinforcement, fire resistance, easy formability, and economical production. Typically, cement production requires crushing and grinding the raw materials and mixing them with additives (i.e., limestone, and clay mixed with iron or ash). Afterward, the mixture is heated up to 1450 °C in cylindrical kilns. This so-called calcination process produces calcium oxide, long with carbon dioxide (CO_2) as a byproduct. Thus, cement production is one of the most significant environmental pollution sources. It has been 30 times more since 1950, and it is currently responsible for 8% of the carbon dioxide emission of the world [1]. In order to constrain and reduce cement consumption, 3D printing of cementitious composites is an effective alternative to conventional construction methods. 3D printing methods can be separated into two categories; extrusion-based and selective binding processes [2]. This thesis focuses on developing layer extrusion methods and suitable material mixtures.

Layer extrusion of 3D printable cementitious composites has been developing rapidly. Initially, eliminating the formwork, decreasing the unit cost and time, reducing the amount of material are advantages of 3D printable cementitious composites. However, optimization of the extrudability requires certain rheological behavior, and in order to reach these requirements, high cement content in the mix design should be obtained [3]. In the latest studies, the main goal is replacing cement with various pozzolonic or rheological modifiers in order to obtain a more sustainable material with less carbon footprint.

One of the most critical challenges of developing a mix design for 3D printable cementitious materials is optimizing the fresh state properties that will enable the material to flow through the printer's nozzle without segregation or clogging while holding the extruded layer structure stable. In this work, the primary focus is replacing cement, as binder content, with two kinds of clay with 0.5-1%, and VMA as rheological modifiers, and also with 20% fly ash (FA) for increased workability and test possible mixture combinations. Furthermore, fly ash replacement makes the material more sustainable, as fly ash is a byproduct of iron production. According to Ferron *et al*. [4], the particle structure of clays is used as rheological modifiers. They also point out that the needle-like structure of sepiolite increases the chord length between the particles and forms a more flocculated network. So as the flocculation grows, the structural build-up develops. On the other hand, only a small portion of VMA could improve the cohesion, stability, and viscosity of cementitious materials [3].

Through these replacements, the buildability parameters of prepared twelve mixtures were obtained at fresh and hardened states. In order to obtain the fresh state buildability properties, the green strength and buildability tests are performed. For the hardened state, compressive and flexural strength tests were performed on 28-day cured specimens.

Within the scope of this work, the following works were performed:

- An on-site and field-friendly testing solution (i.e., buildability test) according to the Murata model and built-up theory as an alternative to the existing laboratory testing method (i.e., green strength tests) was evaluated with specific parameters:
  - Two superplasticizers (SP) were compared to optimize mix design,
  - Buildability parameters of fresh state were assessed via green strength test,
  - The influence of two clay types (i.e., nano-montmorillonite (NM) and sepiolite (SEP)), along with VMA, on the yield stress and buildability were identified.
  - The green strength, buildability, and mechanical properties of 12 mixtures were correlated,
  - For strength-based failure and buckling failure, critical and transitional heights of printable structure were obtained and tabulated.

2. LITERATURE REVIEW

2.1. Concrete 3D Printing Technology

3D printing of cementitious materials is a rapidly developing technology, and it is subjected to a rapidly increasing attention [5-8]. As Van Damme [9] stated, *"The demand on concrete will not decrease in the near future due to developing countries such as China and India investing greatly in construction and also developed countries to rebuild"*. The demand on concrete also affects the climate change because of the cement production. Due to these concerns, new methods have been the focus of construction industry. Compared to conventional methods of construction, 3D-printing has the potential for automation; reduction of construction cost (in terms of labor and formwork), time, material waste, and energy; and fabrication of geometrically complex structures. It is an attractive alternative for both on-site and off-site construction applications [7].

With the 4th industrial revolution, additive manufacturing has been the priority of several sectors. The ever-increasing adaptation of additive manufacturing principles by the construction industry is leading the rapid digitalization of

(i) materials and process,
(ii) structure and performance,
(iii) applications [9].

One of the main advantages of the digitalization of concrete is reducing the carbon footprint while increasing material and shape efficiency. Pressuring the material to flow, extracting the mortar through a nozzle, and letting material self-place without a formwork, is called extrusion. There are numerous kinds of extrusion methods in the construction industry, such as Contour Crafting developed by Koshnevis [9], formwork printing used in London Tube station, printing temporary supports, Slip forming, specifically Smart

Dynamic Casting, developed by Lloret *et al*. [10] and particle bed fusion method. In this study layer-by-layer extrusion of cementitious materials was aimed to be performed.

There are, understandably, some challenges related to the 3D printing of cement-based materials. Besides the compatibility with externalities, especially the weather conditions, one of the most critical factors is materials processibility. The cement-based material should be pumped out of a nozzle practically, yet stiff enough to support itself. Therefore, a specific yield stress value is chosen for acceptable thixotropic behavior. Suitable additions (e.g., clay powders) and admixtures enable the optimization of targeted thixotropic behavior [11].

The inclusion of superplasticizers, nano clays, thixotropy additives, and VMA increases the mixtures' overall printability and buildability performance [6,7] as seen in Figure 2.1. The nano clays play a role in increasing the strength and stiffness of cementitious materials due to the flocculation of colloidal NC particles [12,13].

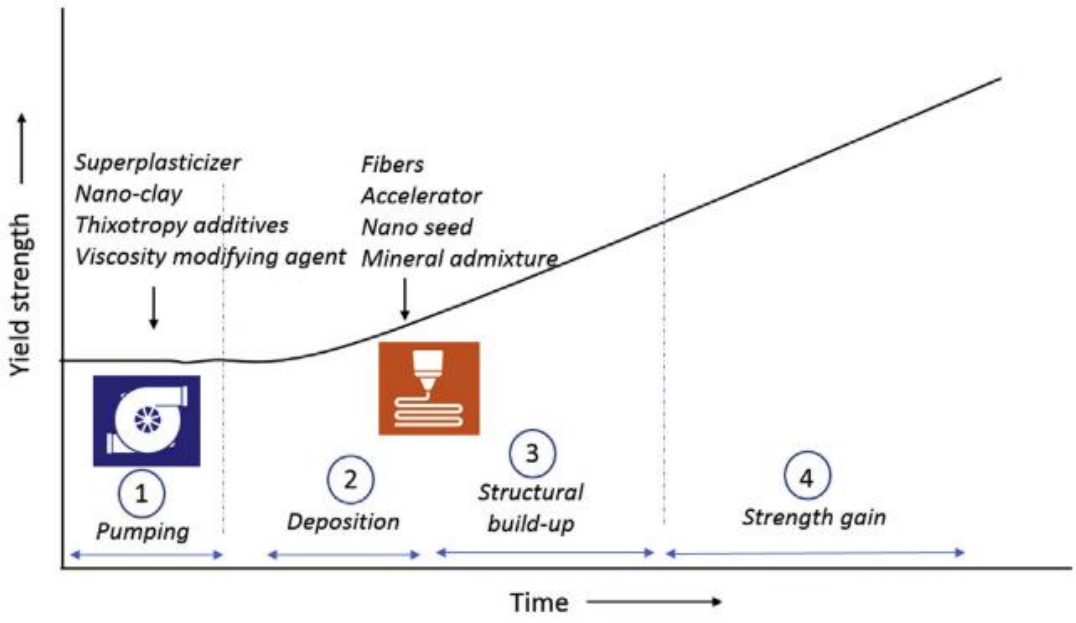

Figure 2.1. Admixture inclusion in 3D printing process. Adapted from [6].

Although these inclusions increase the fresh state strength performance of the printed object, the inclusion amount should be balanced. Low stiffness can cause elastic

deformation, whereas lack of adequate green strength may result in plastic failure, gradually becoming a more brittle failure for older age specimens [6].

2.2. Buildability of 3D printable cementitious materials

For 3D printing of cementitious materials, fresh state properties of the material are essential. After extrusion, the investigation of the plastic state shows material strength and layer quality. Layer-by-layer printed objects should be stable under their own weight. During the printing process, layers should sustain their shape, but they tend to deform under gravity-induced forces. Due to these forces, the yield stress increases with time. Different kinds of failure mechanisms may occur during or after the printing process, such as losing (a) layer stability or (b) geometrical shape stability. Both stabilities are dependent on material characteristics.

Roussel [6,13] developed an analytical model evaluating the yield stress, which may exceed or lack the needed threshold value.

Fresh state testing is a valuable method to evaluate the quality shape stability [10]. Based on fresh state testing, Wolfs *et al*. [14], the proposed a linear stress-strain analytical model of the material until the failure and a related time-dependent Mohr-Coulomb failure criterion. Their work showed that Young's modulus and the cohesion have a linear correlation, and it would further increase with the age of the fresh material. In addition, compressive and shear strength values increase with time. On the other hand, Poisson's ratio and angle of internal friction remain constant as time passes.

The experimental analysis on the 3D printed composites so far shows two failure mechanisms, strength-based failures, and in-print failures. In-print failures can be described as the lack of layer stability due to the defects originated from the print process [14]. These problems occur mainly at the built structure's bottom layer, hence named the critical layer. The green strength tests show the critical layer's load capacity, along with the vertical and horizontal displacements.

Wolfs *et al*. stated that fresh concrete's inter-particle friction, and cohesion behaviors are similar to that of soil, and the Mohr-Coulomb yield criterion applies to cement-based materials. For determining Mohr-Coulomb parameters, "cohesion *C(t)* and angle of internal friction *φ(t)"*, direct shear tests were conducted.

It is also pointed out that Young's modulus *E(t)* and Poisson ratio *v(t)* are crucial parameters besides *C(t)* and *φ(t)*, because the failure of the layers can be caused by instability as well. Due to it intrinsic non-uniform stress distribution, the direct shear test is not suitable, so an unconfined compression test is preferred. To evaluate *E(t)* and *v(t)*, the green strength test, as an unconfined compression test, was carried out. The direct shear test was compared with a uniaxial unconfined compression test, and the results were validated with the printed specimen's buildability check. [14]

The uniaxial unconfined compression test carried out by Wolfs *et al*. was designed according to ASTM D2166. Mold's aspect ratio was chosen as *h/d=2* to enable diagonal shear failure plane form. For measuring the time-dependent uniaxial, unconfined compressive strength, material ages were selected as t=0, 15, 30, 60, and 90 minutes. [14]

After the displacement-controlled procedure, vertical and lateral deformations of the specimens were measured at mid-height of the sample. As seen in Figure 2.2, the printed material should have a low or zero-slump to prevent shape deformation after extrusion.

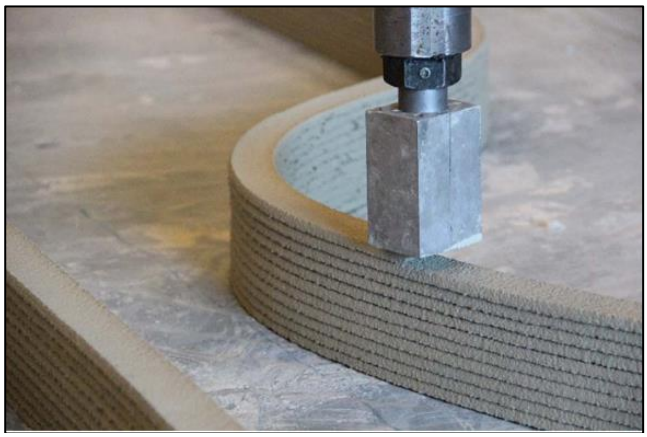

Figure 2.2. 3D printing tests by Wolfs *et al.*. Adapted from [14].

Wolfs *et al*. also stated that the older the material age, the more the maximum load capacity of the specimen is. Also, younger specimens form a lateral displacement, and the 'barreling' effect occurs through specimen failure. On the other hand, older specimens fail with a shear failure plane formation (Figure 2.3). As the soil has similar mechanical behavior, barreling or shear plane formations depend on the ductility and brittleness of the material as it gets older. [14]

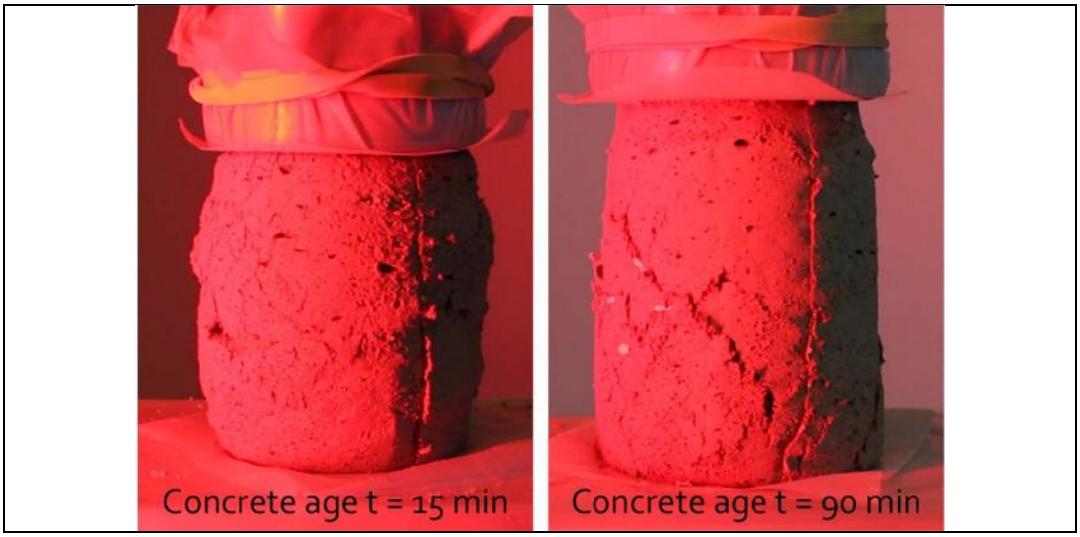

Figure 2.3. The effect of aging time on the mechanical response of concrete.
15 mins (left), 90 mins (right) as introduced in [14].

In addition to the observations on the failure behavior of specimens at different ageing times, the mechanical response of the specimen was analyzed by monitoring the changes in specimen dimensions under loading. The actual diameter was measured for determining the lateral displacement, and the corresponding stress value was determined according to the *true stress method*. Also, the self-weight was excluded from calculations as the failure plane occurs at the cylinder's center, not the bottom. So, including the self-weight of the whole specimen would not be accurate for comparison. The corresponding mechanical results of Wolfs *et al.* [14] are represented in Figure 2.4. The maximum green strength σ_y increases with concrete age, also Young Modulus μ_E and density ρ_ρ of each mixture at each concrete age was found. It was stated by Wolfs *et al.*, that there is a linear fit between stiffness and compressive green strength. In conclusion, assumed failure and

deformation were validated by the results of printed samples investigation of mechanical properties. [14]

Concrete age [min]	Compressive strength σ_y [kPa]		
	$\mu_{\sigma y}$	$\sigma_{\sigma y}$	RSD
0	6,37	1,07	17%
15	7,71	1,42	18%
30	10,05	1,31	13%
60	15,52	2,29	15%
90	18,93	3,92	21%

Young's modulus E [MPa]			Density ρ [kg/m^3]		
μ_E	σ_E	RSD	μ_ρ	σ_ρ	RSD
0,074	0,015	21%	2039	15,0	0,7%
0,099	0,022	22%	2007	8,90	0,4%
0,117	0,016	14%	2033	9,15	0,4%
0,154	0,021	14%	2030	10,6	0,5%
0,186	0,036	19%	1994	15,0	0,8%

Figure 2.4. Green strength test analysis of Wolfs *et al.* [14].

Kruger *et al.* [15] constructed a lower bound analytical model combining material strength, building rate, and failure modes. In this work, Kruger *et al.* stated that it is possible to obtain fresh state properties of the mortar from rheological tests.

According to Kruger's analytical model, the fresh state buildability is limited to plastic deformation, not the elastic buckling, which is also a non-linear failure of the material depending on geometrical nonlinearity. Therefore, plastic flow behavior is simplified with the Mohr-Coulomb failure criterion. Also, Tresca and Rankine limit functions are considered depending on the angled restraint. In conclusion, according to the rheological test results, re-flocculation rate R_{thix} and structuration rate A_{thix} parameters align with green strength test results. Therefore, rheological parameters re-flocculation rate R_{thix} and structuration rate A_{thix} can give the buildability rate of the deposited material with Kruger's analytical model.

However, the model offered by Kruger *et al.* is limited with rheological tests, which are very sensitive to the protocols and operating procedures. They are also sensitive to the

temperature, material preparation time and constrained by laboratory conditions. According to Tay *et al.* [16], results obtained from rheometers vary among different apparatus and do not apply to varying conditions. In addition to these aspects, rheometer tests are time-consuming and costly. Jayathilakage *et al.* [17] stated that the Kruger *et al.* model predicts only the lower bound limit of the plastic failure, and the numerical model overestimated actual strength and stability by 27.5%.

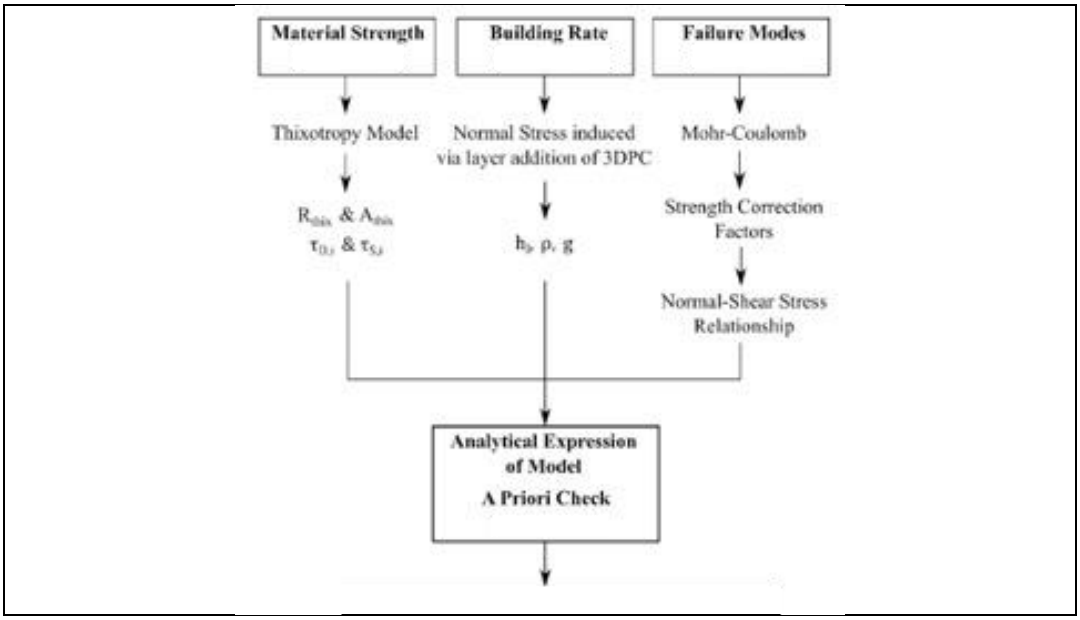

Figure 2.5. Alternative methods to evaluate buildability. Adapted from [16].

An alternative buildability test was presented by Zhang *et al.* [18], named the *buildability test performed according to the Murata model* related to gravity and built-up theory. Slump test can be used to evaluate the buildability of the 3D printable cement-based materials as it works using gravity [19-24]. According to the Murata model, the slump test's only dominant forces are formed by vertical stress. For the lower slump values, vertical stresses are more dominant than lateral ones, and for their evaluation, the von Mises yield criterion was used. As schematically represented in Figure 2.5, the vertical stress, σ_1, increase as the object's height decreases. At the bottom, the vertical stress σ_1 reaches its maximum value corresponding to $\sigma_1 = \rho g H_0$ at the initial state, where ρ is the density of the sample, g is the gravitational constant, and H_0 is the height of the object. As

a uniaxial compressive strength is applied to the sample, the form (b) (Figure 2.6) occurs according to equation:

$$H_1 = \frac{\sigma_y}{\rho g}. \tag{2.1}$$

In (2.1), H_1 is the uniform height of the object, where σ_y denotes the maximum uniform compressive strength [8].

As the object slumps, the lower region of the object expands to decrease the vertical stress σ_1 to $\rho g H_1$. The yielded region's height is depicted as H_2, and the yielded region's yield point is τ_s, where the von Mises condition $\sqrt{3}\tau_s = \sigma_y$ describes the uniaxial yield stress [18]. In the Murata model, the development of yield stress through time is ignored. During printing, compressive stress will increase at the bottom layer. If the compressive stress at the bottom layer is greater than the uniaxial compressive stress, deformations will occur at the bottom layer [18].

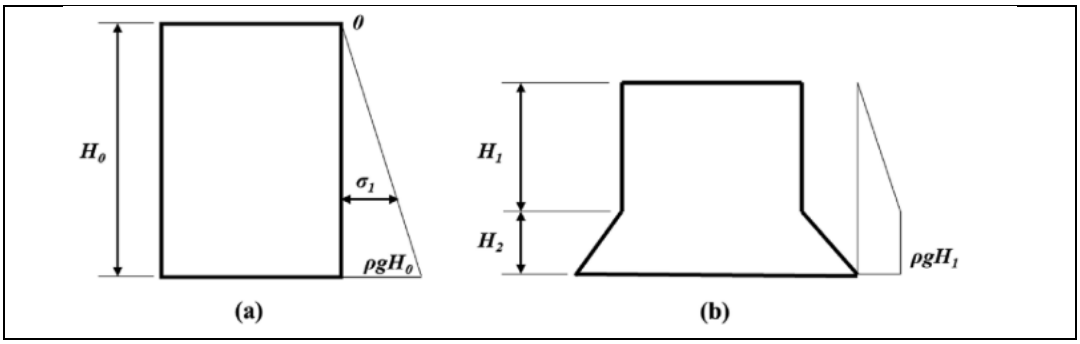

Figure 2.6. Schematic description of the Murata model. Adapted from [10].

Also, Perrot *et al.* described a model [25], the so-called *"built- up theory"*, which can be stated as $H = \alpha\tau_s/(\rho g)$, where H is the height and α is the geometric factor of the printed structure. Both the Murata Model and the built-up theory correlate yield stress and buildability. With these models, it can be concluded that *the higher the yield stress is, the more buildable 3D printable cement-based material will be* [18]. However, the material must also flow through the nozzle. Therefore, it should have adequate dynamic yield stress.

In conclusion, the material should have high static yield stress, but it should also have appropriate dynamic yield stress to be printable. [18]

From individual geometry control of one layer, the overall stability of the printed objects can be achieved and amended. As the gravity-induced stress on layers increases, deformations can be detected on the printed object. Each extruded layer increases the stress of the layers below by $\rho g h_0$ under gravity force [26,27]. As the structuration of the material is non-linear, the yield stress can be defined as $\tau_c > \rho g H t \sqrt{3}$ [26]. With each layer deposited on top of the last extruded one, the strength-based failure begins. Besides the strength-based failure, stability loss or buckling failure can be observed. The critical height H_c is crucial to determine the printed height. The critical height can be defined as

$$H_c \cong \left(\frac{2E\delta^2}{3\rho g} \right)^{\frac{1}{3}}. \tag{2.2}$$

In (2.2), E is the elastic modulus of the material, obtained from the green strength test results, and δ is the width of a one linear meter high wall, which is set by the Tübitak project proposal as 0.5 m [26]. In the project block elements with dimensions of 1 m length, 0.5 m width and 0.8 m height will be produced. 20 layers are to be printed. The relation between E modulus and shear modulus G can be described as

$$E = 2G(1+\nu) \text{ and } \tau_c = G\gamma_c. \tag{2.3}$$

Following (2.3), minimum E-modulus from the strength-based failure is implemented in

$$E > \frac{2\rho g H}{\sqrt{3}\gamma_c}(1+\nu). \tag{2.4}$$

In equation (2.4), the Poisson's ratio v of the material is calculated from the green strength test [26].

Using equations (2.1) and (2.3), a transition height (H_T) between two failure criteria (i.e., strength-based failure and buckling failure), where the strength-based failure is dominant if the print height is lower, and the buckling failure is crucial if the print height is higher than the threshold [17]. Hence, H_T is defined as follows [26]:

$$H_T = 2\delta \sqrt{\frac{1+v}{3\sqrt{3}\gamma_c}}. \tag{2.5}$$

At the transition height, failure modes switch from strength-based failure to buckling failure. From the green strength data, the buildability performance of a 0.5 m x 0.8 m block with NM or sepiolite rheological modifiers along with fly ash substrate, can be calculated.

In addition to the early age buildability of the material, the hardened state mechanical performance parameters are also critical for the 3D printing of cement-based materials. In [27], for mechanical tests, compressive and tensile strength tests, the approach described by Wolfs *et al*. [14] was applied. Flexural tension tests were done according to EN-196-1 on 40x40x160 mm^3 prismatic samples, which were cured seven days. Free span length l was kept 100 mm, and the loading rate was 50 N/s as suggested in [27]. As the specimen fails, the flexural strength f_f can be calculate by the equation:

$$f_f = \frac{1.5F_f\, l}{b^3}. \tag{2.6}$$

In (2.6), F_f is the recorded load, f_f denotes the flexural strength, l is the free length span between supports (i.e., 100 mm), and b is the edge length of the square section (i.e., 40 mm) [27].

Compression tests were conducted according to EN 12390-3 standards on 40x40x40 cubic specimens. The tests were carried out with a loading rate of 960 N/s. 7 days compressive strengths of the samples were obtained. For each specimen, maximum load to failure was read, and stress was calculated based on [27] using the equation:

$$f_c = \frac{F}{A_c}. \tag{2.7}$$

In (2.7), F is the maximum load at failure in N, f_c is the compressive strength in MPa, and A_c is the cross-sectional area of the specimen (i.e., 1600 mm^2). As Wolfs *et al*. stated there were no relevance between nozzle height and bond strength of the layers. Also, there were no relevance between layer orientation and interlayer interval time. In addition to these results, compressive test results showed no relevance between compressive strength and layer direction. However, a strength reduction of 14% dependent of the layer direction and 16% dependent of layer interval time were found [27]. Also, casted compressive strength test results overestimated the printed compressive strength 31% [27].

3. MATERIALS & METHODS

3.1. Materials

One of the main ingredients of the cement based composite targeted to achieve in this work is Ordinary Portland Cement (OPC) CEM I 42.5R from Akçansa. As a binder, cement was replaced with fly ash and two clay alternatives (i.e., nano-montmorillonite, and sepiolite). Most 3D concrete printers have restricted nozzle openings. Therefore, the particle size of the sand as fine aggregate was chosen to be maximum 2 mm in diameter.

A Mastersizer 2000 particle size analyzer equipped with a Hydro MU 200 wet dispersion unit (Malvern, Worcestershire, United Kingdom), and a sonicator were used to determine the particle size distribution (PSD) of cement in Özyeğin University [28]. The average particle size of the cement is 15 µm, fly ash is 65µm and sepiolite is 57 µm; and the maximum particles size of NM was reported as 20 µm by Sigma-Aldrich [29]. Figure 3.1 represents the particle size distribution for the FA and OPC used in the study.

There are two kinds of clays to replace cement as rheological modifiers of the composite. The surface modified nano-montmorillonite (NM) supplied from Sigma Aldrich has maximum particle size of 20 µm [29]. This nano-clay is in powder form and surface modified. On the other hand, sepiolite is supplied from a local source and sieved by 150 µm (micron) sieve. Fly ash is replaced with cement to increase workability. The chemical compound of fly ash is given in Table 3.1.

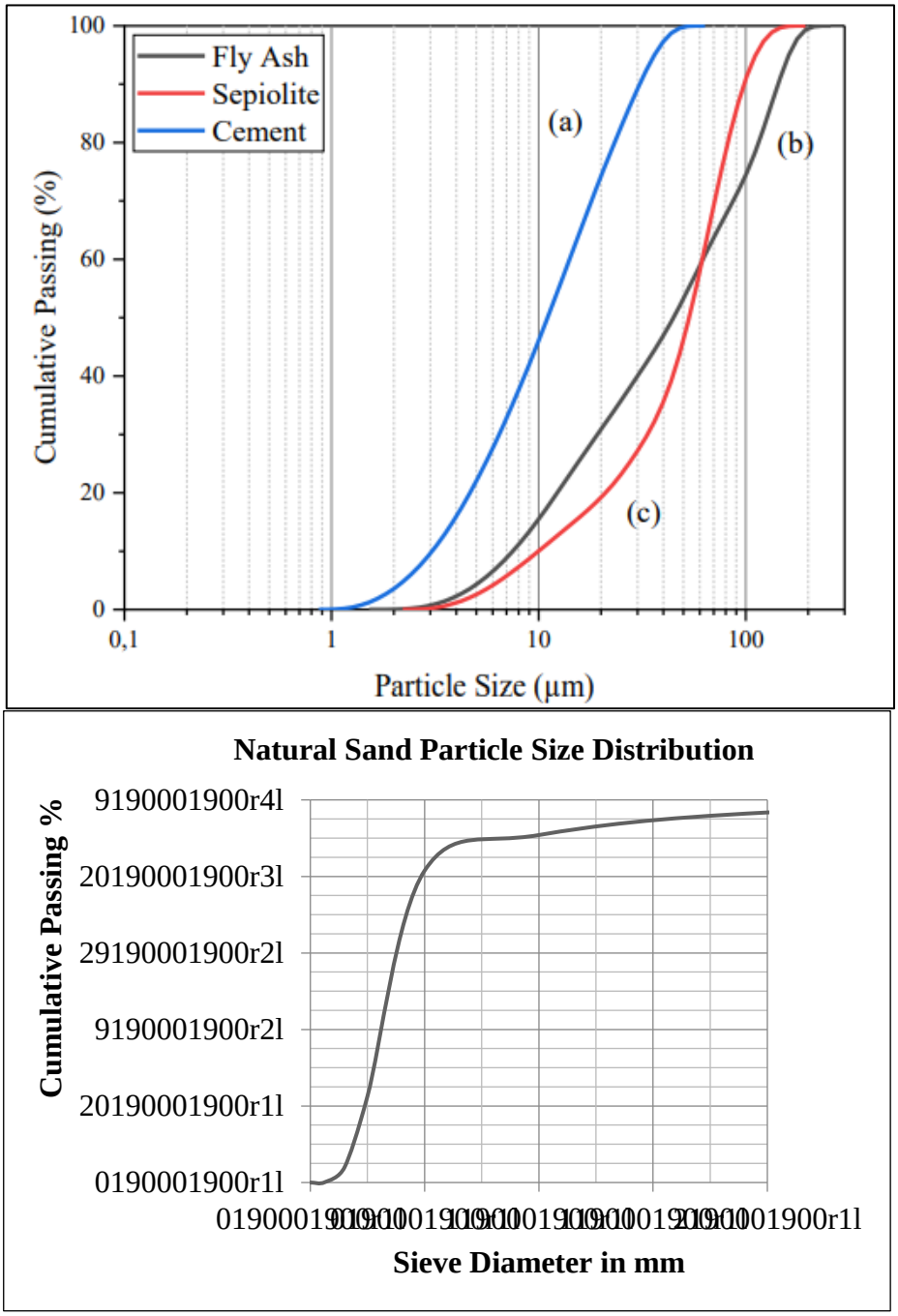

Figure 3.1. Particle size distributions. Above: Particle size of (a) Akçansa CEM I 42,5R, (b) Class F Fly Ash and (c) Sepiolite [28]. Below: Natural sand particle size distribution.

Table 3.1. Fly Ash Chemical Compound in %.

Loss on Ignition	**SiO_2**	**Al_2O_3**	**Fe_2O_3**	**CaO**	**MgO**	**SO_3**	**Na_2O**
2.74	55.38	25.20	6.14	2.02	2	0.14	0.62
K_2O	**Total Alkali**	**TiO_2**	**Cl**	**Free CaO**	**28 days pozzolonic activity**	**Density kg/m^3**	
3.80	3.12	1.20	0.0014	0.18	87.8	2100	

Two kinds of superplasticizers were sent to Boğaziçi University Construction Materials Lab along with VMA for this work. These superplasticizers were also compared in this study to optimize the mix design. One of the superplasticizers is SP_1, a high-performance superplasticizer as a concrete additive. It is PCE (Polycarboxylate Ether) based, making it very suitable for self-compacting concrete. Another one is SP_2, a high-performance superplasticizer based on a modified PCE composition. According to Marchon *et al.*, superplasticizers enable cementitious material to reduce yield stress and viscosity for improving workability at defined solid volume. SPs help to decrease water content, shrinkage, porosity and therefore improve mechanical properties [30].

Besides, VMA contributes to improving the shape stability, printability, and buildability of the layers. A stabilizer is used as VMA, which increases the yield stress slightly according to the data acquired from Sika. The VMA contains a modified starch complex, which increases stability and segregation resistance of concrete mixes without significant reduction of slump or flow, resulting in improved surface quality and aesthetics.

3.2. Methodology

3.2.1. Preparation of the mixes

Cement paste is prepared according to ASTM C305 and the mortar is prepared according to the following procedure:

1) 30 sec. slow mixing of binder with water
2) Sand addition
3) 30 sec. slow mixing
4) 30 sec high-speed mixing
5) Stop
6) 30 sec. scraping
7) Wait 75 sec.
8) 60 sec. high speed mixing.

With a constant w/b ratio of 0.36, the mixture was prepared according to the mix combinations in Table 3.2.

Table 3.2. Mix Design Content in %.

Sample Name	Cement	Fly Ash	NM	SEP	SP	VMA
C_SP	100	-	-	-	0.35	-
C_SP_FA	80	20	-	-	0.35	-
NM_0.5	99.5	-	0.5	-	0.35	-
NM_0.5_FA	79.5	20	0.5	-	0.35	-
NM_1	99	-	1	-	0.35	-
NM_1_FA	79	20	1	-	0.35	-
SEP_0.5	99.5	-	-	0.5	0.5	-
SEP_0.5_FA	79.5	20	-	0.5	0.5	-
SEP_1	99	-	-	1	0.5	-
SEP_1_FA	79	20	-	1	0.5	-
VMA_SP	100	-	-	-	0.5	0.3
VMA_FA	80	20	-	-	0.5	0.3

Vicat Needle Test: Initial setting time of cement paste is measured by vicat needle test. The test is conducted according to ASTM C191-13 standard.

Workability - Flow Table Test: To evaluate workability of the material, slump and flow table tests were carried out. For this purpose, prepared mortar mixtures were tested on

the flow table to obtain flow diameter of each sample. The tests were carried out according to ASTM C230/ C230 M- 14 standard in t = 0, 15, 30, 60 min.

Green Strength Test: A Uniaxial Compressive Machine by ELE with 3kN maximum loading was used to measure displacement under quasi-static load. The samples were tested in t=0, 15, 30 and 60 minutes. For this test a special testing apparatus was designed and manufactured as represented in Figure 3.2. Prepared samples are filled in cylindrical mold, which has 6.75 cm diameter and 13.5 cm height. h=2d is intentionally selected in order to maintain a shear failure plane. As Wolfs *et al.* stated, the diameter is chosen to eliminate size effects due to particle size distribution [14]. The mold is pulled upwards and removed. Two transparent PVC plaques are put above and under the sample to reduce the friction on top and bottom of the sample.

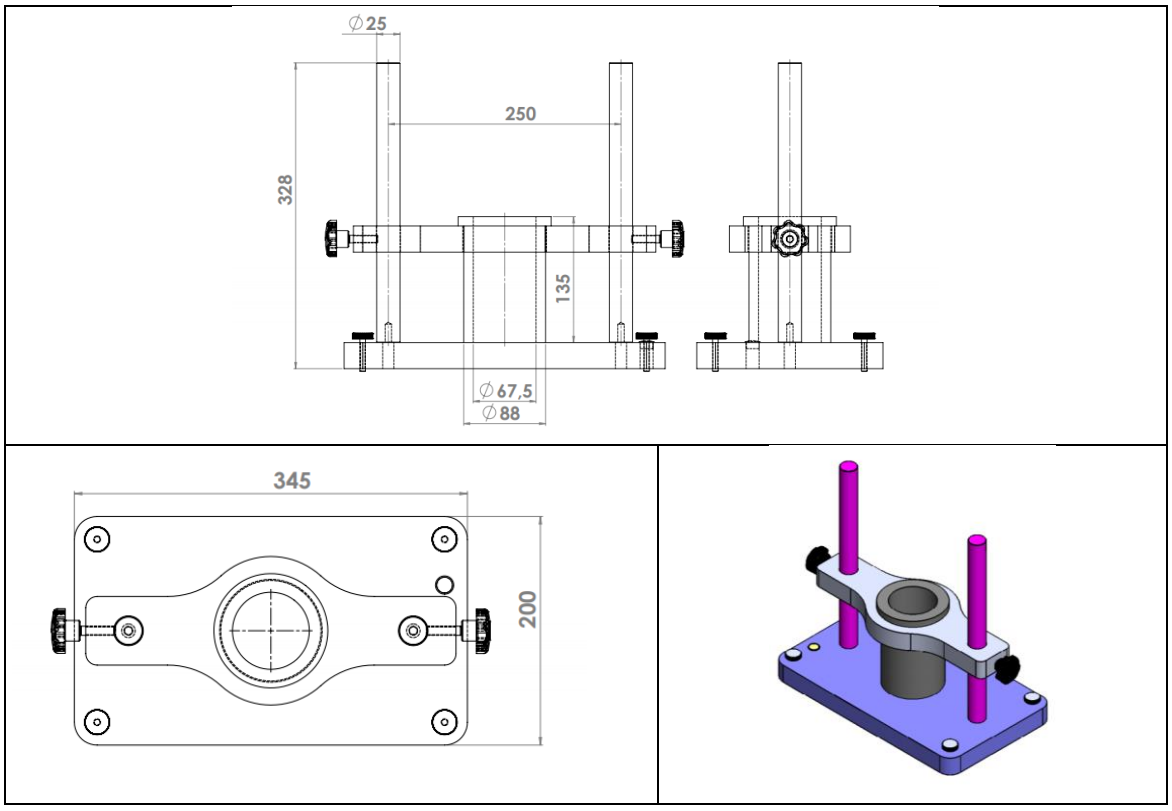

Figure 3.2. Green strength test apparatus.

The tests were executed with a rate of 10 mm/min. Also Wolfs *et al.* stated it is important to simulate the loading rate of real printing process and allow the test to be performed fast enough to neglect effects of thixotropic build-up [14]. For each mixture, three specimens were prepared and tested at fresh state in four different measuring times. From loading and reloading the sample, each test took about 4.5 to 5 minutes in total. Totally, 144 tests were recorded with a Canon High Resolution Camera for further processing. Afterward, the recordings were post-processed by ImageJ, a Java-based image processing program. Each snapshot was extracted from the recordings at 0, 30, 60, 120, 180 and 240 seconds of the experiment and processed by ImageJ as shown in Figure 3.3.

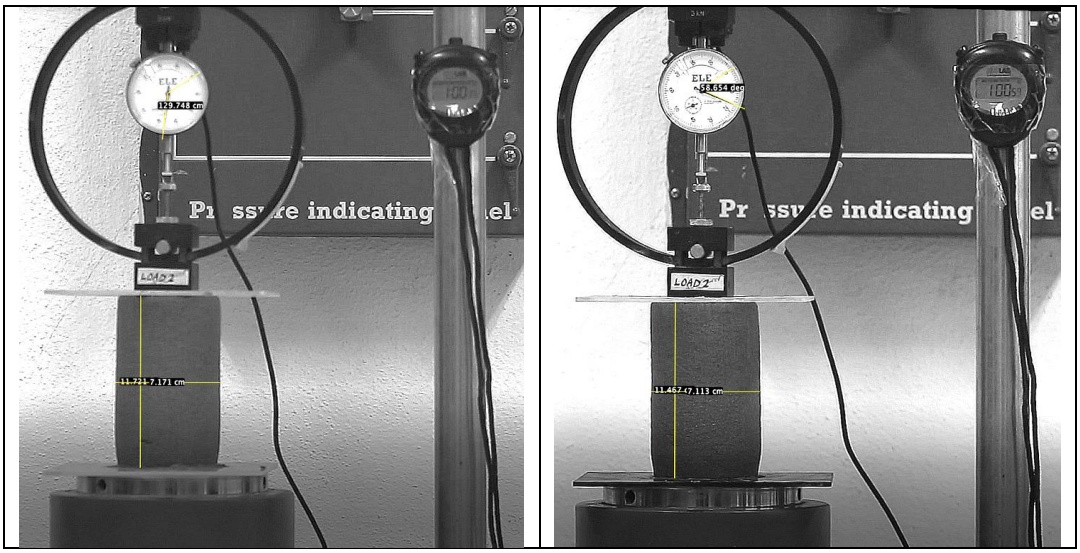

Figure 3.3. SEP_1_FA and VMA_FA green strength test result at 15 mins material age. SEP_1_FA (left) and VMA_FA (right). The deflections, and the force readings on both images are processed via ImageJ.

At each vertical deflection of these six time checkpoints, the lateral deflection in the middle of the sample and the vertical deflection were measured and compared with the initial diameter and height at 0 seconds. The displacement was related to the load at the given time. The tests were performed under conditions of 18 C^o ± 1 and 57% humidity approximately.

Buildability Test: In sight of Murata model and built-up theory, under the gravity force the yield stress and buildability of remaining height and aspect ratio of the slumped concrete are to be evaluated. This shows the layer's ability of standing stability [16]. This test ran with 6.75 cm diameter and 13.5 cm height cylindrical plastic mold. Initially the mold is filled to its 1/3 volume with mortar and compacted with a wooden rodding stick 20 times, this is repeated 3 times till the mold is full. Then the mold is removed vertically with the apparatus in order to keep it perfectly vertical. To assess the buildability, the height and diameter is measured, photographed, and processed by ImageJ. The deformation after the removal of the mold gives the *buildability index b.*

Compressive Strength Test: Compressive strength specimens were casted in 40x40x40 mm molds and tested according to EN 12390-3 standards. U Test 3000 kN Automatic Compression Testing Machine was used with a loading rate of 1kN/s. 28-day compressive strengths of the samples were obtained. Unmolded samples were stored in a curing pool at 20 C° until the test day. For each specimen, the maximum force was read, and stress was calculated using equation (2.6).

Flexural Strength Test*:* Flexural Strength Tests was carried out by using an MTS Machine with a maximum capacity of 100kN. 3 point bending test procedure was applied on 40x40x160 mm beams according to EN 196-1 to obtained comparative results. The free span length *l* was set to be 100 mm and loading rate was 50 N/s until failure. After curing in water at 20^{o}, 28 day flexural strength was obtained from the samples. As the specimen fails, for determining the flexural tensile strength f_f, equation (2.7) should be applied:

4. RESULTS & DISCUSSION

4.1. Preliminary Tests

In order to compare two superplasticizers and prepare the mix design, a preliminary study has been conducted. Same mixtures with Hi-tech and SF-18 superplasticizers and without superplasticizers were compared by means of fresh state performances. Below are the comparison done by Vicat needle test, flow (spread slump) test and, the green strength test. Figure 4.1 gives initial setting times of cement paste with varying w/b ratios, and without superplasticizers, clay, fly ash, or VMA. Setting times were found to be very similar after a threshold water-to-cement ratio was exceeded. At the same time, as it's shown in Figure 4.2, there is no significant difference between cement paste mixtures cast by using SF-18 and Hi-tech.

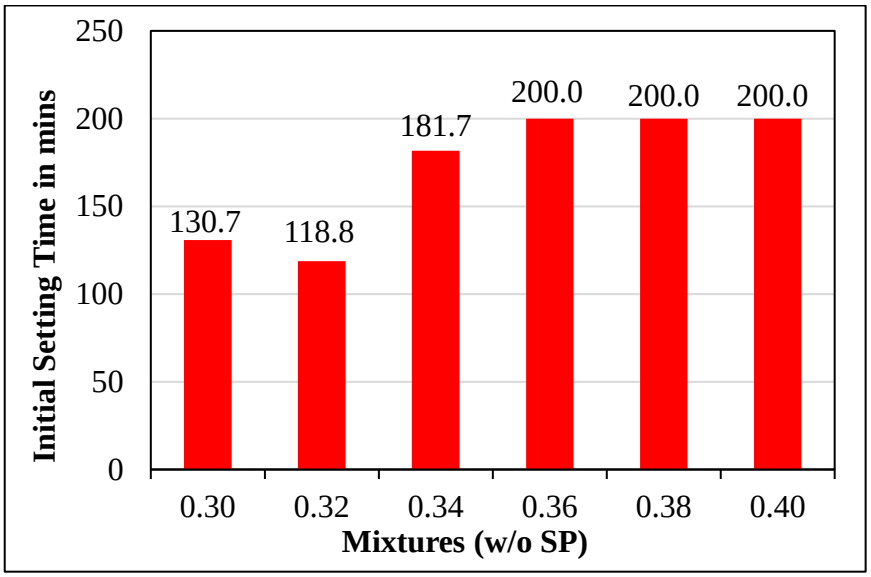

Figure 4.1. Initial setting times of varying w/b ratios without SP.

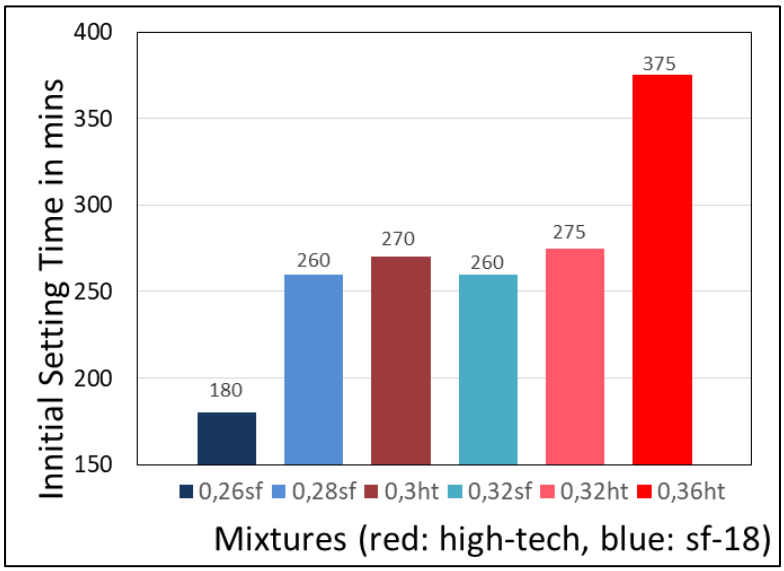

Figure 4.2. Comparison of initial setting time for the mixtures. These mixtures are cast using different chemical admixtures.

4.1.1. Comparison of Slump and Flow

Spread and slump are other parameters to observe superplasticizer performance however these tests were only done to observe the range of the superplasticizers. The spread behavior of the to-be-printed mixtures can be a distinctive parameter to optimize during a mix-design process. The slump loss and spread flow diameter change of the mixes cast by using 2 different admixtures were given in Figure 4.3. Slump loss of SF-18 SP from 0 minute to 15 minutes was found to be very steep. Spread loss for SF-18 SP was relatively steeper.

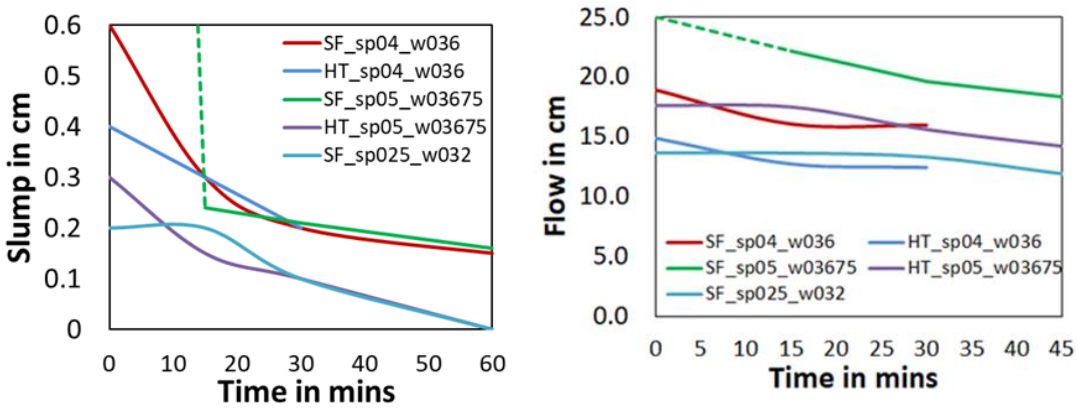

Figure 4.3. Slump and spread test results.

4.1.2. Comparison of Green Strength

As shown in Figure 4.4, the green strength load-bearing capacity at fresh state of the mixture with Hi-tech SP is higher than the mixture with SF-18 superplasticizer. w/b and sp/b ratios are kept constant for both mixtures.

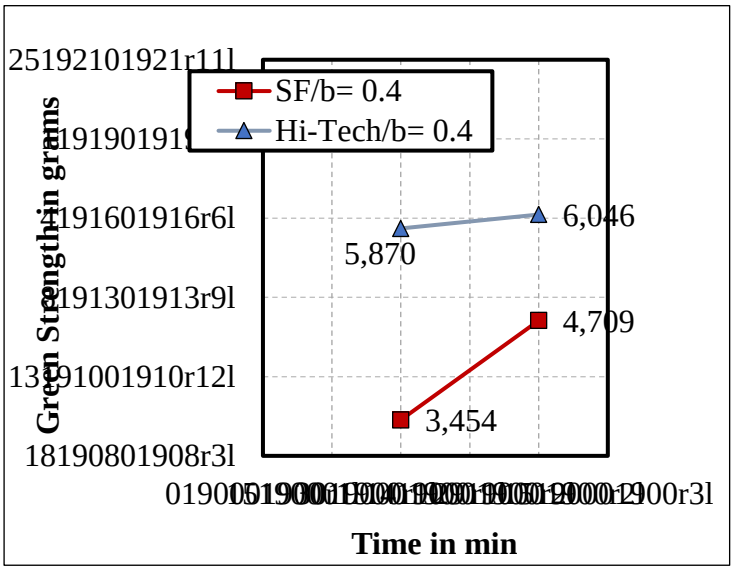

Figure 4.4. Green strength load bearing capacity.

4.1.3. Observations & Conclusions

Our observations and conclusions regarding to the advantages and disadvantages of Hi-tech and SF-18 SPs are summarized in Table 4.1.

As most important parameters are spread-slump and green strength, the decision was made according to these parameters. From spread-slump, it can be seen that, in general Hi-tech SP has lower slump compared toSF-18 SP. Therefore, Hi-tech SP has higher static yield stress than SF-18 SP. Depending on observation; Hi-tech SP has less fluctuation in spread and slump results, which makes Hi-tech SP stable and predictable. In addition to these, Hi-tech SP had greater green strength values than SF-18 SP; therefore, Hi-tech SP increases the buildability of the mix design. As a conclusion, Hi-tech SP is chosen for this work as a superplasticizer.

Table 4.1. Pros and cons of SP_1 and SP_2.

	PROs	**CONs**
SF-18	• Works with lower w/b ratios • Works similar to Self-Compacting Concrete (SCC) • Shorter Initial Setting Time (may need additional retarder, may be better for secondary phase, so preparing in small proportions)	• Flocculation is observed • Less Green Strength • Bleeding is observed
Hi-tech	• Works with higher w/b ratios • Has a higher range of w/b ratio • Higher Green Strength	• Longer Initial Setting Time (may not need any retarder) (better for taking from bulk, no need for small portion preparation for printing)

4.2. Results

4.2.1. Green Strength Test Results

In developing 3D printable concrete, there are new challenges to overcome, which one may not come across while producing conventional concrete. One of the main challenges is the elimination of formwork during the printing process. It is essential to secure the layer stability after the extrusion. In order to maintain the shape and stability, early age and hardened state mechanical properties of the mixtures should be thoroughly examined and analyzed. In this study, strength development was acquired by following, the green strength, buildability test, and compressive strength at 28 days. The first part, the green strength is the uniaxial compressive strength at the fresh state. According to Perrot *et al.* [25], the duration of the print process of a large concrete component is approximately three hours with a simulated building rate of 1.1-6.2 m/hr. Also, the hydration process of the mixes starts approximately at the 4-5th hour, giving a printing process with mixing, and transporting approximately 4-5 hours in total. Therefore, the green strength can be measured shortly before the hydration process starts. However, it is a difficult process to obtain green strength. As an alternative to the conventional green strength test process, Wolfs *et al.* [14] offered to measure green strength with a uniaxial testing machine as a quasi-static load simulating the print rate. In order to acquire targeted results, fresh mortar's green strength was measured at varying material ages, such as t=0, 15, 30, and 60 mins.

Each mixture was tested at each material age t=0, 15, 30, 60 min, in triplicates. Preparation of each test lasts 5.5 minutes, while each test lasts approximately 4-5 min. 0, 30, 60, 120, 180, and 240th seconds of each video's screenshots were taken and processed via image processing software ImageJ. In addition, screenshots of the maximum force at each video were recorded and processed with the same software. Initially, the experiment setup was calibrated by correlating the dial gauge units with 2 kg dead-weights. Afterward, the 2 kg weight change was read at the dial and noted as load calibrator to measure force. Figure 4.5, the load scale graph is shown as an indicator for force measurement.

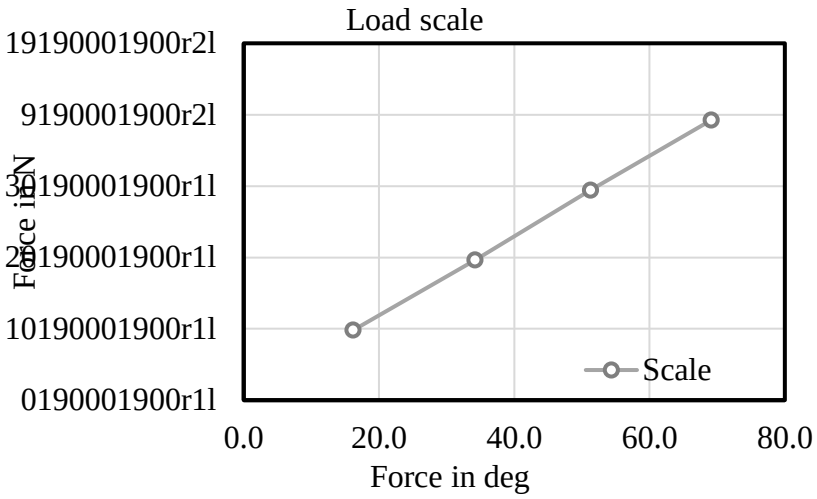

Figure 4.5. Calibration of dial scale in degrees to load in N.

At first, in Figure 4.5, initial vertical and horizontal measurements of each material age were taken via ImageJ. For detecting the vertical and the horizontal displacements, the half-height and width of each specimen were calculated and processed via ImageJ for each time frame (i.e., t=0, 30, 60, 90, 120, 180, and 240 sec.) of each material age. These stated as *Y displacement in vertical axis*, and *X at ½ displacement* in the figures below. The horizontal and the vertical displacements were plotted against force calculated from the dial gauge pointer degree and load converter graphic. They were stated as force and not as stress due to the constant changing diameter of the specimen.

4.2.2. Results for the mix C-SP-FA

Below green strength test results were given for C_SP_FA mixture at material ages of t=0, 15, 30 and 60 minutes. The tests were repeated three times for all four material ages and average values were calculated. In Figure 4.6a-d, uniaxial compressive strength read from the dial gage versus vertical displacement of the specimens were shown. In the last graph average results were summarized for C_SP_FA_ (Figure 4.6e).

At material age t=0 minute (Figure 4.6a), the prepared specimen was tested by a uniaxial compressive testing machine, and the average peak value was found to be 64.334 N at the 119th second of the test with a vertical displacement of 1.722 cm. At

material age t=15 minutes (Figure 4.6b), the tested average peak value is 54.71 N at the 123rd second, and vertical displacement is 2.135 cm. At material age t=30 minutes (Figure 4.6c), the tested average peak value is 85.29 N at the 119th second, and vertical displacement is 1.765 cm. At material age t=60 minutes (Figure 4.6d), the tested average peak value is 84.41 N at the 122nd second, and vertical displacement is 2.112 cm.

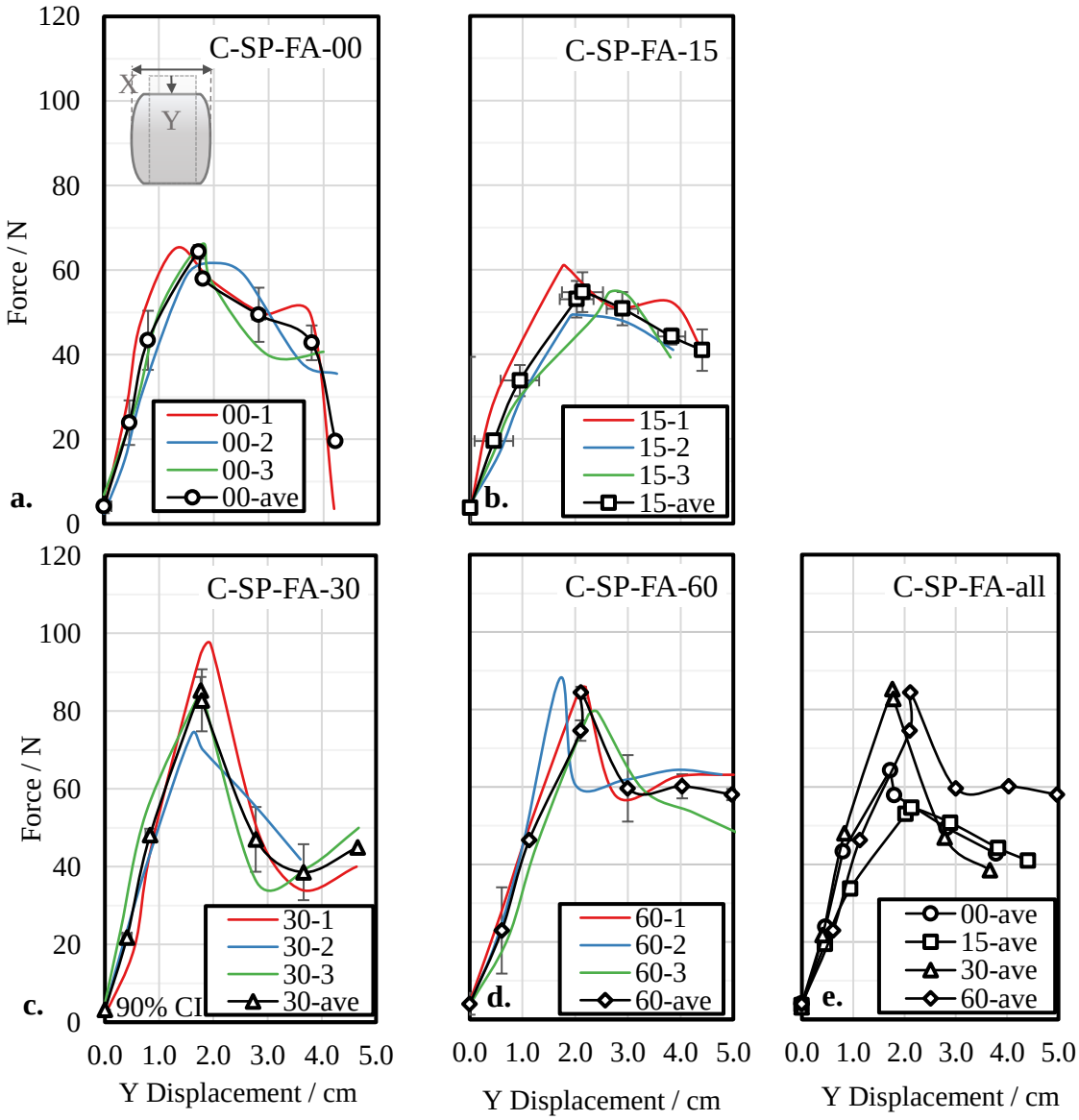

Figure 4.6. Force response of C-SP-FA mixture. The experiments are performed at various material ages during green strength tests.

In Figure 4.7, horizontal displacement, X at ½ lengths in cm, versus vertical displacement, Y displacement in cm was plotted at material ages of t=0, 15, 30, and 60 min. At material age t=0 min. (Figure 4.7a), lateral length of specimen at the maximum compressive force of 64.334 N is 7.644 cm with a vertical displacement of 1.722 cm.

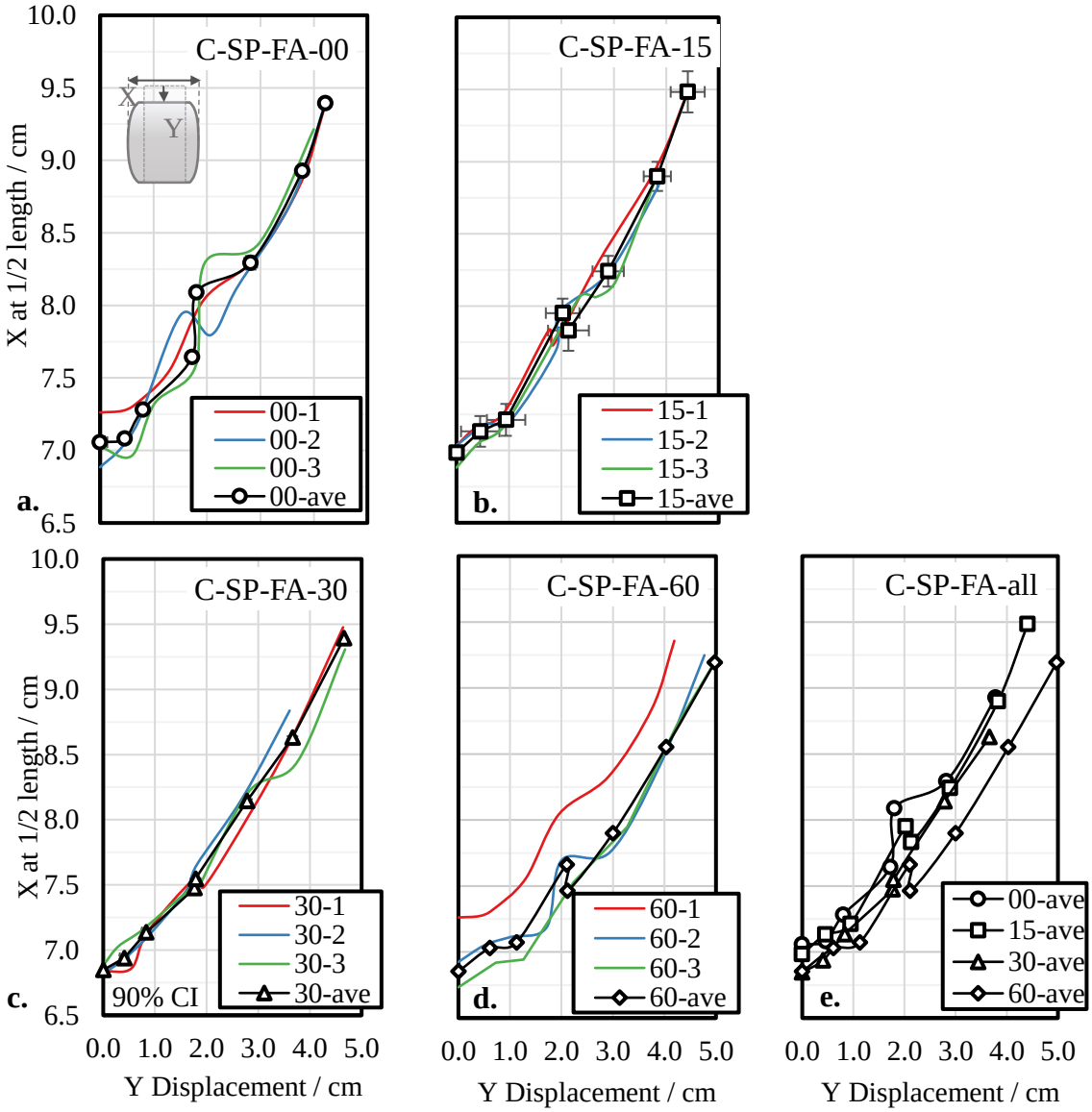

Figure 4.7. Lateral displacement of C-SP-FA mixture. Experiments are performed at various material ages during green strength tests.

At material age t=15 min. (Figure 4.7b), lateral length of specimen at the maximum compressive force of 54.71 N is 7.831 cm with a vertical displacement of 1.66 cm. At material age t=30 min. (Figure 4.7c), lateral length of specimen at maximum compressive force of 85.29 N is 7.547cm with a vertical displacement of 1.765 cm.

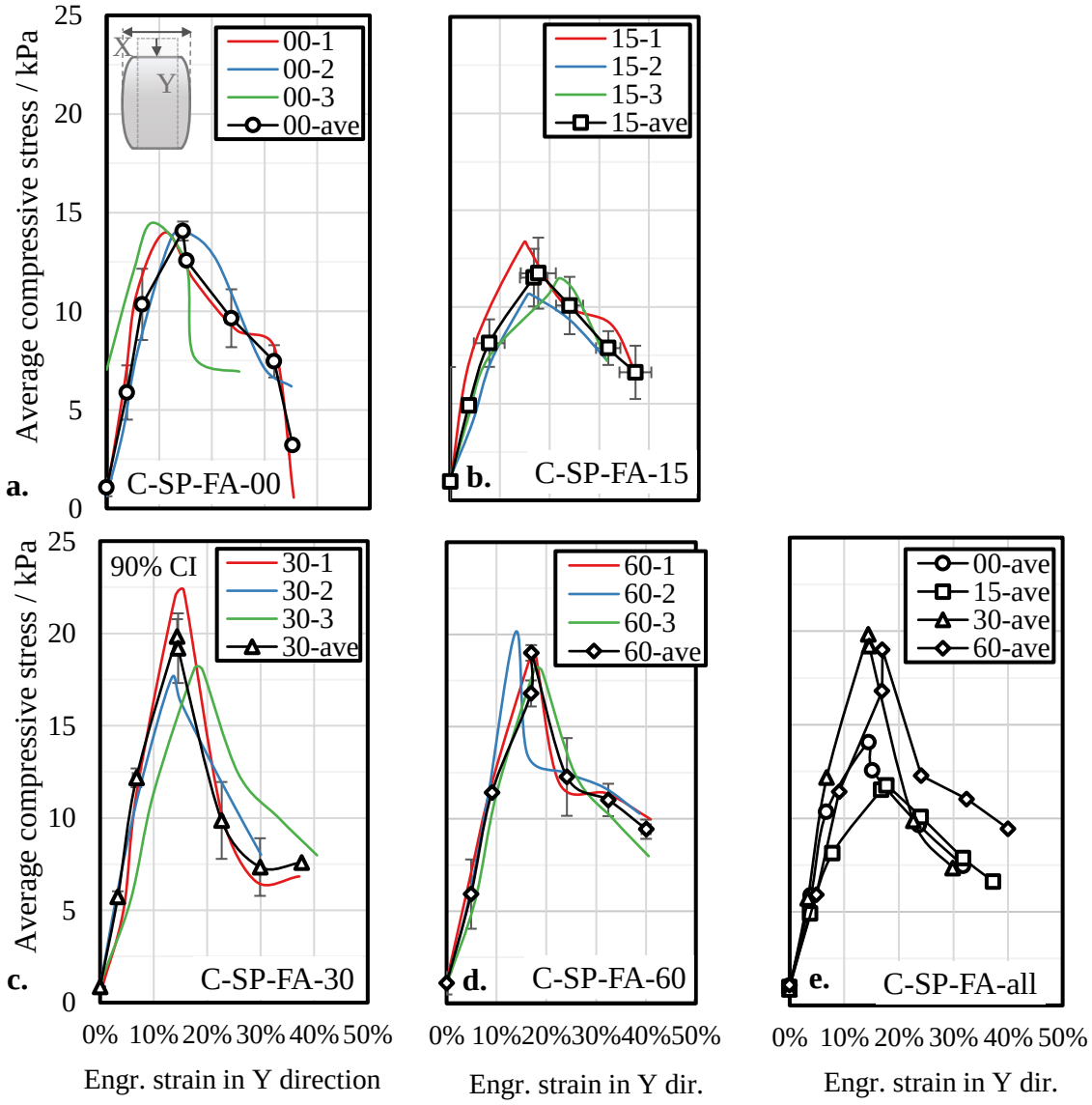

Figure 4.8. Average stress of C-SP-FA mixture. The experiments are performed at various material ages via green strength tests.

At material age t=60 min. (Figure 4.7d), lateral length of specimen at a maximum compressive force of 84.41 N is 7.464cm with vertical displacement of 2.112 cm. Overall,

material at age of 30 minutes has the highest lateral displacement while material age t=60 min has the lowest lateral displacement.

In Figure 4.8, average compressive stress in kPa versus vertical engineering strain (final height/initial height) in percentages is shown at material ages of t=0-, 15-, 30-, and 60-min. Specimen's height at the age of 0 min. (Figure 4.8a) has decreased 14.5% under the average maximum compressive load of 64.334 N. At the material age of t=15 min. (Figure 4.8b), specimen's height got 17.7% less with an average maximum compressive load of 54.71 N. Specimen's height at the age of 30 min. (Figure 4.8c) has decreased 14.4% under the average maximum compressive load of 85.29 N. Lastly, the specimen's height at the age of 60 minutes has decreased 17% under the average maximum compressive load of 84.41 N (Figure 4.8d).

4.2.3. Green strength result summary

All 12 mixtures green strength results can be found in Appendix. Table 4 summarizes the test results for all mixtures and ageing times at the peak force. Along with the mean peak force response, the mean values of the vertical displacement and the deflection in x direction at the maximum force point are tabulated. In addition to the measured quantities (i.e., time at peak force, peak force, Y displacement, and X displacement), the calculated mechanical responses namely the mean engineering strain and the corresponding mean uniaxial stress are represented. The uniaxial stress is calculated assuming the cross-section of the specimen is uniform, and stress is distributed uniaxial. It is seen that the highest peak stress occurs in SEP1 mixtures, whereas SEP1-FA mixtures reach their peak force point the earliest.

Table 4.2. Green strength test results summary at maximum force.

		Time at max. force in secs	Max. Force in N	Y displacement at max. force in cm	X displacement at max force in cm	Engr. strain at max. force in cm/cm	Uniaxial stress at max. force in kPa
CS-SP	0	132	52.9	2.123	7.699	0.178	11.4
	15	112	85.4	1.655	7.644	0.140	19.6
	30	138	71.4	2.126	7.655	0.176	15.8
	60	101	98.1	1.545	7.459	0.127	22.6
CS-SP-FA	0	119	64.3	1.722	7.644	0.145	14.1
	15	123	54.7	2.135	7.831	0.177	11.7
	30	119	85.3	1.765	7.475	0.144	19.8
	60	122	84.4	2.112	7.464	0.170	19.0
VMA-SP	0	128	57.8	2.056	7.788	0.171	12.1
	15	131	67.8	2.019	7.697	0.167	15.1
	30	125	68.9	1.957	7.582	0.160	15.5
	60	118	83.2	1.845	7.679	0.152	18.4
VMA-FA	0	131	53.9	1.943	7.641	0.158	12.2
	15	145	60.1	2.279	7.772	0.187	13.4
	30	119	72.6	1.803	7.542	0.147	17.0
	60	120	74.6	1.888	7.595	0.152	17.2
NM0.5	0	171	51.8	2.622	8.048	0.217	10.7
	15	143	67.8	2.201	7.804	0.181	14.3
	30	130	73.3	2.029	7.591	0.167	16.2
	60	120	113.4	1.871	7.391	0.154	26.1
NM0.5-FA	0	127	58.0	2.084	7.817	0.174	12.0
	15	109	67.8	1.853	7.468	0.147	15.2
	30	118	83.0	1.845	7.709	0.152	18.4
	60	93	94.5	1.499	7.301	0.121	22.2
NM1	0	119	65.0	1.737	7.548	0.143	14.9
	15	132	71.4	2.078	7.476	0.171	15.7
	30	108	87.8	1.564	7.429	0.126	20.9
	60	119	138.2	1.999	7.472	0.157	32.2
NM1-FA	0	121	52.7	1.988	7.682	0.165	11.0
	15	121	63.9	1.946	7.522	0.158	14.4
	30	110	76.3	1.692	7.618	0.141	16.7
	60	88	89.9	1.460	7.273	0.119	21.2
SEP0.5	0	101	106.5	1.579	7.285	0.126	25.2
	15	92	131.3	1.524	7.211	0.121	32.2
	30	95	147.8	1.517	7.311	0.120	35.3
	60	98	157.6	1.557	7.201	0.120	38.9
SEP0.5-FA	0	115	116.7	1.601	7.365	0.122	27.4
	15	98	110.4	1.593	7.423	0.125	26.1
	30	83	152.6	1.035	7.287	0.081	38.7
	60	91	137.5	1.696	7.369	0.132	31.0
SEP1	0	100	147.3	1.527	7.263	0.119	36.1
	15	79	214.8	1.152	7.158	0.090	54.0
	30	70	250.1	1.011	7.016	0.078	64.5
	60	75	217.1	1.155	7.140	0.089	53.3
SEP1-FA	0	72	129.3	1.061	7.197	0.082	32.6
	15	78	168.9	1.077	7.121	0.085	43.2
	30	65	166.2	0.946	6.933	0.074	43.5
	60	67	195.3	1.113	7.181	0.087	49.9

4.3. Buildability Test

The buildability test of 3D printable concrete stated by Zhang *et al.* [18] shows the stability of the casted specimen's post-cast height. Due to self-weight in accordance with Murata model and built-up theory, specimen slumps after removal of the mold. According to Zhang, specimen with least deformation after removal has the best buildability.

The mold's height is 13.5 cm, and its diameter is 6.75 cm. The mold was filled with mixture to its 1/3 height and compacted with a rod 20 times, then this procedure was repeated twice till the specimen is full. Then mold is removed with the apparatus vertically.

Presently there are no standard methods to measure buildability or extrudability. In various researches, the prepared mix design content and properties vary dramatically. Also, rheometers like oscillatory rheometer or rotational rheometer test results differ significantly due to different instrument suppliers. These susceptible test results may also differ due to different protocols and sample preparation. This approach is convenient due to on-site and off-site practicing. In addition to these, this field-friendly approach is very economical considering the rheometer prices.

In this study, the buildability properties were investigated on the mixtures with VMA, NM, and SEP. Twelve mixtures' height and diameter displacements were photographed and processed via ImageJ. All tests were repeated three times. As shown in the representative photos in Figure 4.9, VMA_SP has the lowest height after demolding. According to Zhang *et al.* [18], high yield stress improves the buildability and layer stability of 3D printable cementitious; however, it is not very beneficial for extrudability. As seen from the flow table results of VMA_SP, the spread, and slump were less than other mixtures, which means VMA_SP has high yield stress. The combination of these two tests also confirms the buildability test approach. Interestingly, the most printable mixtures, SEP_1_FA, VM_FA, and NM_1_FA, have the lowest horizontal displacement.

Table 4.3. Buildability test results.

Mixture name	Height in cm	Diameter in cm	Aspect ratio h/d	Mixture name	Height in cm	Diameter in cm	Aspect ratio h/d
C_SP	11.91	6.97	**1.71**	**SEP_0.5**	12.49	6.87	1.82
C_SP_FA	11.89	7.06	**1.68**	**SEP_0.5_FA**	12.75	6.87	1.86
NM_0.5	12.07	6.94	**1.68**	**SEP_1**	13	6.81	1.90
NM_0.5_FA	11.98	7.12	**1.68**	**SEP_1_FA**	12.9	6.82	1.89
NM_1	11.84	6.91	**1.71**	**VMA_SP**	12.01	7.1	1.69
NM_1_FA	12.04	7.14	**1.69**	**VMA_FA**	12.26	6.88	1.78

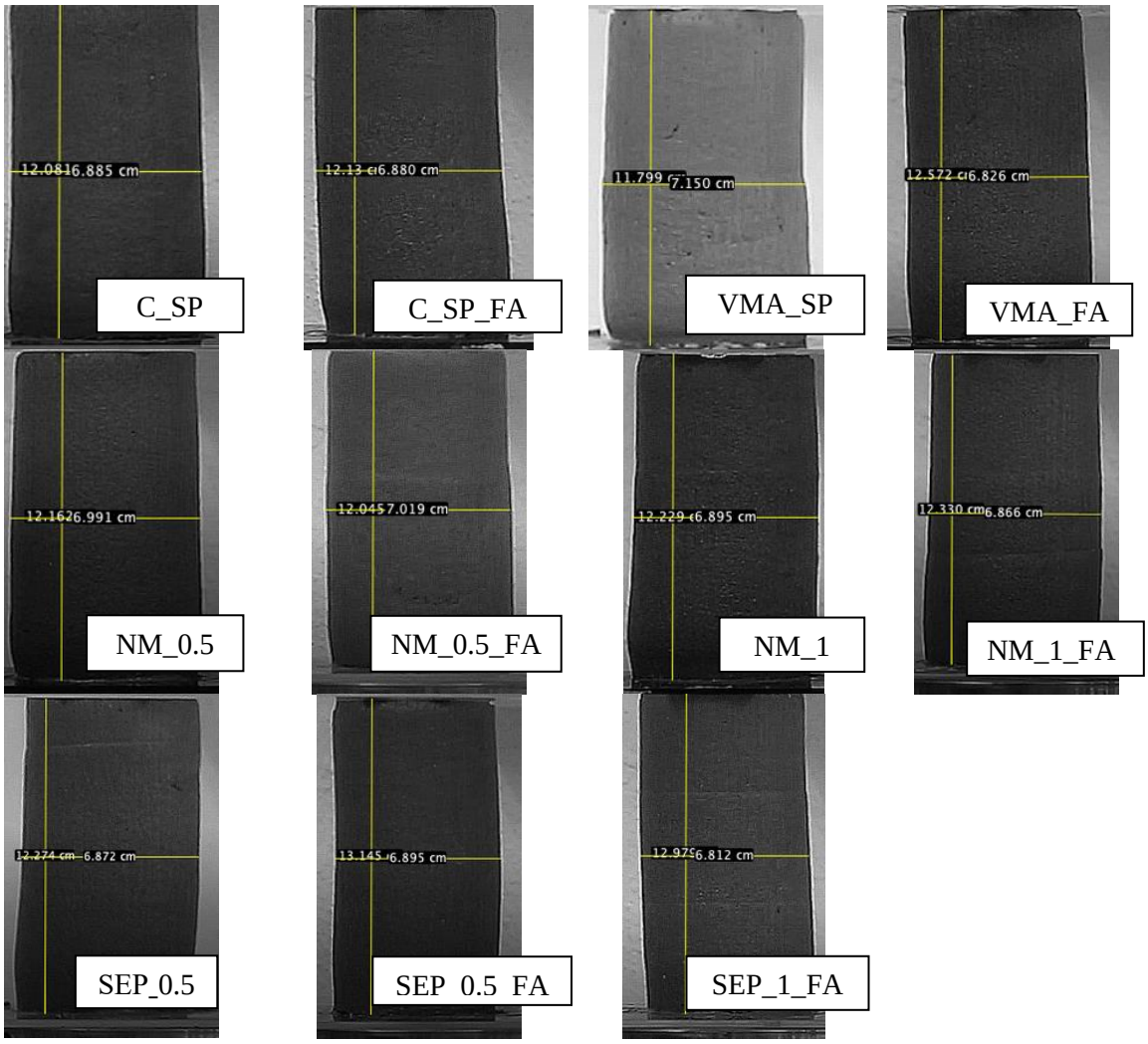

Figure 4.9. The samples and measurements for the buildability test.

In addition, the tests were repeated three times, and the average and standard deviation values were reported. The specimen measurements are represented in Figure 4.10. As represented in Table 4.3 and Figure 4.10, the maximum height belongs to SEP_1, SEP_1_FA, and SEP_0.5_FA, respectively. As seen from the results, the minimum height deformations were seen in the mixtures with sepiolite. In addition, the smallest diameter belongs to SEP_1, SEP_1_FA and SEP_0.5_FA respectively as well as the heights.

On the other hand, the shortest of height belongs to NM_1, followed by C_SP_FA, and C_SP, while the largest diameter belongs to NM_1_FA, followed by NM_0.5_FA, and VMA_SP. According to buildability test results in Figure 4.10, SEP1 has the highest yield stress σ_y, which means can carry maximum number of layers on top of bottom layer.

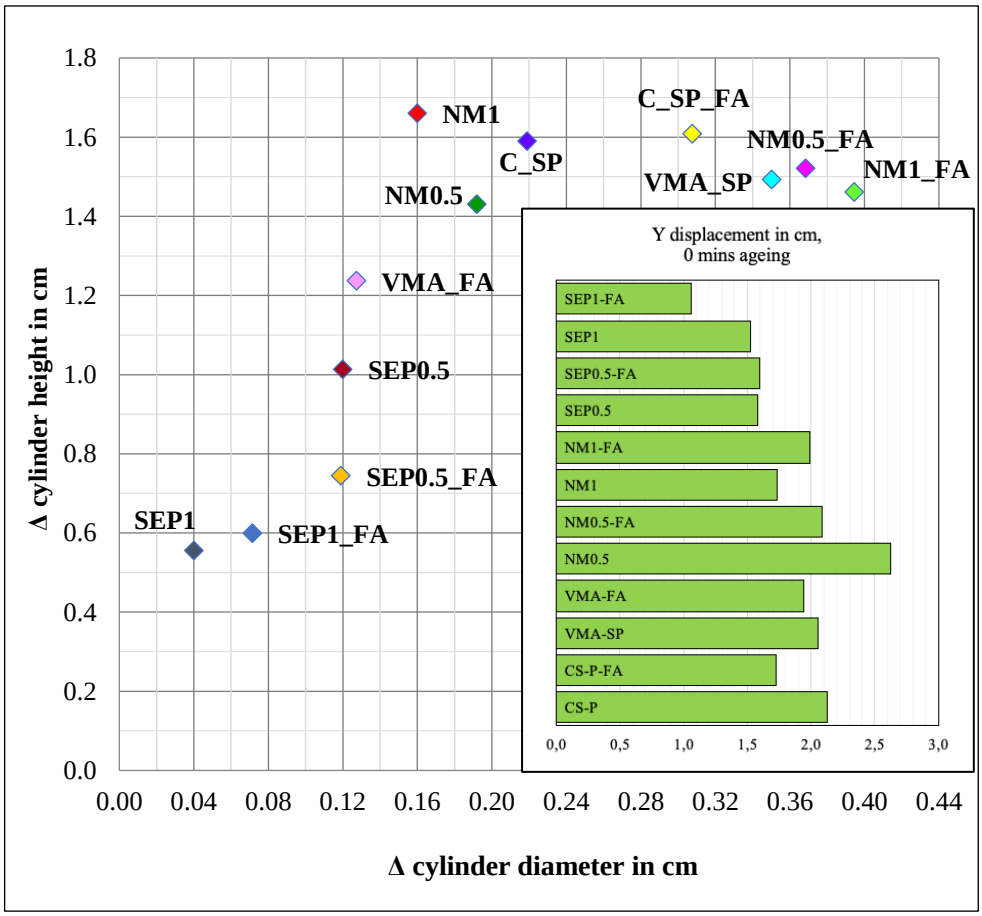

Figure 4.10. Buildability test for all samples.

In this work, the flowability of mortar was determined by flow table test instead of the cement paste due to dramatic change in shearing history when the aggregates are added. Mortar flowability was chosen as the flowability parameter to observe the change in the packing density and the water film thickness when the aggregate is added to the varying cement and nano clay contents.

As seen in Figure 4.11, mixtures with fly ash have lower compressive strength than the ones without fly ash. Naturally, as the cement content decreases by a minimum of 20%, the hydration process decelerates leading to decreased mechanical performance for the first 28 days. However, it is well established that this decrease is compensated by the 90^{th} day for the cement-based materials produced by using mineral admixtures.

On the other hand, partial substitution of the cement by fly ash results in a decrease in the water content of the mix due to round-shaped particles of fly ash. Under the same content of ingredients, the fly ash replacement of 20% reduces the water demand by 10%. The mixtures without fly ash have the same w/b ratio of 0.36 as the ones with fly ash. So, a decrease in the compressive strength can be expected, especially for the first 28 days [31,32].

The addition of sepiolite resulted in the highest compressive strength when 28-day compressive strength results were examined. The lowest compressive strength, 38.6 MPa, belongs to the mixture C_FA, which is without clay or VMA. Therefore, it can be concluded that sepiolite, NM, and VMA have a positive effect on the compressive strength of the mixtures, respectively.

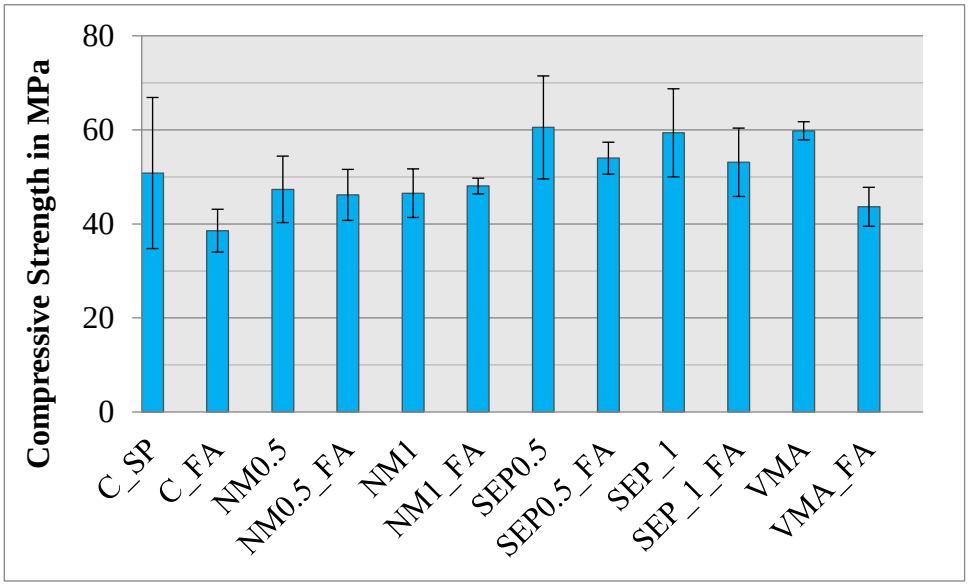

Figure 4.11. 28 days compressive strength results of the mixes.

Due to its needle-like structure, sepiolite clay holds water and contributes to the hydration process by building stronger bridges between water and the puzzolonic particles. According to Ferron *et al.* [4], sepiolite increases the chord length between the particles and forms a more flocculated network. So as the flocculation grows, structural build-up develops.

According to Boukendakdji *et al.* [33,34], VMA, as a colloidal agent, increases compressive and flexural strength along with modulus of elasticity. Also in this study, it can be seen VMA contributes to the compressive and flexural strength gain.

As shown in Figure 4.12, in each case, fly ash addition decreases the flexural strength of the mixtures. VMA mixture with 0.3 VMA inclusions has the highest flexural strength. As mentioned above VMA increases the flexural strength as a colloidal agent behavior. Among the mixtures without fly ash, SEP_1 has the lowest flexural strength with 8.4 MPa.

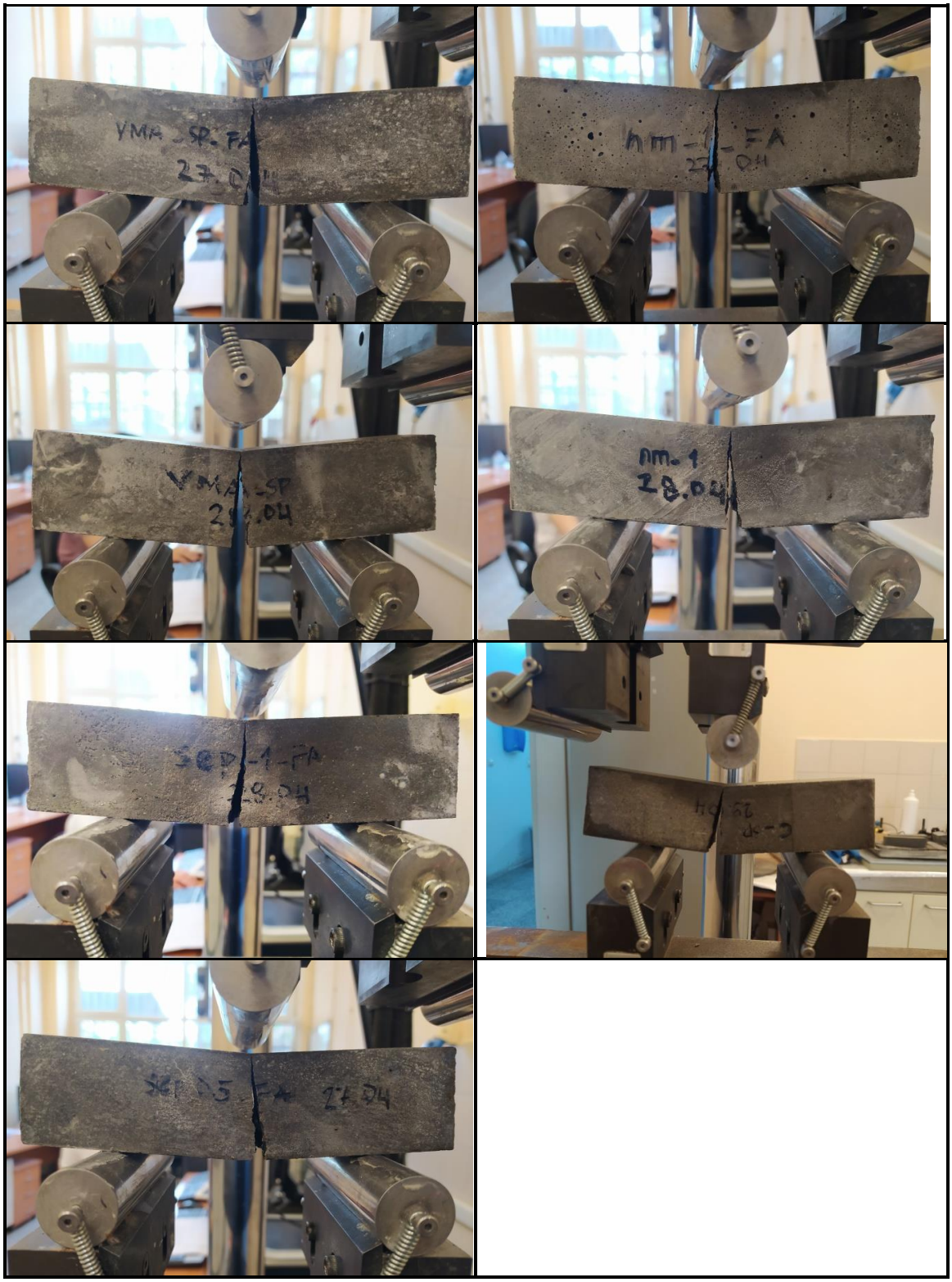

Figure 4.12. Flexural tensile test process.

As expected, both clay additions containing fly ash have the lowest flexural strength values although the removal of fly ash from these mixtures ends up with higher flexural strengths. It should be also pointed out that, the mixtures with fly ash reaches full strength at 90 days of curing. As represented in Figure 4.11, the fly ash removal affects mixtures with NM more than mixtures with sepiolite. This may be due to particle size of NM, which is approximately 20 µm, much smaller than regular fly ash and cement particles.

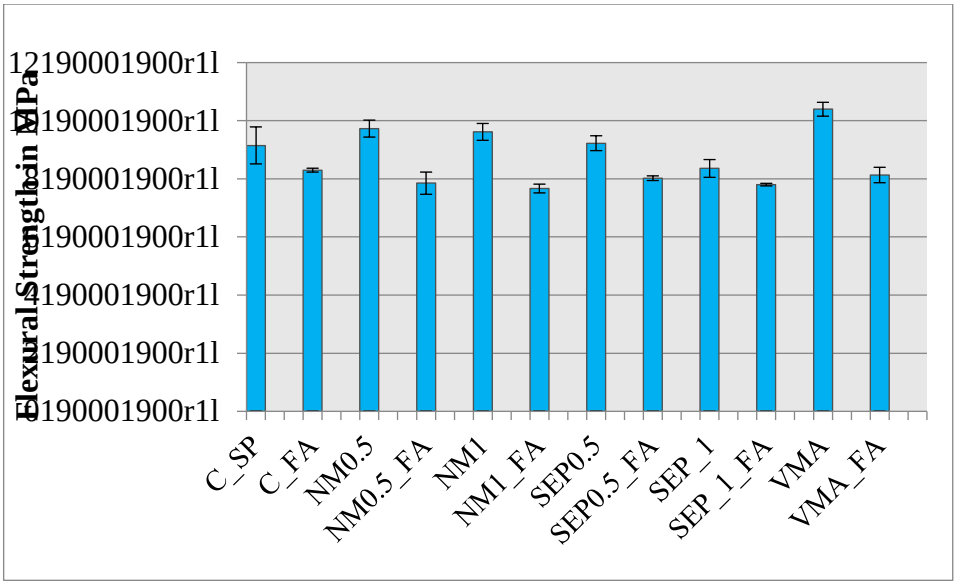

Figure 4.13. 28 days flexural strength results of the mixes.

Using material properties obtained from the green strength tests and using equations (2)-(5), the critical height and the transition height are calculated for a 3D printed concrete block of 0.5 m width and 0.8 m height, with NM and sepiolite as rheological modifiers and fly ash substrate. The determined values are tabulated in Table 4.4. Also ageing time dependent critical height and transition height values are plotted in Figure 4.14.

In Figure 4.14, it was observed that, mixture with sepiolite reaches higher height than other two mixtures. Due to sepiolite clay's needle like structure and non-swelling clay properties, it forms a gel like structure and increases the structuration rate of the mixture. As a result, the mixture gains more strength due to interaction with water. Therefore, mixtures with sepiolite reach higher printable height than other mixture. Surface modified NM, although it is swelling clay, forms Van der Waals bridges between particles. So, there

occurs an increase in strength although not as much as sepiolite inclusion. Especially, first 15 minutes printing process of mixtures without clay and NM inclusion are critical due to self-buckling. Critical heights of these mixtures are close to the printed height H of 0.8 m.

Table 4.4. E-modulus and Poisson's ratio of mixtures. C-SP-FA, NM1-FA, SEP0.5-FA.

Sample	Ageing time (in mins)	E-modulus (in kPa)	Poission's ratio (in -)	Critical height H (in m)	Shear strain (in -)	Transition height (in m)
C-SP-FA	0	88.27	0.61	1.00	0.25	1.12
C-SP-FA	15	56.77	0.78	0.86	0.43	0.90
C-SP-FA	30	131.8	0.66	1.14	0.17	1.37
C-SP-FA	60	98.9	0.62	1.04	0.22	1.18
NM1-FA	0	61.25	0.51	0.89	0.33	0.93
NM1-FA	15	83.29	0.64	0.98	0.27	1.09
NM1-FA	30	114.27	0.56	1.09	0.19	1.27
NM1-FA	60	176.58	0.46	1.26	0.11	1.58
SEP0.5-FA	0	202.61	0.65	1.32	0.11	1.69
SEP0.5-FA	15	210.96	0.61	1.34	0.10	1.73
SEP0.5-FA	30	320.31	0.70	1.54	0.07	2.13
SEP0.5-FA	60	331.51	0.54	1.55	0.06	2.17

Transition height is higher than critical height, which is to be expected. Also, all the mixture's critical height is above H =0.8 m, so strength-based failure is dominant. It should also be noted, the difference between critical and transitional height of mixture with sepiolite is far higher than other two mixtures. It can be inferred that self-buckling is not dominant failure in mixtures with sepiolite as much as the other mixtures. However, mixtures with surface modified NM and without clay's difference between critical and transitional height is far less. Therefore, transition from strength-based failure to buckling is more possible.

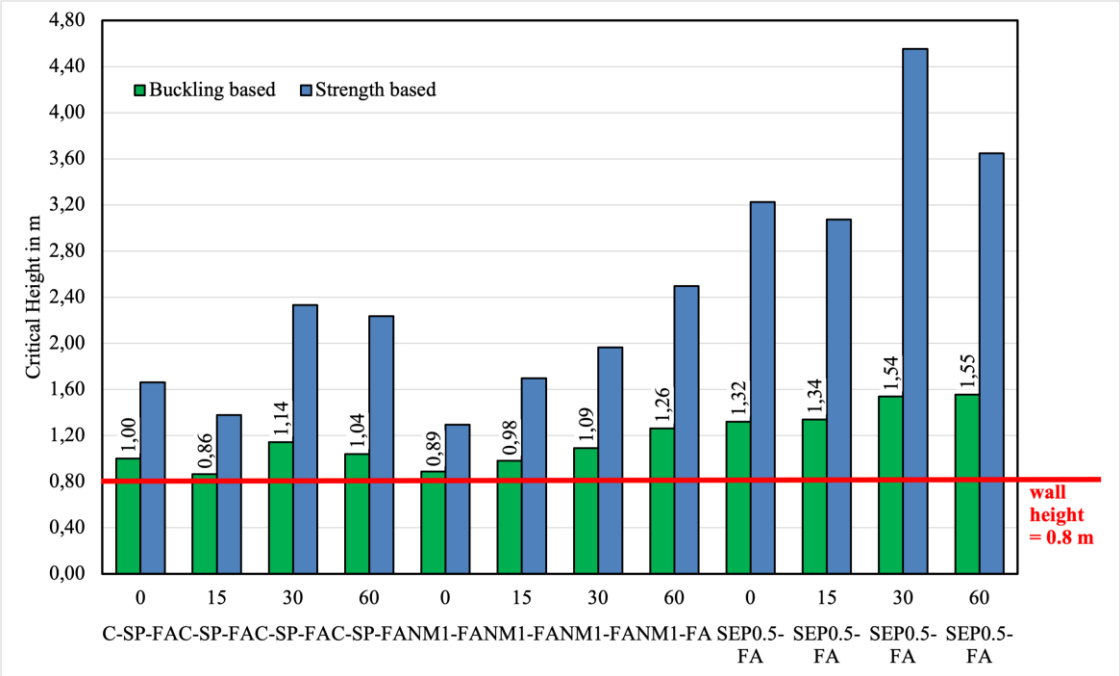

Figure 4.14. Critical and transition heights for selected mixtures w.r.t. ageing time.

4.4. Fiber Optimization

In order to improve mechanical performance of the printable mixture NM_1_FA, fibers are included to the mix design. According to Hambach *et al.* [35] carbon fibers contribute to improve mechanical performance of the mixtures and provide strain hardening after cracking. By this way toughness of the mixture can be increased. In this study carbon fibers were included at each experiment by 5‰ per volume, which equals to 9.58 gr. In Table 4.5 properties of the carbon fibers are tabulated.

Table 4.5. The mechanical properties of the carbon fiber.

Tensile Strength in MPa	E-Module in GPa	Electrical conductivity in ohm-cm	Specific Gravity in g/cc	Diameter in µm	Carbon percentage in %	Length in mm
3800	228	0.00155	1.81	7.2	95	12

In order to optimize fiber content, first, spread and slump values of the printable mixture NM_1_FA were measured. Tay *et al.* [16] stated spread- slump ratio gives a

certain buildability index. Buildability index of the printable mixtures indicates a parameter to iterate more printable mixtures with different content. By keeping the buildability index constant, carbon fibers were included to the mixture.

Figure 4.15 shows the spread- slump values of NM_1_FA mixture without fibers. These values are kept constant and taken as reference values to produce more printable mixtures. To compare NM_1_FA with C_SP_FA and NM_0.5_FA and also differentiate the effect of NM included mixtures' spread slump values with fibers were also acquired.

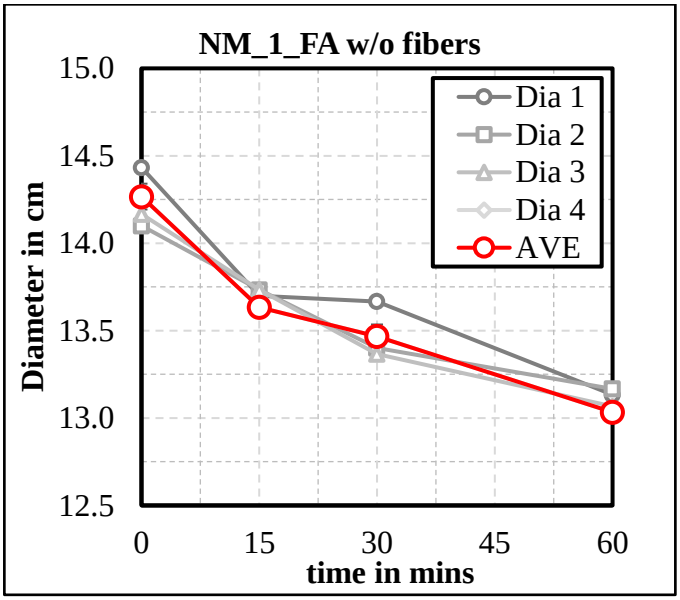

Figure 4.15. The spread values of NM_1_FA mixture without fibers.

Table 4.6. Slump values at different time intervals without fibers.

min	0	15	30	60
Slump in cm	0.25	0.25	0.2	0.1

The effect of fiber thickness on the results are investigated via testing two kinds of carbon fibers with lengths 12 mm and 6 mm. Fibers with shorter length acquire more water due to the increase of the fiber surface area when w/b and sp/b ratios are kept constant. As

seen in Figure 4.16, the mixture with NM_1_FA with 6mm carbon fibers having w/b and sp/b ratio of 0.4 results with less spread and slump values.

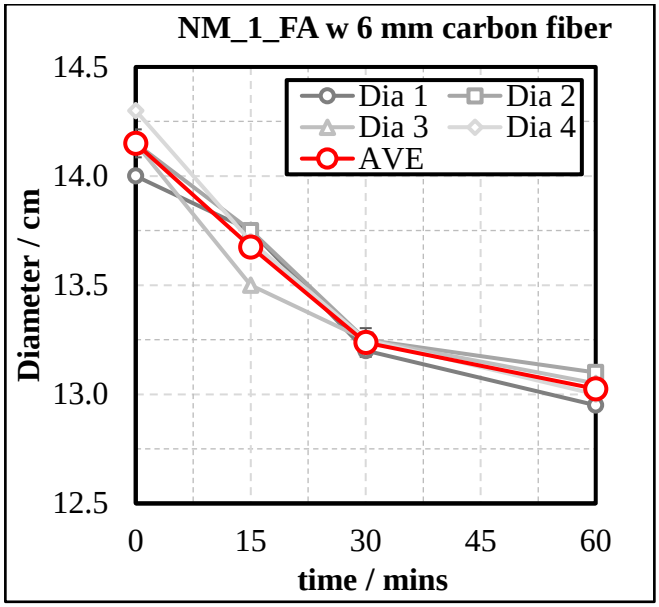

Figure 4.16. The spread values of NM_1_FA mixture with 6 mm fibers.

The evolution of slump values is tabulated in Table 4.7. The results indicate a higher yield stress than the printable NM_1_FA mixture without fiber inclusion.

Table 4.7. Slump values with 6 mm carbon fiber.

time in min	0	15	30	60
Slump in cm	0.2	0.165	0.1	0.1

In Figure 4.17 and Figure 4.18, C_SP_FA and NM_0.5_FA mixtures with 12 mm fiber diameters are represented. These mixtures were also prepared with w/b ratio of 0.4 and sp/b with 0.4. These optimal ratios are determined according to a series of test campaigns. The results of these campaigns are tabulated in Table 4.8 and Table 4.9.

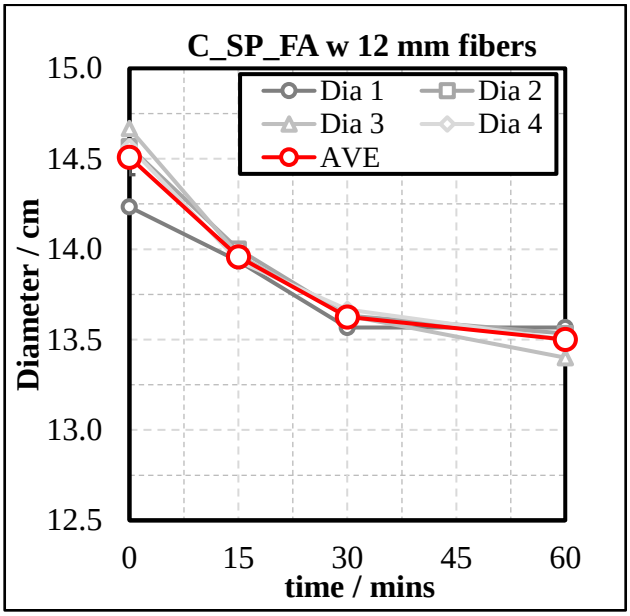

Figure 4.17. The spread values of C_SP mixture with 12 mm fibers.

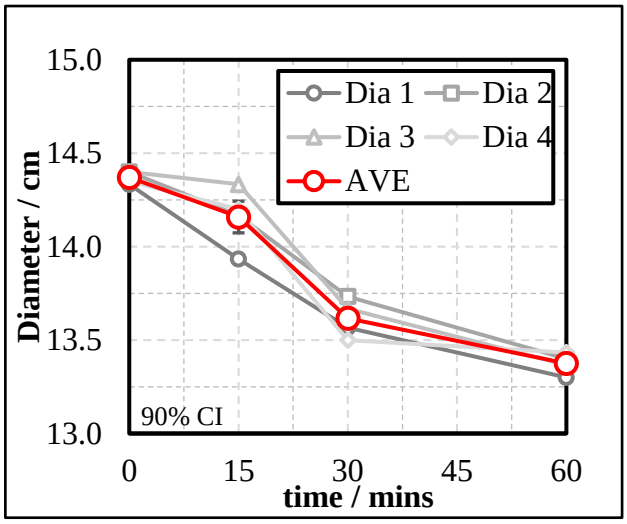

Figure 4.18. The spread values of NM0.5-FA mixture with 12 mm fibers.

As can be seen from Table 8 and Table 9, mixtures prepared by using 12 mm fibers yielded spread and slump values closer to the results obtained from non-fibrous mixtures. Therefore, fibers with 12 mm length were found more adequate for trial experiments.

Table 4.8. Slump values with 12 mm fiber for C-SP.

time in min	0	15	30	60
Slump in cm	0.2	0.2	0.2	0.1

Table 4.9. Slump values with 12 mm fiber for NM0.5-FA.

time in cm	0	15	30	60
Slump in cm	0.3	0.2	0.1	0.1

After rheological experiments on non-fibrous mixtures, yield stresses of the mixtures were acquired [16]. The yield stress obtained from rheological experiments can also be obtained roughly from flow table test. In order to obtain minimum change in the yield stress, w/b ratio was kept constant and only sp/b ratio was altered during fiber inclusion.

Figure 4.19 represents the iterative flow table experiments with varying percentages of sp/b ratio such as 2, 1.8, 1.2, 1.1 and 1‰. As seen in Figure 4.19, among the varying percentages, 1.1‰ of sp/b ratio flow table experiment results was nearest to the non-fibrous NM_1_FA. However, 1.1‰ of sp/b ratio is too high; therefore, it was assumed that mechanical properties will decrease dramatically. So, w/b and sp/b ratio of 0.4 was found more adequate for printing.

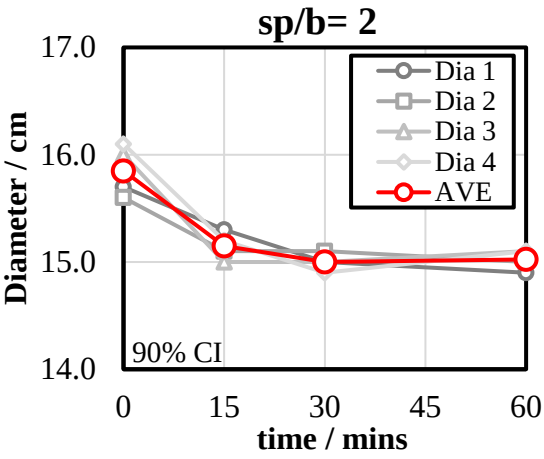

time in min	0	15	30	60
Slump in cm	0.35	0.3	0.3	0.25

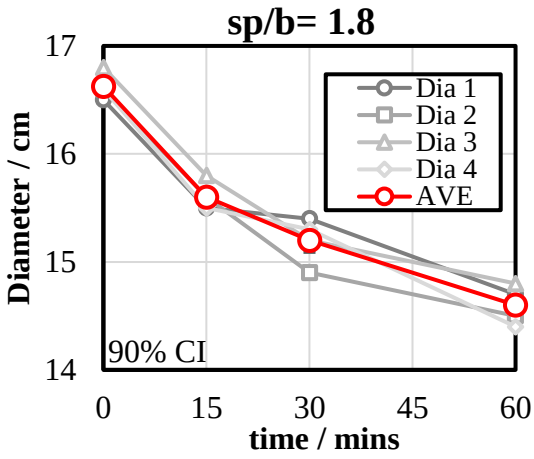

time in min	0	15	30	60
Slump in cm	0.35	0.3	0.2	0.2

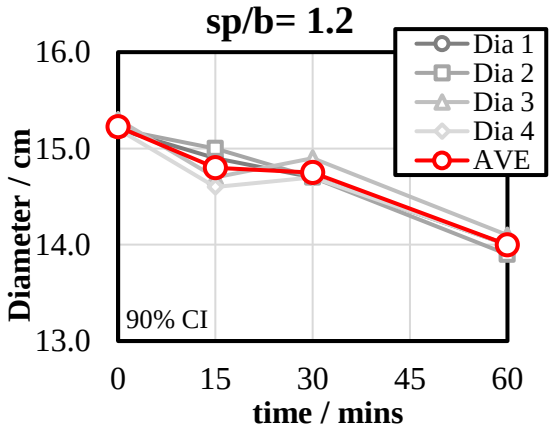

time in min	0	15	30	60
Slump in cm	0.3	0.25	0.25	0.15

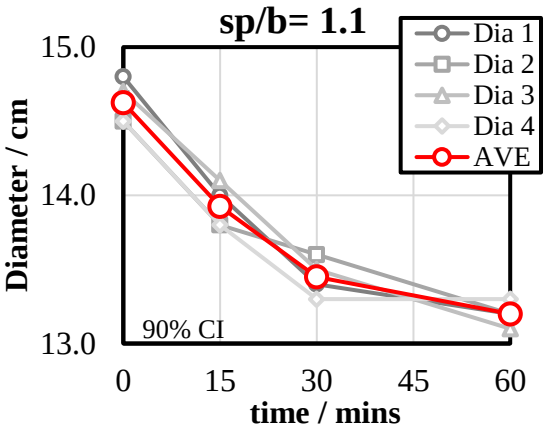

time in min	0	15	30	60
Slump in cm	0.3	0.2	0.1	0.1

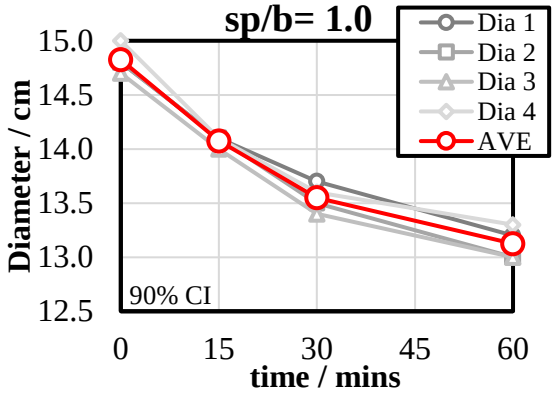

time in min	0	15	30	60
Slump in cm	0.25	0.1	0.1	0.1

Figure 4.19. sp/b ratio flow table experiment results.

Finally, 12 mm carbon fiber included mixtures with w/b and sp/b ratio of 0.4 were printed at Özyeğin University. Unfortunately, problems occurred during printing process. It was found that mixture should be improved for increasing its compatibility with the printer. Although the spread –slump values of fiber reinforced mixture were similar to non-fibrous mixture of NM_1_FA, **the fiber reinforced mixture was not printable**. This shows similar static and dynamic yield stress values do not make the mixture as printable as the non-fibrous mixture. Although the yield stress values were similar, fiber dispersion was observed to be not homogenous during mixing. As shown in the Figure 4.20, carbon fibers were not dispersed properly and were stuck at the nozzle of the printer. Also, the mixture was segregated during printing process since applied force was excessive due to carbon fibers.

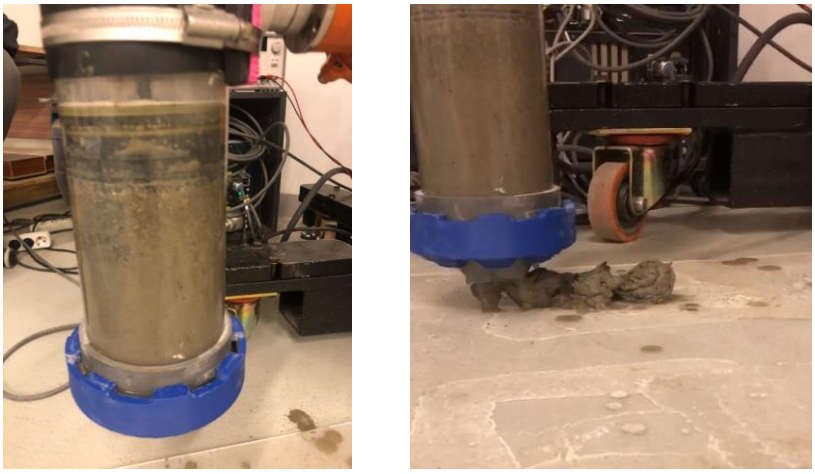

Figure 4.20. Printing trials at Özyegin University.

In order to eliminate the problems occurred during printing following precaution and improvements can be made. First, according to Hambach *et al*. [35] carbon fibers need pre-process to improve the mechanical performance, such as heating up to 400 C^{o}. Other than that, fiber inclusion can be reduced up to 1‰ per volume and mixed with higher rpm and longer in time. However, this increases the energy spend during the production. On the other hand, PP fibers can also be used in order to control cracks. As stated by Tay *et al.* [16] and Zhang *et al.* [18], packing density is crucial by including fibers. Packing density experiments will be most useful in the process of including fibers. A numeric model can be built up by flowability of the cement paste and aggregate and fiber inclusion.

5. CONCLUSIONS

3D printing of cement-based materials has been an emerging alternative to conventional concrete construction techniques. In this study, it was targeted to predict fresh state and hardened state characteristic properties of 12 mixtures with 2 different clay types and VMA as rheological modifiers after deposition. The aim of these tests was to simulate after printing process and predict stability of the printed object.

5.1. Green strength of mixtures:

Compared to control mix design without fly ash, substitution of binder with fly ash by 20% decreased the load bearing capacity by 13%. Also fly ash addition decreased the time that the material reaches before failure, meaning mixtures with fly ash will fail quicker than the mixtures without any fly ash.

As it can be seen from Table 4, NM and SEP increased the average stress the specimen can carry. While 0.5% sepiolite substitution of binder content doubled the load carrying capacity, 1% sepiolite substitution of the binder almost tripled compared to control mixture. In addition to sepiolite, substitution of fly ash by 20% doubled the load bearing capacity with 0.5% sepiolite substitution and tripled the compressive strength by 1% sepiolite substitution compared to the control mixture with fly ash.

0.5% substitution of binder by Nano-montmorillonite increased the green strength of the cement-based material by 15%. 1% substitution of control mixture with NM increased the load bearing capacity by 43%. Adding fly ash to the mix design with NM did not change the load bearing capacity at all.

VMA substituting the binder by 0.3% ended up with decreasing the load bearing capacity of cement-based material at fresh state by 19%. Adding 20% substitution of fly ash to VMA inclusion ended up with 10% decrease of green strength compared to the

control mixture with fly ash. Overall, mixtures with VMA decrease the load bearing capacity of the mixture and have low buildability.

Also, sepiolite decreases the lateral displacement at half height significantly, while NM and VMA do not change the lateral displacement at all. In addition to that sepiolite enables the material to reach maximum stress much earlier in time than NM or VMA, meaning after deposition of the material with sepiolite, it will fail much earlier than mixtures with NM or VMA.

Mixtures with NM and VMA slightly increase the vertical displacement under force, while mixtures with sepiolite decreases it to almost half value compared to control mixture. This means mixture with sepiolite will be built with more layers than mixtures with NM or VMA and also object printed by sepiolite mixture will have a great height than with other mixtures. On the other hand, it will deform much earlier than the objects printed with other mixtures.

Combined with flow table test results, buildability test results give similar results with green strength results. Mixtures with sepiolite have lower spread and slump results, meaning higher yield stress, and also higher buildability according to buildability test. Although these clay inclusions increase fresh state strength performance of the printed object, inclusion amount should be balanced. Low stiffness can cause elastic deformation, whereas lack of adequate green strength may result in plastic failure, which will gradually become a more brittle failure for older age specimens [6]. Mixture with 1% sepiolite was observed to be too stiff from the findings. A mix design update, with increasing superplasticizer of the mixture with 1% sepiolite, may increase the flowability of the material while decreasing the failure time due to strength.

It should be noted that these tests give a robust and not so accurate results; however, they are an easy alternative compared to green strength test.

5.2. Green strength and buildability

When the average peak stress of mixtures and the flow table test results are analyzed together as represented in Figure 5.1, the following conclusions can be stated:

Despite the higher load bearing capacity of sepiolite at fresh state, the flow diameter of mixtures with sepiolite is rather low. This means dynamic yield stress of the mixtures with sepiolite is rather low while static yield stress is high. This makes the mixtures with sepiolite harder to print.

On the other hand, the mixtures with NM have maximum dynamic yield stress compared to other mixtures. Mixtures with NM are more flowable, which makes them easier to print.

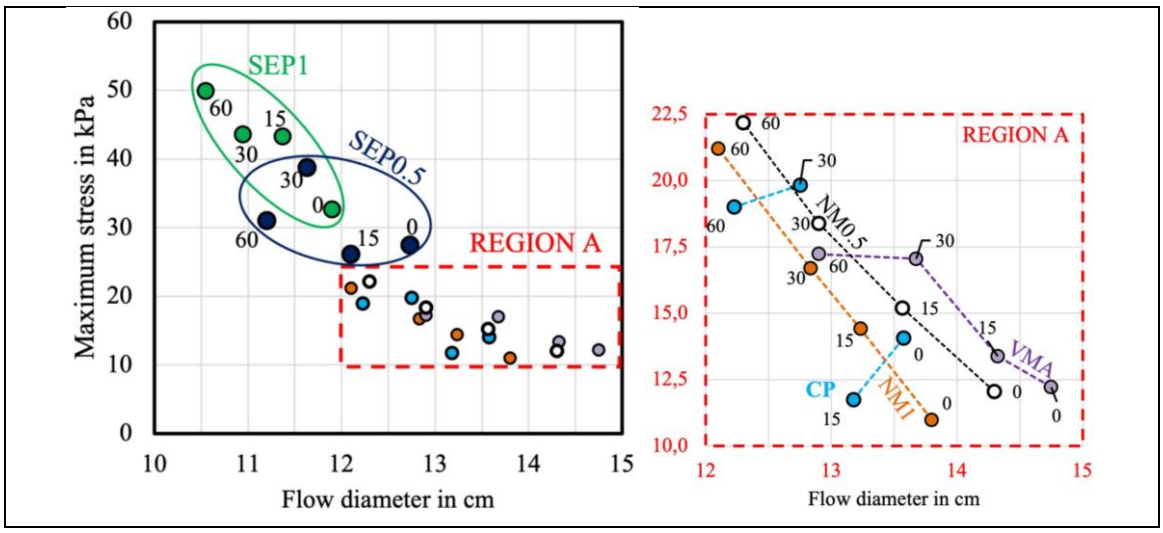

Figure 5.1. Correlation of unconfined uniaxial compressive true stress vs. flow diameter. The measurements are conducted at fresh state.

5.3. Green strength and compressive & flexural strengths

Figure 5.2 and Figure 5.3 display the maximum load carried by mixtures at fresh state (on the vertical axis), and the maximum average load carried by mixtures at hardened state (on the horizontal axis). As seen in Figure 5.2, the mixtures with sepiolite have high

compressive strength both at fresh and hardened state. NM_1_FA and SEP_0.5_FA mixtures have the closest fresh and hardened compressive strength values to C_SP.

Figure 5.4 and Figure 5.5 display the maximum load carried by mixtures at fresh state (on the vertical axis), and the flexural strength of mixtures at hardened state (on the horizontal axis). It can be concluded from the results that the binder content substitution with fly ash by 20% had a negative effect on the flexural strength. When the flexural strength is correlated with fresh state compressive stress, it can be seen mixtures with sepiolite have optimal values. The mixtures with NM combined with fly ash have lowest values according to flexural and green strength tests.

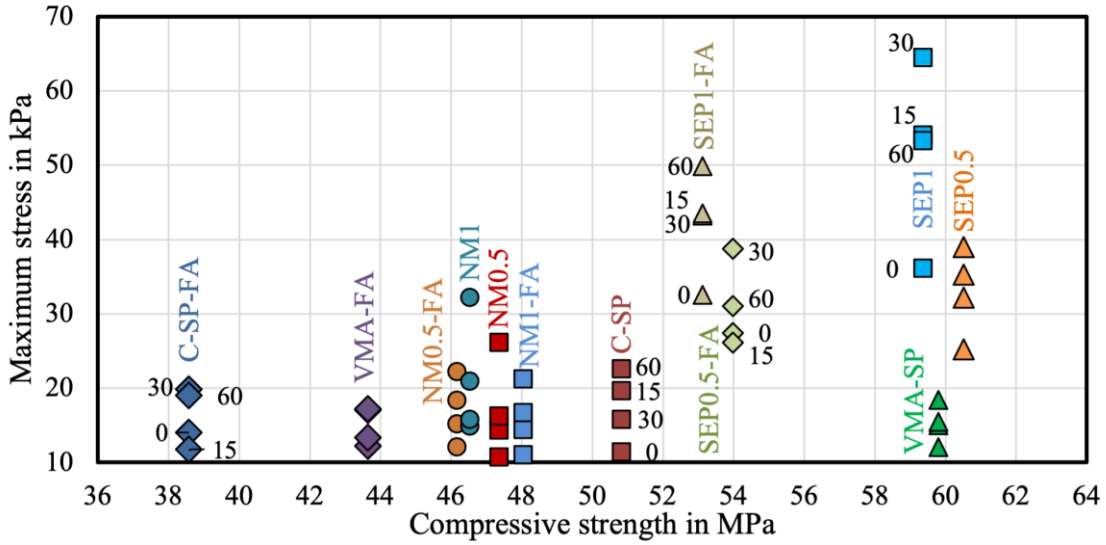

Figure 5.2. Maximum stress in comparison to compressive strength. The results are obtained from green strength tests. For each mixture, maximum stress increases with ageing, unless otherwise specified.

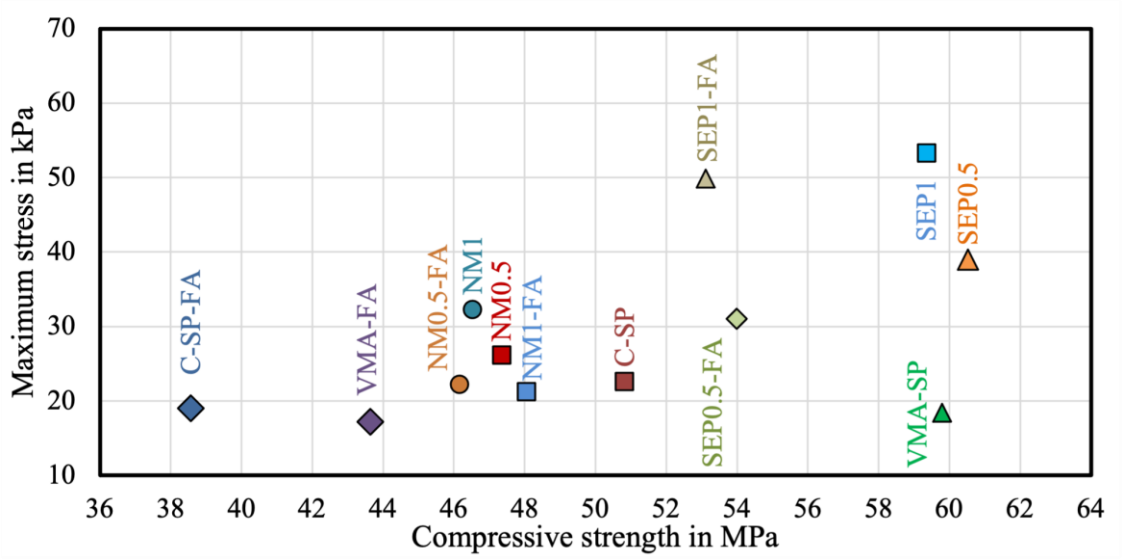

Figure 5.3. Max. stress in comparison to compressive strength of 60 mins aged samples. The results are obtained from green strength test.

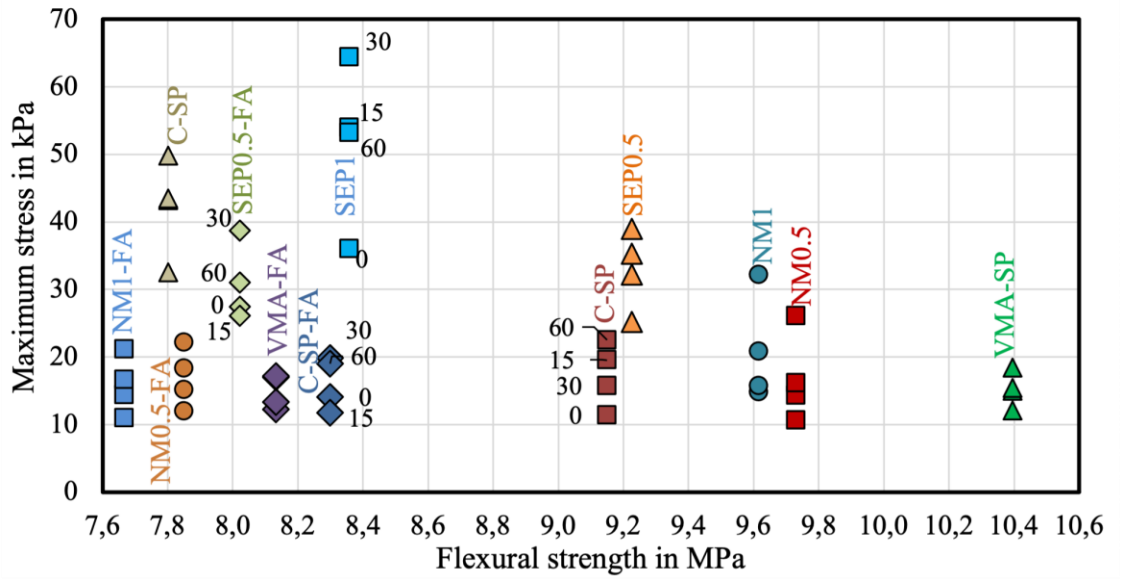

Figure 5.4. Maximum stress in comparison to flexural strength. The data is obtained from green strength tests. For each mixture, maximum stress increases with ageing unless otherwise specified.

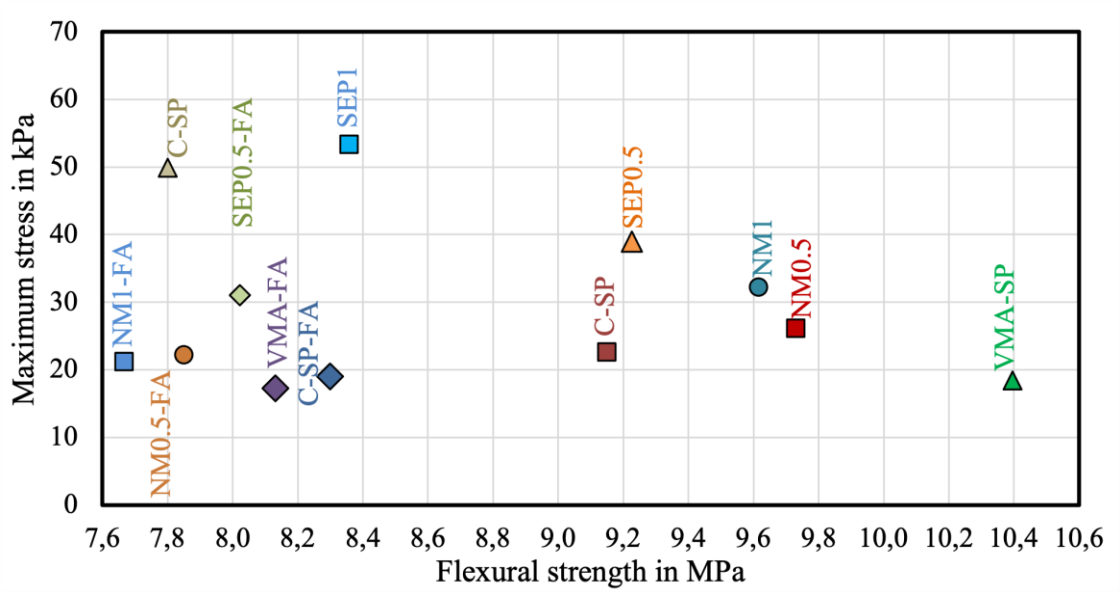

Figure 5.5. Max. stress in comparison to flexural strength for 60 minutes aged samples.

5.4. Green strength and ageing time

From Figure 5.6 to Figure 5.8 represent the average increase of peak stress for each mixture with and without FA substitution with respect to ageing time as seen from the figures, the yield stress increases with time, if the average of peak stress at a given ageing time is fit against concrete age. Also, for each mixture, it should be noted that FA substitution slightly decreases this trend (i.e., slope).

The trend analysis on the effect of ageing on the yield stress assumes that a linear relationship in fact exists. Although this assumption was applicable to most mixtures, the R^2 values of some mixtures (i.e., NM1-FA, SEP0.5-FA) were found contradictory.

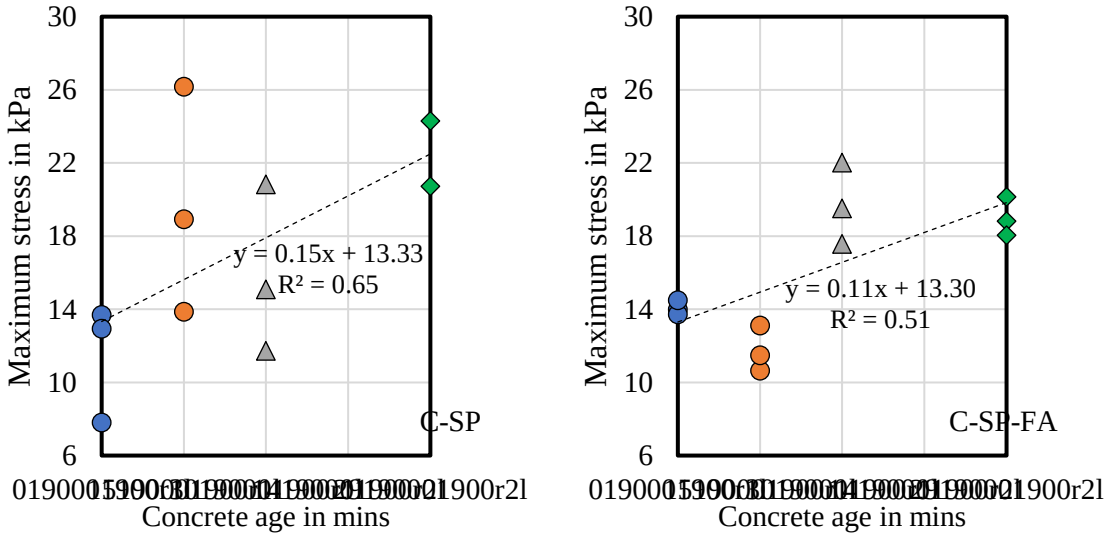

Figure 5.6. The effect of concrete aging on max. strength of C-SP and C-SP-FA. C-SP (left) and C-SP-FA (right).

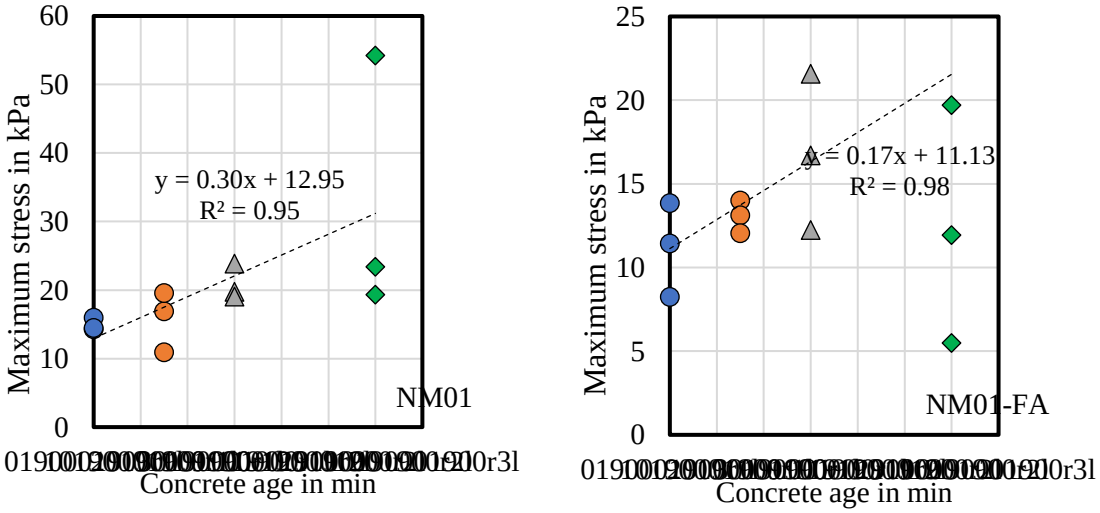

Figure 5.7. The effect of concrete aging on max. strength of NM1 and NM1-FA. NM1 (left) and NM1-FA (right).

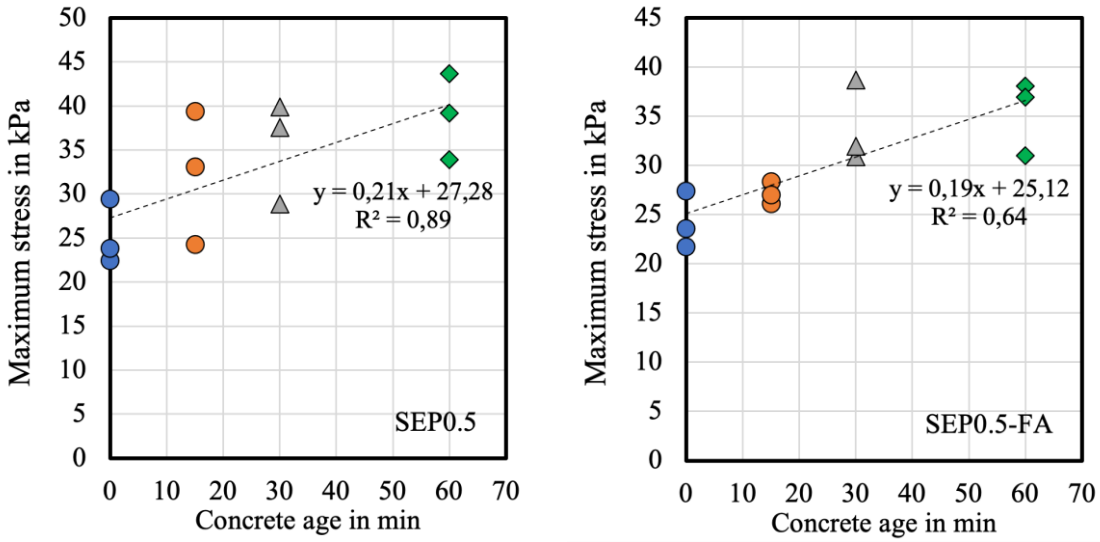

Figure 5.8. The effect of concrete aging on max. strength of SEP0.5 and SEP0.5-FA. SEP0.5 (left) and SEP0.5-FA (right).

5.5. Overall stability of the printed object

Elasticity modulus *E*, Poisson's ratio *v* and maximum stress obtained from green strength test can be used to calculate strength based failure and buckling failure. With a given width of 0.5 m and height of 0.8 m of print object, critical height for strength based failure and critical height for self-buckling were obtained from equations mentioned by Roussel [26].

As a conclusion, mixtures with sepiolite reach higher heights when printed without strength based or self-buckling failures. However, mixtures without clay inclusion or surface modified NM may have difficulties with first 15 minutes of the printing process due to closeness of their critical height H_c to targeted print object height 0.8 m.

5.6. Future Work

The compressive and flexural tests can be done for the 1st and the 7th day, in order to obtain mechanical properties at earlier ages. These tests can also be done for printed specimens and obtain more realistic mechanical test results.

In addition, static yield stress results can be compared with rheological parameters obtained from rheometer tests.

Green strength tests can be further done up to average setting time of the mixtures and not only first hour. Also, ultrasound pulse velocity tests can be run to correlate with compressive test results at fresh and hardened state.

Carbon fibers can be heat treated and fiber content can be reduced. On the other hand, PVA or PP fibers can be added to optimize mixtures for reinforcement. It is necessary to lead a study with packing density with alternative fibers.

6. REFERENCES

1. Andrew, R. M., “Global CO2 Emissions from Cement Production, 1928-2018”, *Earth System Science Data*, vol. 11, no. 4, pp. 1675–1710, 2019.

2. Buswell, R. A., W. R. Leal da Silva, F. P. Bos, H. R. Schipper, D. Lowkee, N. Hack, H. Kloft, V. Mechtcherine, T. Wangler, and N. Roussel, “A Process Classification Framework for Defining and Describing Digital Fabrication With Concrete”, *Cement and Concrete Research*, vol. 134, p. 106068, 2020.

3. Wangler, T., N. Roussel, F. P. Bos, T. A. M. Salet, and R. J. Flatt, “Digital Concrete: A Review”, *Cement and Concrete Research*, vol. 123, p. 105780, 2019.

4. Ferron, R. D., S. Shah, E. Fuente, and C. Negro, “Aggregation and Breakage Kinetics of Fresh Cement Paste”, *Cement and Concrete Research*, vol. 50, pp. 1–10, 2013.

5. Li, V. C., F. P. Bos, K. Yu, W. McGee, T. Y. Ng, S. C. Figueiredo, K. Nefs, V. Mechtcherine, V. N. Nerella, J. Pan, G. P. A. G. van Zijl, P. J. Kruger, “On the Emergence of 3D Printable Engineered, Strain Hardening Cementitious Composites (ECC/SHCC)”, *Cement and Concrete Research*, vol. 132, p. 106038, 2020.

6. Panda, B., J. H. Lim, and M. J. Tan, “Mechanical Properties and Deformation Behaviour of Early Age Concrete in the Context of Digital Construction”, *Composites Part B: Engineering*, vol. 165, pp. 563–571, 2019.

7. Li, Z., M. Hojati, Z-. Wu, J. Piasente, N. Ashrafi, J. P. Duarte, S. Nazarian, S. G. Bilén, A. M. Memari, and A. Radlinska, “Fresh and Hardened Properties of Extrusion-Based 3D-Printed Cementitious Materials: A Review”, *Sustainability*, vol. 12, no. 14, pp. 1–33, 2020.

8. Reiter, L., T. Wangler, A. Anton, and R. J. Flatt, “Setting on Demand for Digital Concrete – Principles, Measurements, Chemistry, Validation”, *Cement and Concrete Research*, vol. 132, p. 106047, 2020.

9. Van Damme, H., “Concrete Material Science: Past, Present, and Future Innovations”, *Cement and Concrete Research*, vol. 112, pp. 5–24, 2018.

10. Voigt, T., T. Malonn, and S. P. Shah, “Green and Early Age Compressive Strength of Extruded Cement Mortar Monitored With Compression Tests and Ultrasonic Techniques”, *Cement and Concrete Research*, vol. 36, pp. 858–867, 2006.

11. De Schutter, G., K. Lesage, V. Mechtcherine, V. N. Nerella, G. Habert, and I. Agusti-Juan, “Vision of 3D Printing with Concrete — Technical, Economic and Environmental Potentials”, *Cement and Concrete Research*, vol. 112, pp. 25-36, 2018.

12. Tregger, N., M. E. Pakula, and S. P. Shah, “Influence of Clays on the Rheology of Cement Pastes”, *Cement and Concrete Research*, vol. 40, no. 3, pp. 384–91, 2010.

13. Marchon, D., S. Kawashima, H. Bessaiesney, S. Mantellato, S. Ng, “Hydration and Rheology Control of Concrete for Digital Fabrication: Potential Admixtures and Cement Chemistry”, *Cement and Concrete Research*, vol. 112, pp. 96-110, 2018.

14. Wolfs, R. J. M., F. P. Bos, and T. A. M. Salet, “Early Age Mechanical Behaviour of 3D Printed Concrete: Numerical Modelling and Experimental Testing”, *Cement and Concrete Research*, vol. 106, no. May 2017, pp. 103–116, 2018.

15. Kruger, J., S. Zeranka, and G. van Zijl, “3D Concrete Printing: A Lower Bound Analytical Model for Buildability Performance Quantification”, *Automation in Construction*, vol. 106, p. 102904, 2019.

16. Tay, Y. W. D., Y. Qian, and M. J. Tan, “Printability Region for 3D Concrete Printing Using Slump and Slump Flow Test”, *Composites Part B: Engineering*, vol. 174, p. 106968, 2019.

17. Jayathilakage, R., P. Rajeev, and J. Sanjayan, “Yield Stress Criteria to Assess the Buildability of 3D Concrete Printing”, *Construction and Building Materials*, vol. 240, p. 117989, 2020.

18. Zhang, C., Z. Hou, C. Chen, Y. Zhang, V. Mechtcherine, and Z. Sun, “Design of 3D Printable Concrete Based on the Relationship Between Flowability of Cement Paste and Optimum Aggregate Content”, *Cement and Concrete Research*, vol. 104, p. 103406, 2019.

19. Chamberlain, J. A., S. Clayton, K. A. Landman, and J. E. Sader, “Experimental Validation of Incipient Failure of Yield Stress Materials Under Gravitational Loading”, *Journal of Rheology*, vol. 47, no. 6, pp. 1317–1329, 2003.

20. Chamberlain, J. A., J. E. Sader, K. A. Landman, and L. R. White, “Incipient Plane-Strain Failure of a Rectangular Block Under Gravity”, *International Journal of Mechanical Sciences*, 43, pp. 793-815, 2001.

21. Chamberlain, J. A., J. E. Sader, K. A. Landman, D. J. Horrobin, and L. R. White, “Incipient Failure of a Circular Cylinder Under Gravity”, *International Journal of Mechanical Sciences*, 44, pp. 1779–1800, 2002.

22. Pashias, N., D. V. Boger, J. Summers, and D. J. Glenister, “A Fifty Cent Rheometer for Yield Stress Measurement”, *Journal of Rheology*, 40, pp. 1179–1189, 1996.

23. Schowalter, W. R., and G. Christensen, “Toward a Rationalization of the Slump Test for Fresh Concrete: Comparisons of Calculations and Experiments”, *Journal of Rheology*, 42, pp. 865-870, 1998.

24. Murata, J., “Flow and Deformation of Fresh Concrete”, *Materiaux et Construction*, vol. 17, pp. 117–129, 1984.

25. Perrot, A., D. Rangeard, and E. Courteille, “3D Printing of Earth-Based Materials: Processing Aspects”, *Construction and Building Materials*, vol. 172, pp. 670–676, 2018.

26. Roussel, N., “Rheological Requirements for Printable Concretes”, *Cement and Concrete Research*, vol. 112, pp. 76-85, 2018.

27. Wolfs, R. J. M., F. P. Bos, and T. A. M. Salet, “Hardened Properties of 3D Printed Concrete: The Influence of Process Parameters on Interlayer Adhesion”, *Cement and Concrete Research*, vol. 119, pp. 132-140, 2019.

28. Aydin, E. M., “*Extrusion and Rheology Characterization of Cement-Based Materials Containing Different Types of Clays*”, Master Thesis, Ozyegin University, 2021.

29. Sigma Aldrich, *Nanoclay, Surface Modified*, 2020.

30. Marchon, D., S. Kawashima, H. Bessaies-Bey, S. Mantellato, and S. Ng, “Hydration and Rheology Control of Concrete for Digital Fabrication: Potential Admixtures and Cement Chemistry”, *Cement and Concrete Research*, vol. 112, pp. 96–110, 2018.

31. Kwan, A. K. H., and Li Y., “Effects of Fly Ash Microsphere on Rheology, Adhesiveness and Strength of Mortar”, *Construction and Building Materials*, vol. 42, pp. 137–145, 2013.

32. Federal Highway Administration, *Fly Ash Facts for Highway Engineers*, 2007, https://www.fhwa.dot.gov/pavement/recycling/fach03.cfm, accessed on 01 June 2021.

33. Boukendakdji, O., F. Debieb, E. H. Kadri, and N. Benramoul, “Effect of Viscosity Modifying Admixtures on the Workability and Mechanical Resistances of Self-

Compacting Mortars", *Journal of Materials and Environmental Science, vol.* 7, no. 2, pp. 558–565, 2016.

34. Chen, Y., S. C. Figueiredo, Z. Lia, Z. Changa, K. J., O. Çopuroğlu, and E. Schlangen, "Improving Printability of Limestone-Calcined Clay-Based Cementitious Materials by Using Viscosity-Modifying Admixture", *Cement and Concrete Research*, vol.132, p.106040, 2020.

35. Hambach, M., M. Rutzen, and D. Volkmer, "Properties of 3D-Printed Fiber-Reinforced Portland Cement Paste", In: Sanjayan J. G., A. Nazari, and B. Nematollahi, *3D Concrete Printing Technology*, Butterworth-Heinemann, Oxford, 2019.

APPENDIX A: GREEN STRENGTH TEST RESULTS

Green strength at t = 0 seconds

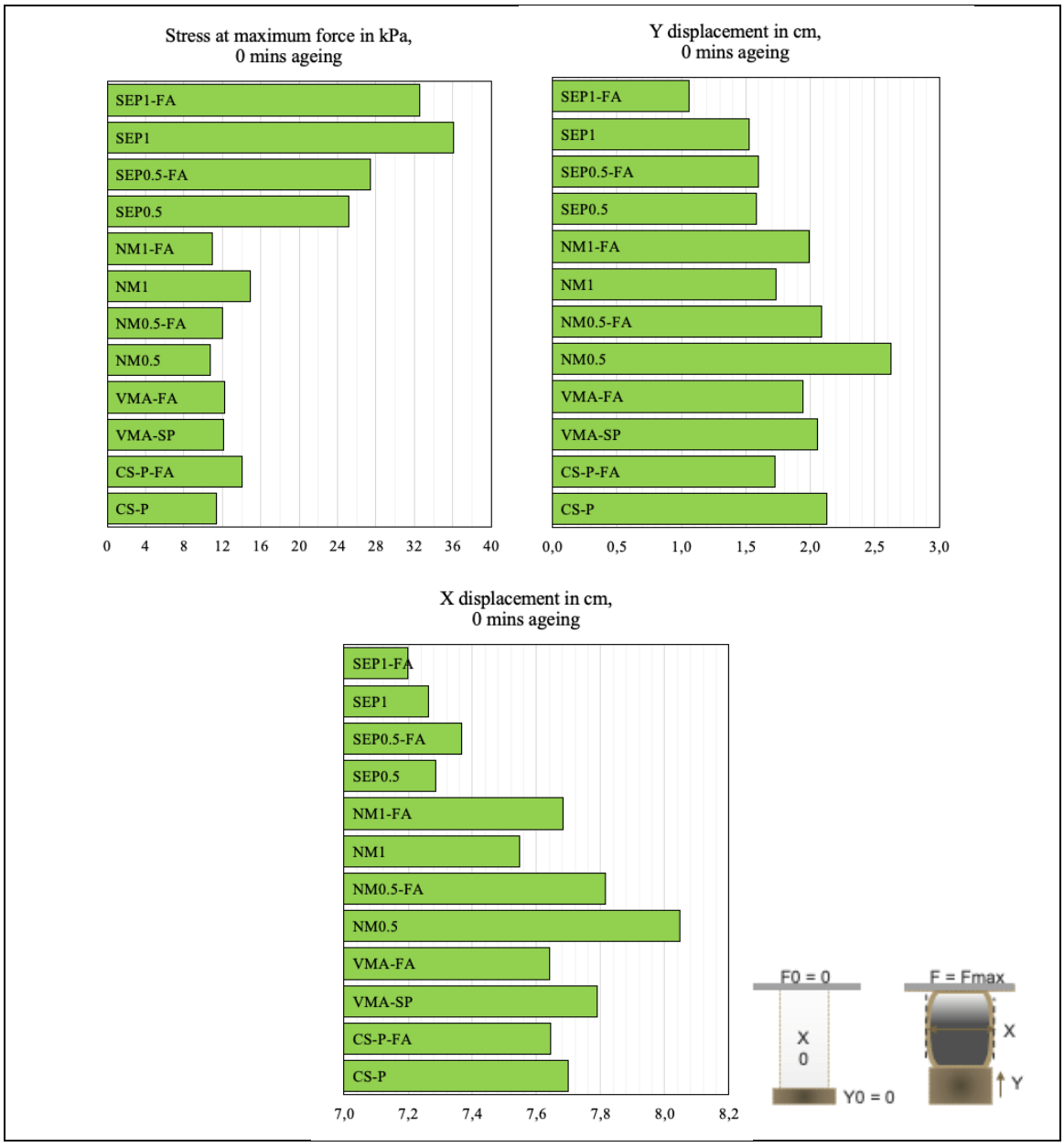

Figure A.1. Results summary, 0 minutes of ageing.

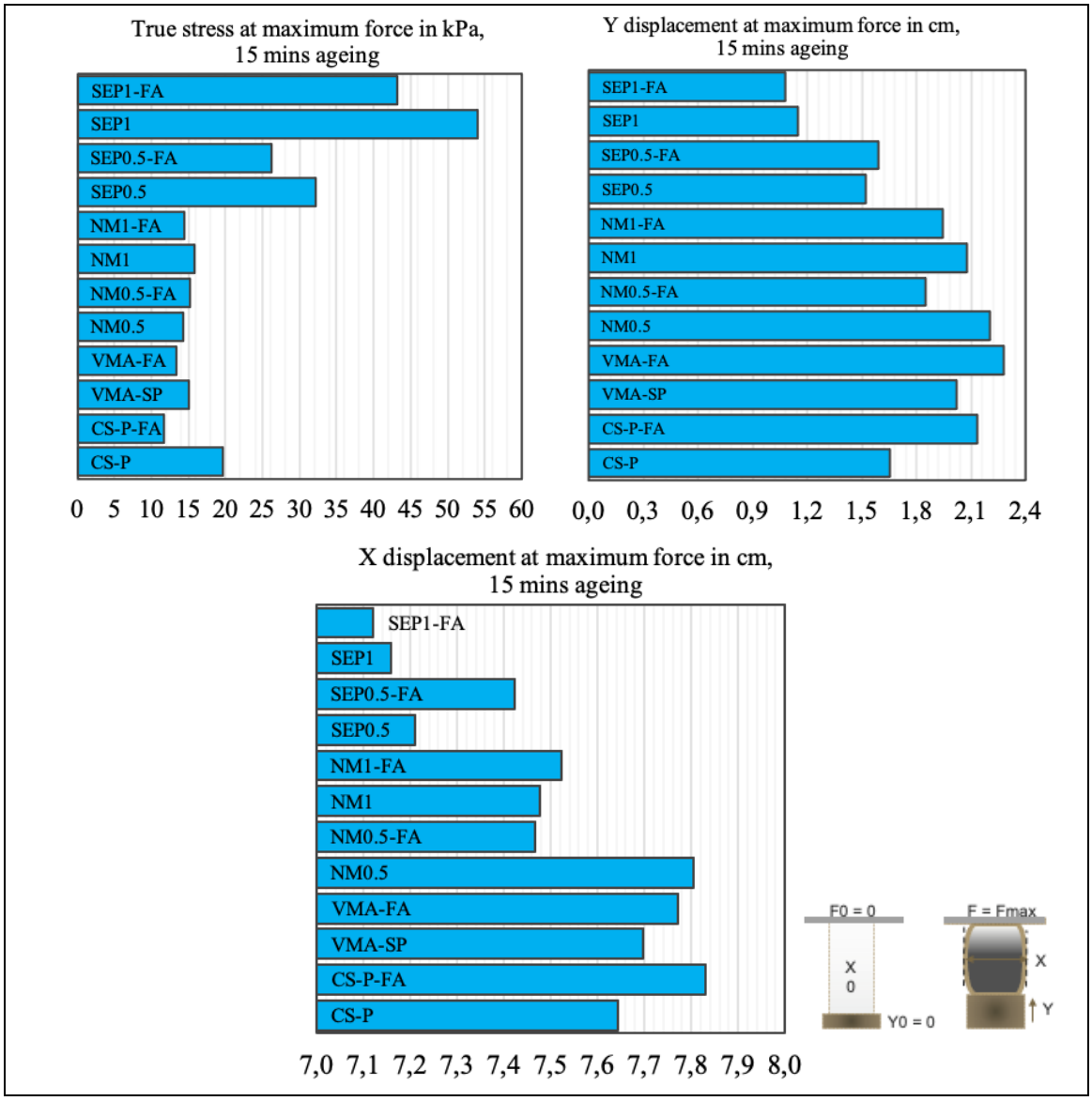

Figure A.2. Results summary, 15 minutes of ageing.

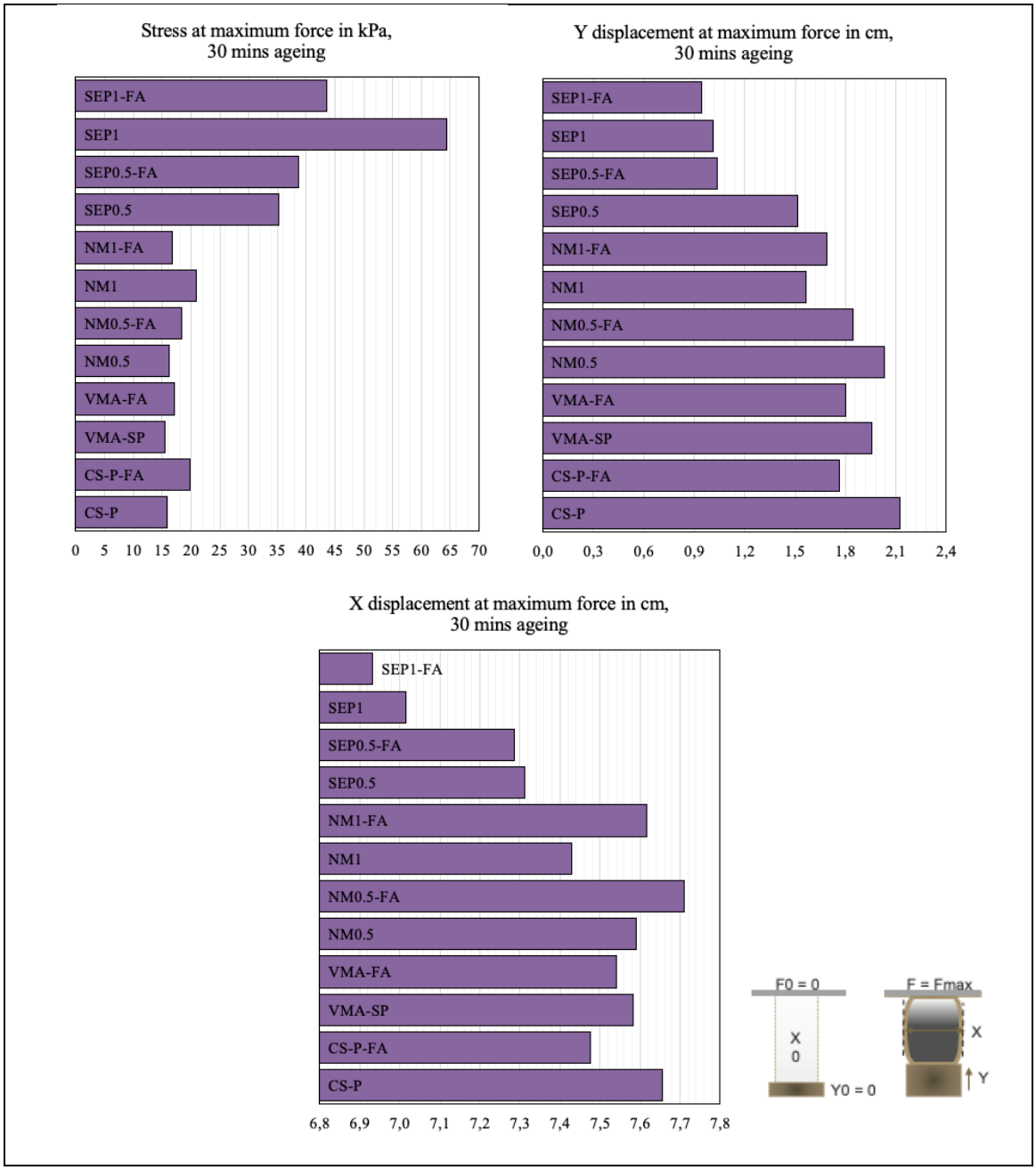

Figure A.3. Results summary, 30 minutes of ageing.

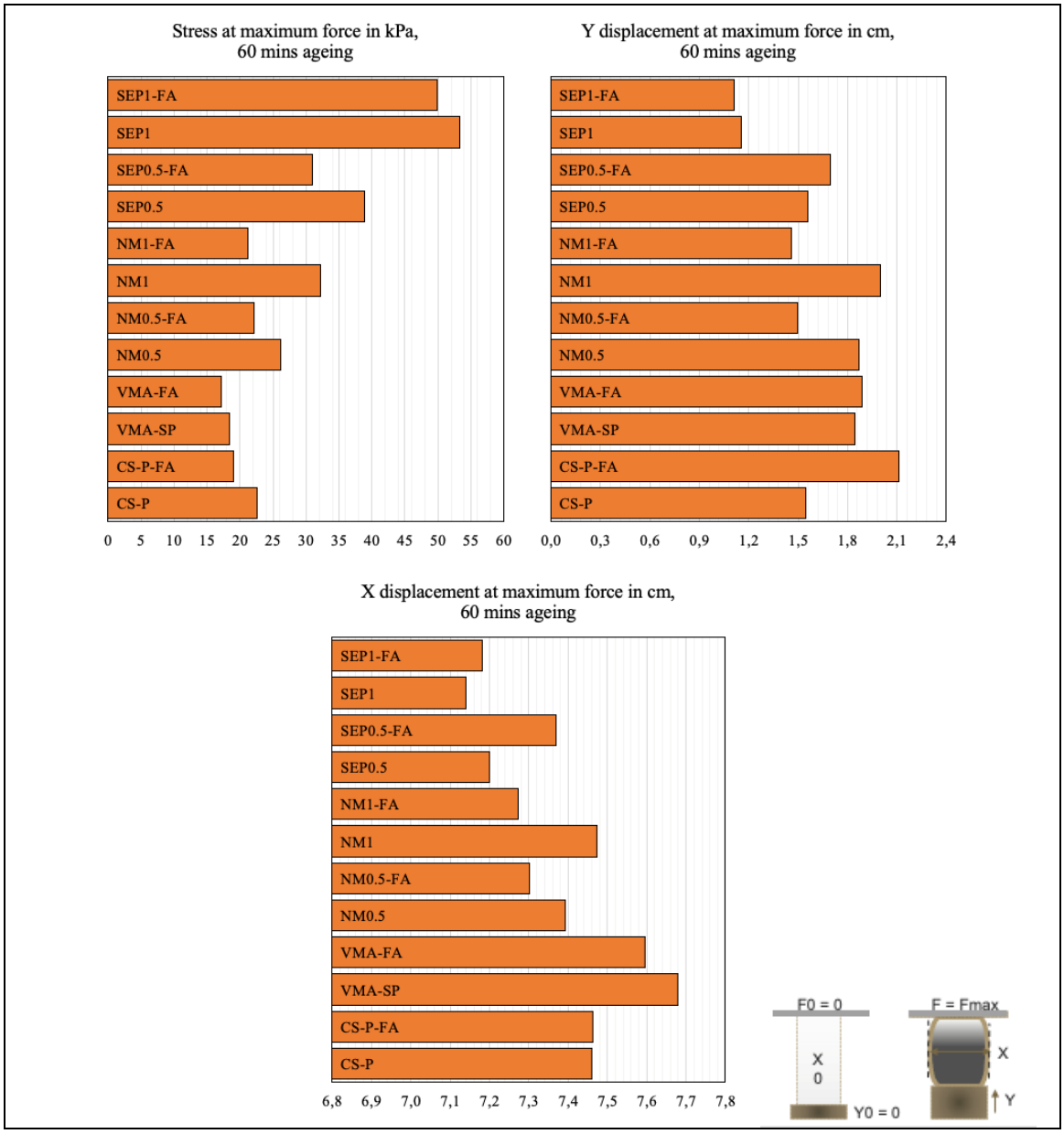

Figure A.4. Results summary, 30 minutes of ageing.

Results for the mix C-SP

Here the C_SP mixture's four green strength test results were shown at material ages of t=0, 15, 30 and 60 minutes. The tests were repeated three times for all four material ages, and average values were determined. In Figure A.5, uniaxial compressive strength

read from the dial gage versus vertical displacement of the specimens are shown. In the last graph (Figure A.5e) average results were summarized for all ages.

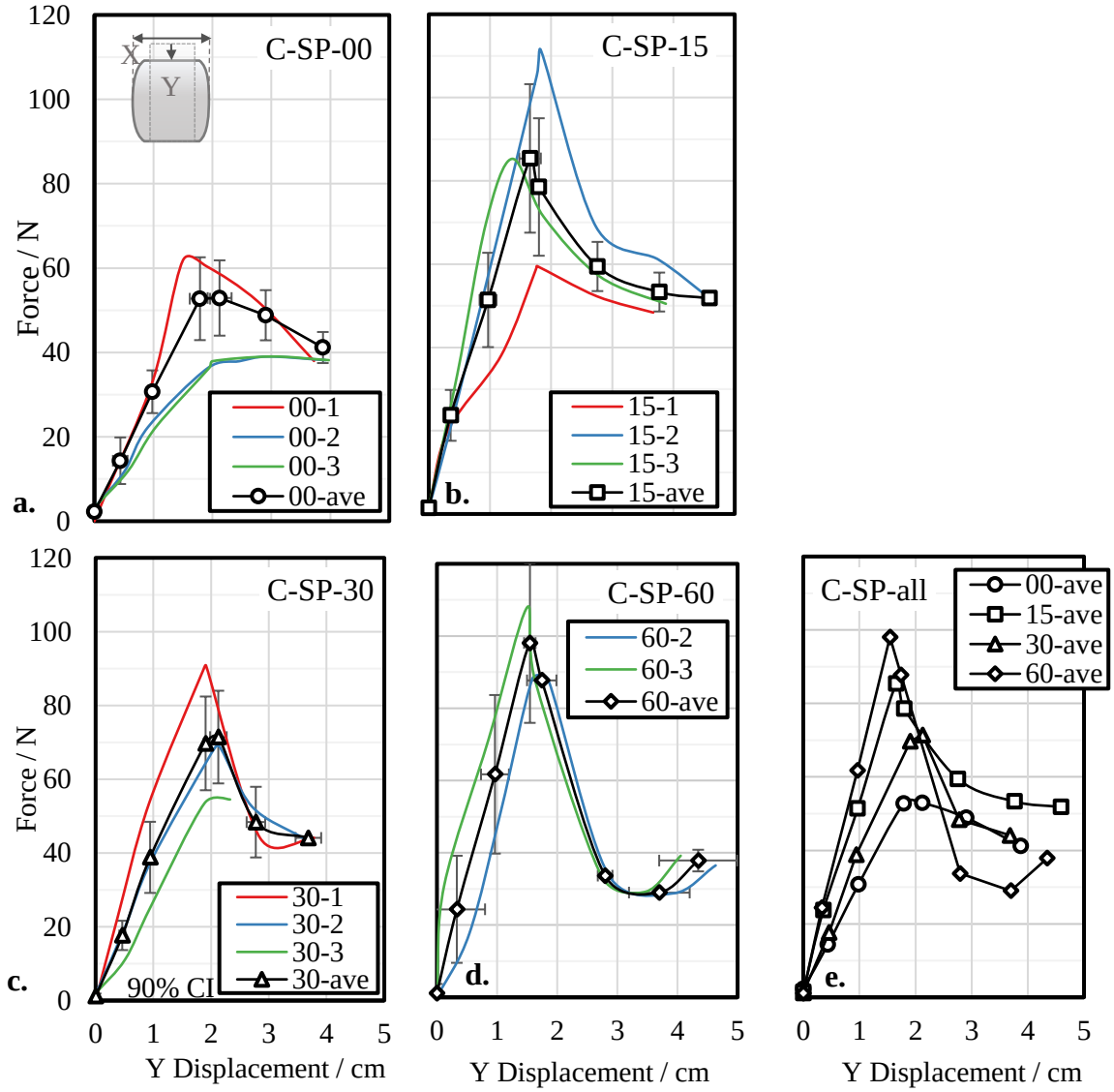

Figure A.5. Force response of C-SP mixture at various material ages. Data gathered via green strength tests.

At material age t=0 minute (Figure A.5a), the prepared specimen is tested by uniaxial compressive testing machine and average peak value is 52.9 N at the 132nd second of the test with a vertical displacement of 2.123 cm. At material age t=15 minutes Figure A.5), tested average peak value is 85.39 N at the 112nd second and vertical displacement is 1.66 cm. At material age t=30 minutes (Figure A.5c), tested average peak value is 71.41 N at

the 128th second and vertical displacement is 2.13 cm. At material age t=60 minutes (Figure A.5d), the tested average peak value is 98.08 N at the 100th second and vertical displacement is 1.55 cm.

In Figure A.6, *the horizontal displacement, X at ½ length*, versus *vertical displacement, Y* is plotted at material ages of t=0, 15, 30 and 60 min. At material age t=0 min. (Figure A.6a), lateral length of specimen at maximum compressive force of 52.9 N is 7.7 cm with vertical displacement of 2.123 cm. At material age t=15 min. (Figure A.6b), lateral length of specimen at maximum compressive force of 85.39 N is 7.644 cm with vertical displacement of 1.66 cm. At material age t=30 min. (Figure A.6c), lateral length of specimen at maximum compressive force of 71.41 N is 7.655 cm with vertical displacement of 2.13 cm. At material age t=60 min. (Figure A.6d), the lateral length of specimen at the maximum compressive force of 98.08 N is 7.459 cm with vertical displacement of 1.55 cm. Overall, material at age of 0 minutes has the highest lateral displacement while material age t=60 min has the lowest lateral displacement as expected.

In Figure A.7, average compressive stress in kPa versus vertical engineering strain (final height/initial height) in percentages was shown at material ages of t=0, 15, 30 and 60 min. Specimen's height at the age of 0 minutes (Figure A.7) has decreased 17.8% under the average maximum compressive load of 52.9 N. At the material age of t=15 min. (Figure A.7), specimen's height got 14% less with an average maximum compressive load of 85.4 N. Specimen's height at the age of 30 min. has decreased 17.6% under the average maximum compressive load of 71.41 N (Figure A.7c). Lastly, specimen's height at the age of 60 min. has decreased 12.7% under the average maximum compressive load of 98.08 N (Figure A.7d).

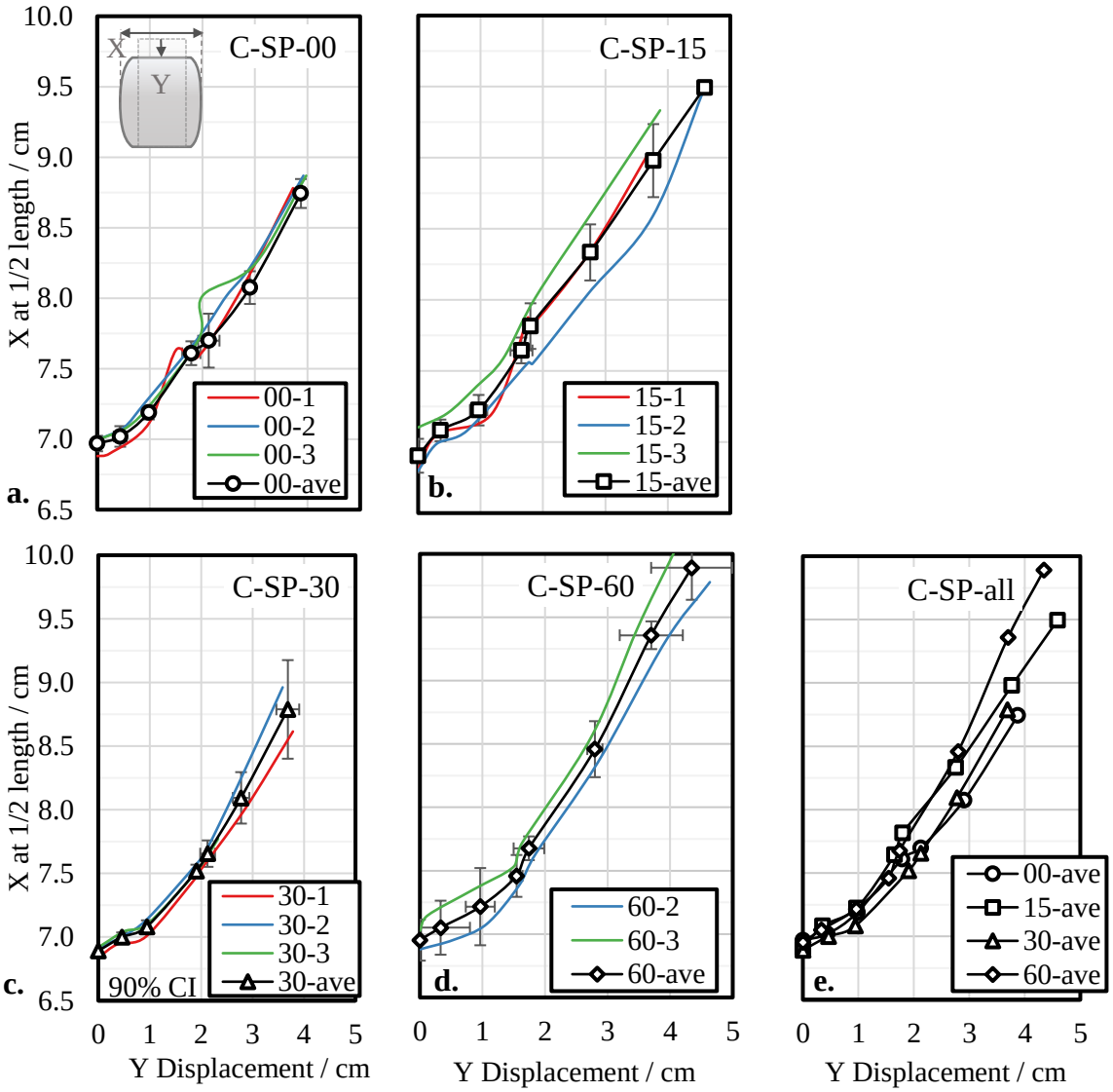

Figure A.6. Lateral displacement of C-SP mixture at various material ages. Data gathered via green strength tests.

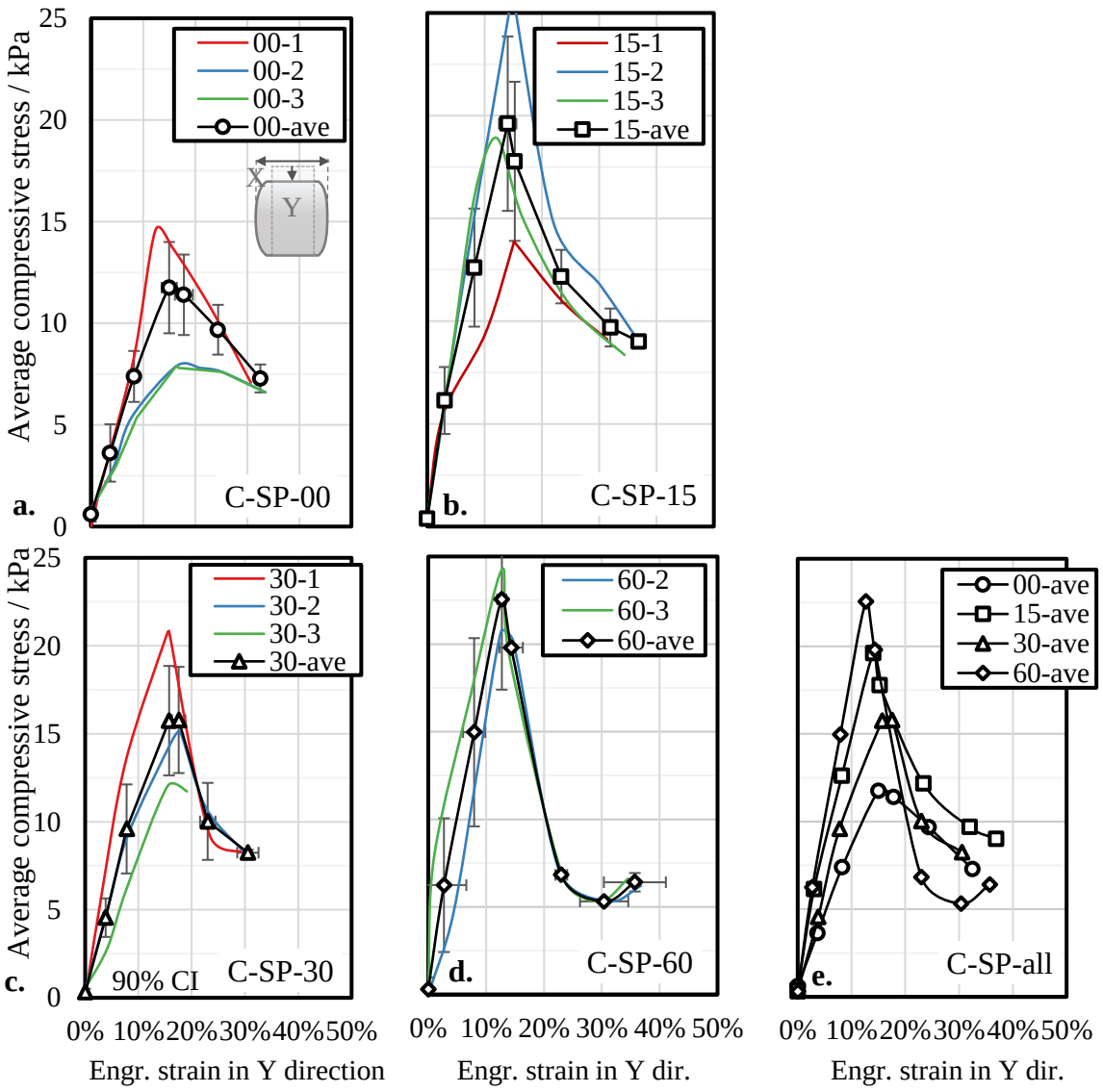

Figure A.7. Average stress of C-SP mixture at various material ages. Data gathered via green strength tests.

Results for the mix VMA-SP

Green strength test results were given below for VMA_SP mixture at material ages of t=0, 15, 30 and 60 minutes. The tests were repeated three times for all four material ages and average values were calculated. In Figure A.8, uniaxial compressive strength read from the dial gage versus vertical displacement of the specimens were shown. In the last graph average results were summarized for VMA_SP mixture

At material age t=0 minute (Figure A.8a), the prepared specimen was tested by uniaxial compressive testing machine and average peak value is 56.12 N at the 120th second of the test with a vertical displacement of 1.890 cm. At material age t=15 minutes (Figure A.8b), tested average peak value is 77.43 N at the 124th second and vertical displacement is 1.775 cm. At material age t=30 minutes (Figure A.8c), tested average peak value is 70.21 N at the 153rd second and vertical displacement is 2.284 cm. At material age t=60 minutes (Figure A.8d), tested average peak value is 85.28 N at the 117th second and vertical displacement is 1.919 cm.

In Figure A.9, the horizontal displacement, *X at ½ length*, versus the vertical displacement, *Y displacement*, was plotted at material ages of t=0, 15, 30 and 60 min. At material age t=0 min. (Figure A.9a), lateral length of specimen at maximum compressive force of 56.12 N is 8.046 cm with vertical displacement of 1.890 cm. At material age t=15 min. (Figure A.9b), lateral length of specimen at maximum compressive force of 77.43 N is 7.564cm with vertical displacement of 1.775 cm. At material age t=30 min. (Figure A.9c), lateral length of specimen at maximum compressive force of 70.21 N is 7.808 cm with vertical displacement of 2.284 cm. At material age t=60 min. (Figure A.9d), lateral length of specimen at maximum compressive force of 85.28 N is 7.705 cm with vertical displacement of 1.919 cm. Overall, material at age of 30 minutes has the highest lateral displacement while material age t=15 min has the lowest lateral displacement.

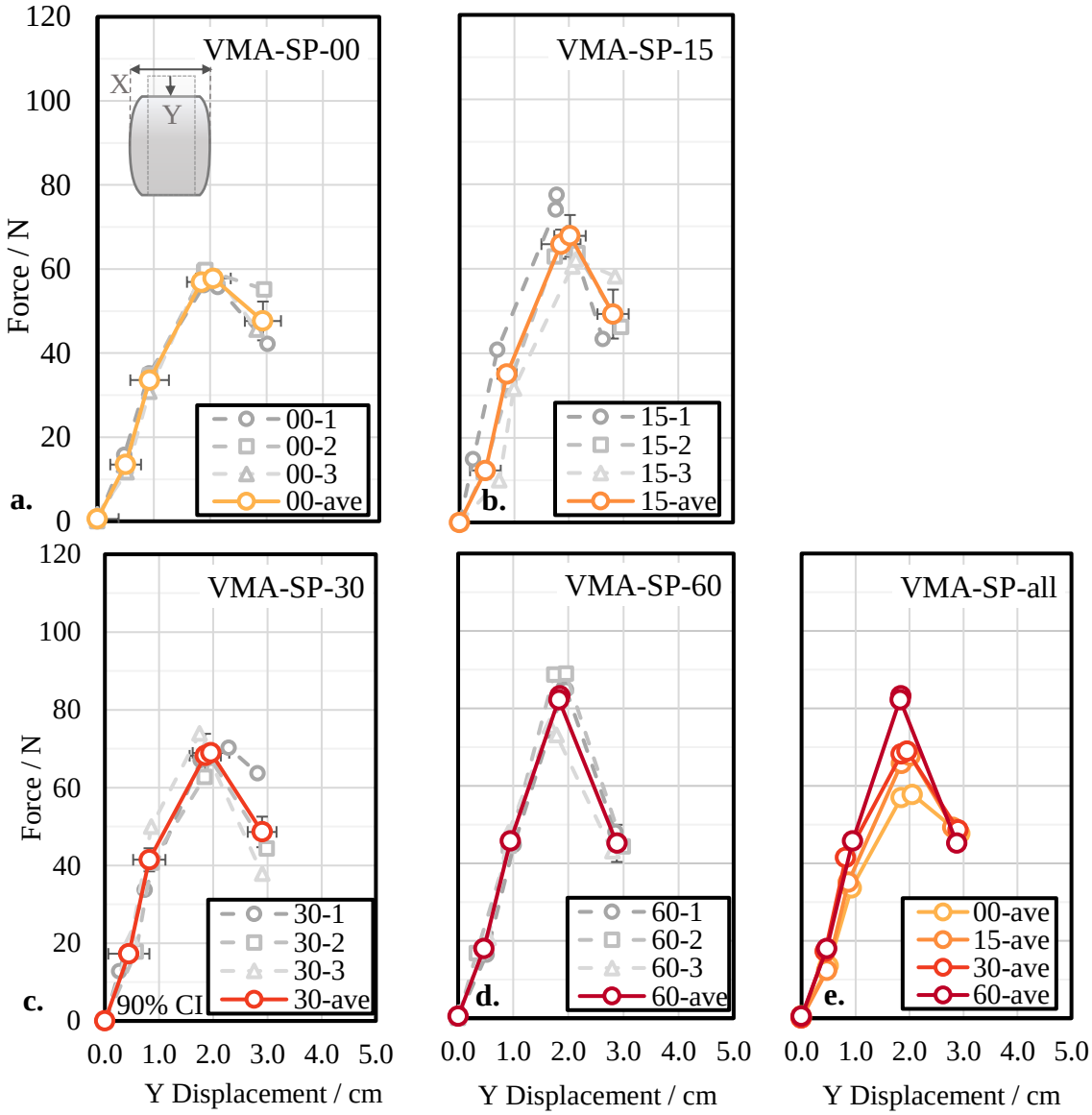

Figure A.8. Force response of VMA-SP mixture at various material ages. Data gathered via green strength tests.

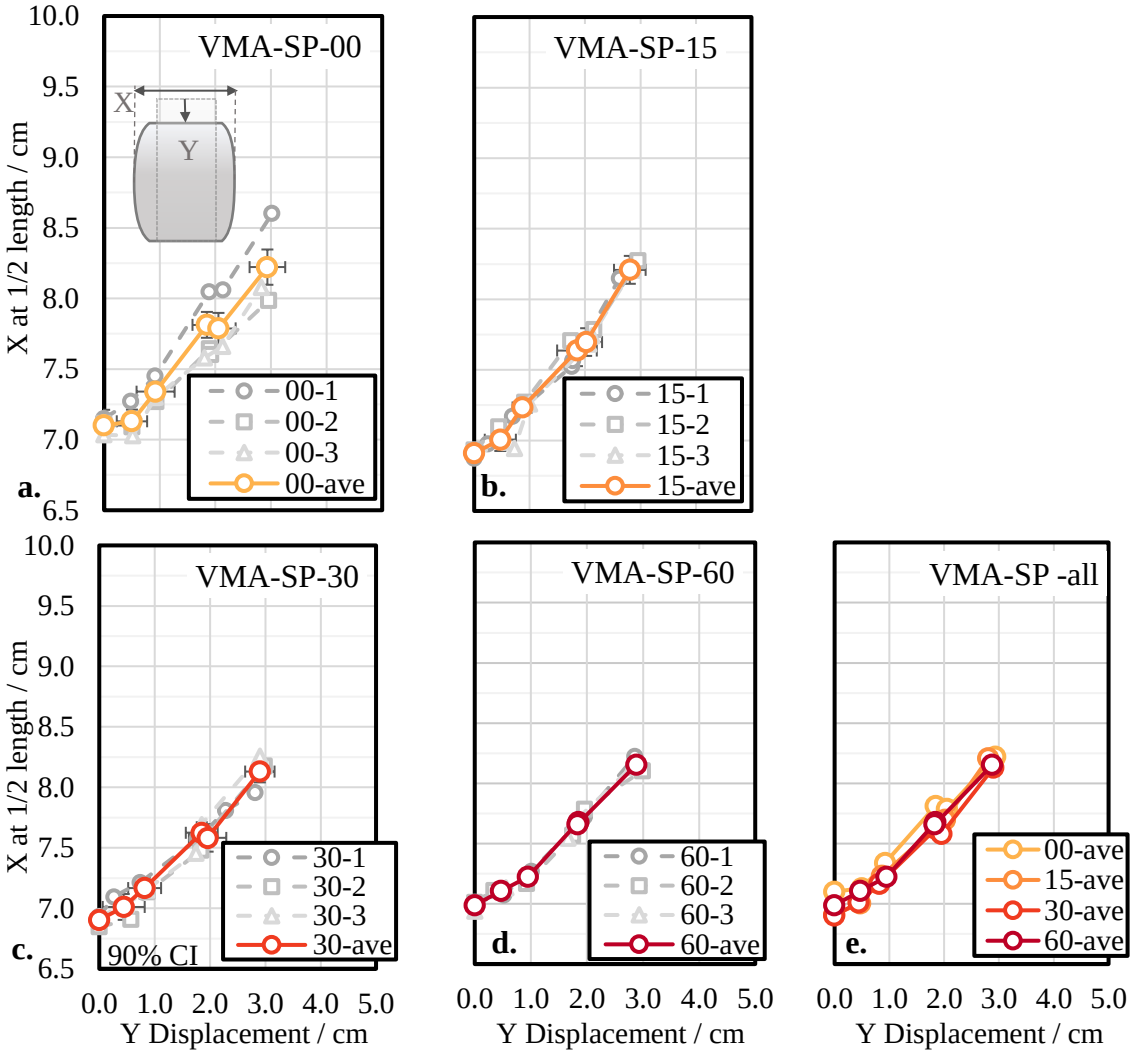

Figure A.9. Lateral displacement of VMA-SP mixture at various material ages. Data gathered via green strength tests.

In Figure A.10, average compressive stress in kPa versus vertical engineering strain (elongation/initial height) in percentages is shown at material ages of t=0, 15, 30 and 60 min. Specimen's height at the age of 0 minutes (Figure A.10a) has decreased 16% under the average maximum compressive load of 56.12 N. At the material age of t=15 minutes (Figure A.10b), specimen's height got 14.8% less with an average maximum compressive load of 77.43 N. Specimen's height at the age of 30 minutes (Figure A.10) has decreased 18.6% under the average maximum compressive load of 70.21 N. Lastly, specimen's height at the age of 60 minutes has decreased 15.6% under the average maximum compressive load of 85.28 N (Figure A.10d).

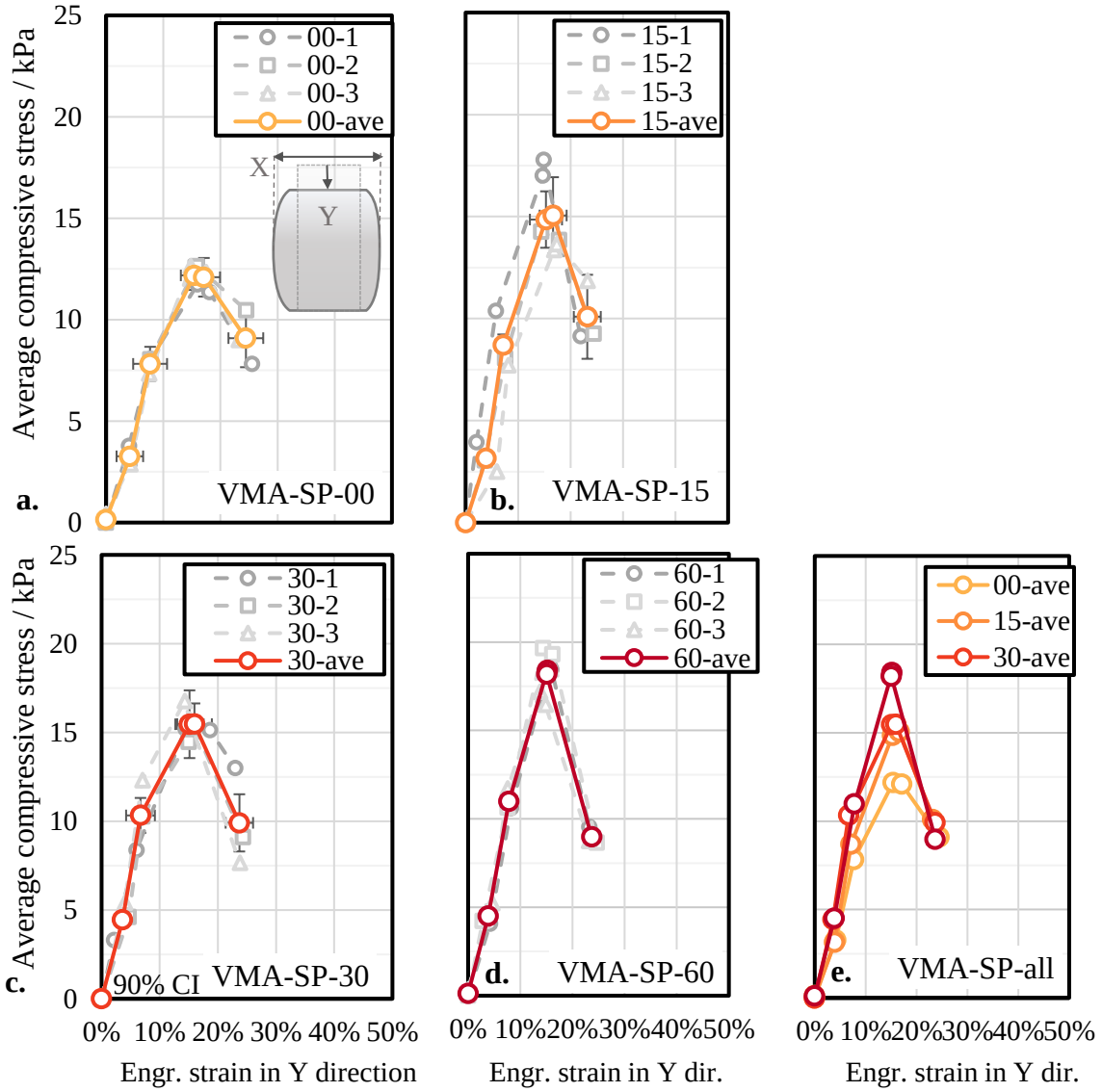

Figure A.10. Average stress of VMA-SP mixture at various material ages. Data gathered via green strength tests.

Results for the mix VMA-FA

Figure A.11 represents the VMA_FA mixture's four green strength test results at material ages of t=0, 15, 30 and 60 minutes. The tests were repeated three times for all four material ages and average values were calculated. In Figure A.11, uniaxial compressive strength read from the dial gage versus vertical displacement of the specimens were shown. In the final graph (Figure A.11e), all results were summarized for VMA-FA-all material age average results are summarized.

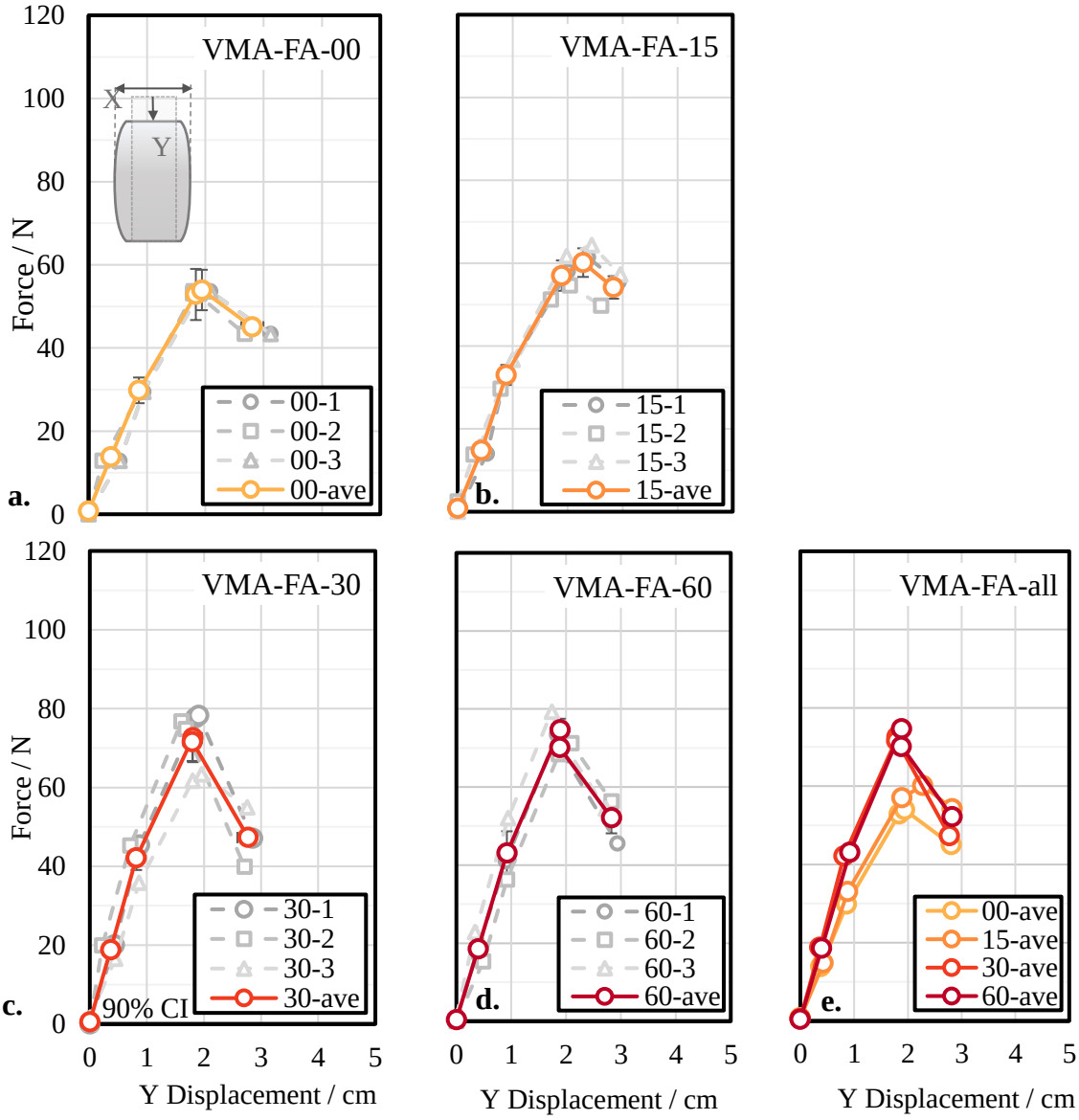

Figure A.11. Force response of VMA-FA mixture at various material ages. Data gathered via green strength tests.

At material age t=0 minute (Figure A.11a), the prepared specimen was tested by uniaxial compressive testing machine and average peak value is 53.935 N at the 130th second of the test with a vertical displacement of 1.943 cm. At material age t=15 minutes (Figure A.11b), tested average peak value is 60.14 N at the 145th second and vertical displacement is 2.279 cm. At material age t=30 minutes (Figure A.11c), tested average peak value is 72.57 N at the 119th second and vertical displacement is 1.803 cm. At

material age t=60 minutes (Figure A.11d), tested average peak value is 74.62 N at the 120th second and vertical displacement is 1.888 cm.

In Figure A.12, the horizontal displacement, *X at ½ lengths*, versus the vertical displacement, *Y displacement* was plotted at material ages of t=0, 15, 30 and 60 minutes. At material age t=0 minutes (Figure A.12a), the lateral length of the specimen at maximum compressive force of 53.935 N is 7.641cm with vertical displacement of 1.943 cm. At material age t=15 minutes (Figure A.12b), the lateral length of specimen at maximum compressive force of 60.14 N is 7.772 cm with vertical displacement of 2.279 cm. At material age t=30 minutes (Figure A.12c), lateral length of specimen at maximum compressive force of 72.57 N is 7.542 cm with vertical displacement of 1.803 cm. At material age t=60 minutes (Figure A.12d), the lateral length of the specimen at maximum compressive force of 74.62 N is 7.595 cm with vertical displacement of 1.888 cm. Overall, material at age of 15 minutes has the highest lateral displacement while material age t=30 minutes has the lowest lateral displacement (Figure A.12e).

In Figure A.13, the *average compressive stress* versus *vertical engineering strain* (i.e., elongation / initial height) in percentages is shown at material ages of t = 0, 15, 30 and 60 minutes. Specimen's height at the age of 0 min. has decreased 15.8% under the average maximum compressive load of 53.935 N (Figure A.13a). At the material age of t = 15 min. (Figure A.13b), specimen's height got 18.7% less with an average maximum compressive load of 60.14 N. Specimen's height at the age of 30 min. has decreased 14.7% under the average maximum compressive load of 72.57 N (Figure A.13c). Lastly, specimen's height at the age of 60 minutes has decreased 15.2% under the average maximum compressive load of 74.62 N (Figure A.13d).

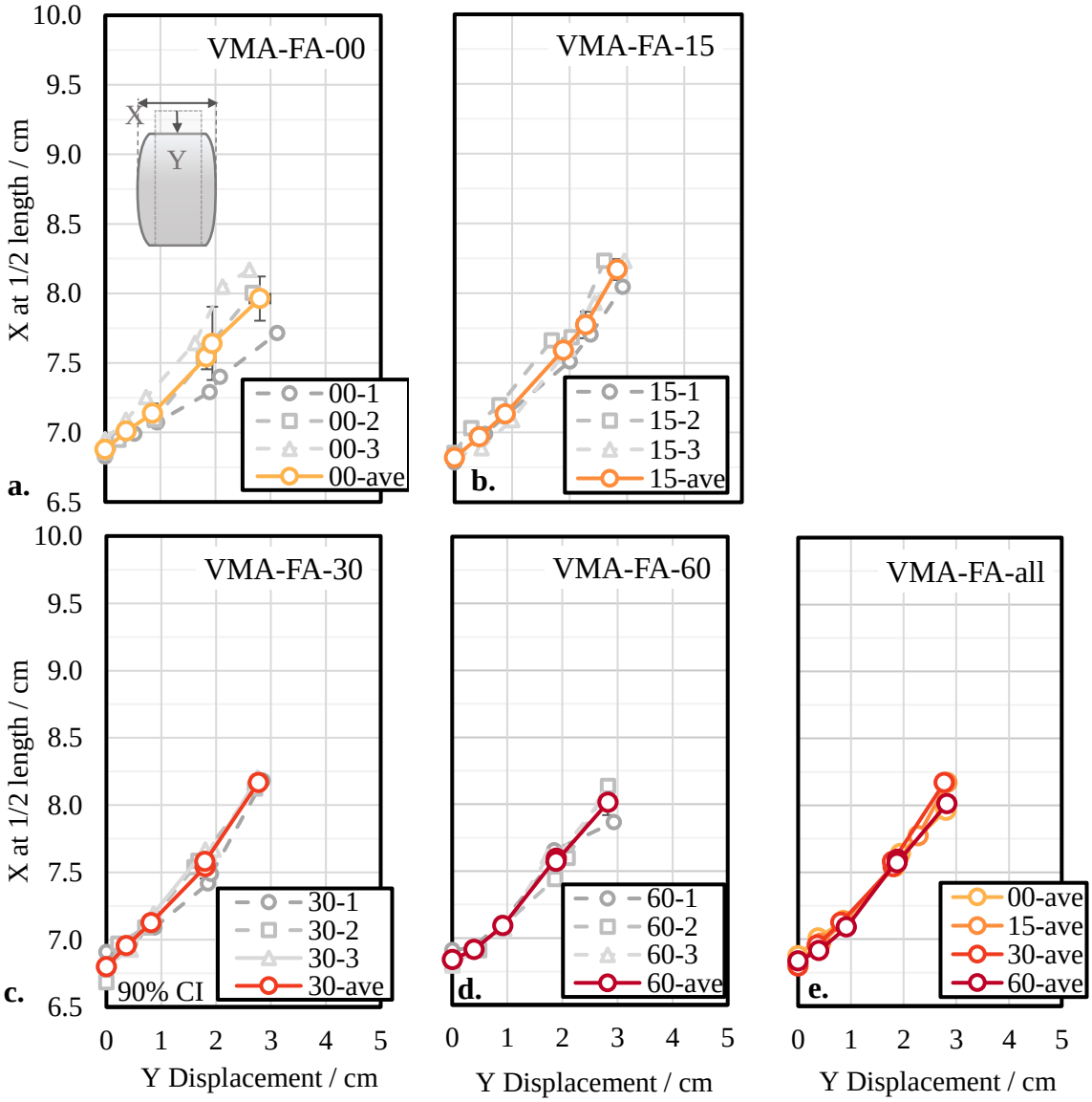

Figure A.12. Lateral displacement of VMA-FA mixture at various material ages. Data gathered via green strength tests.

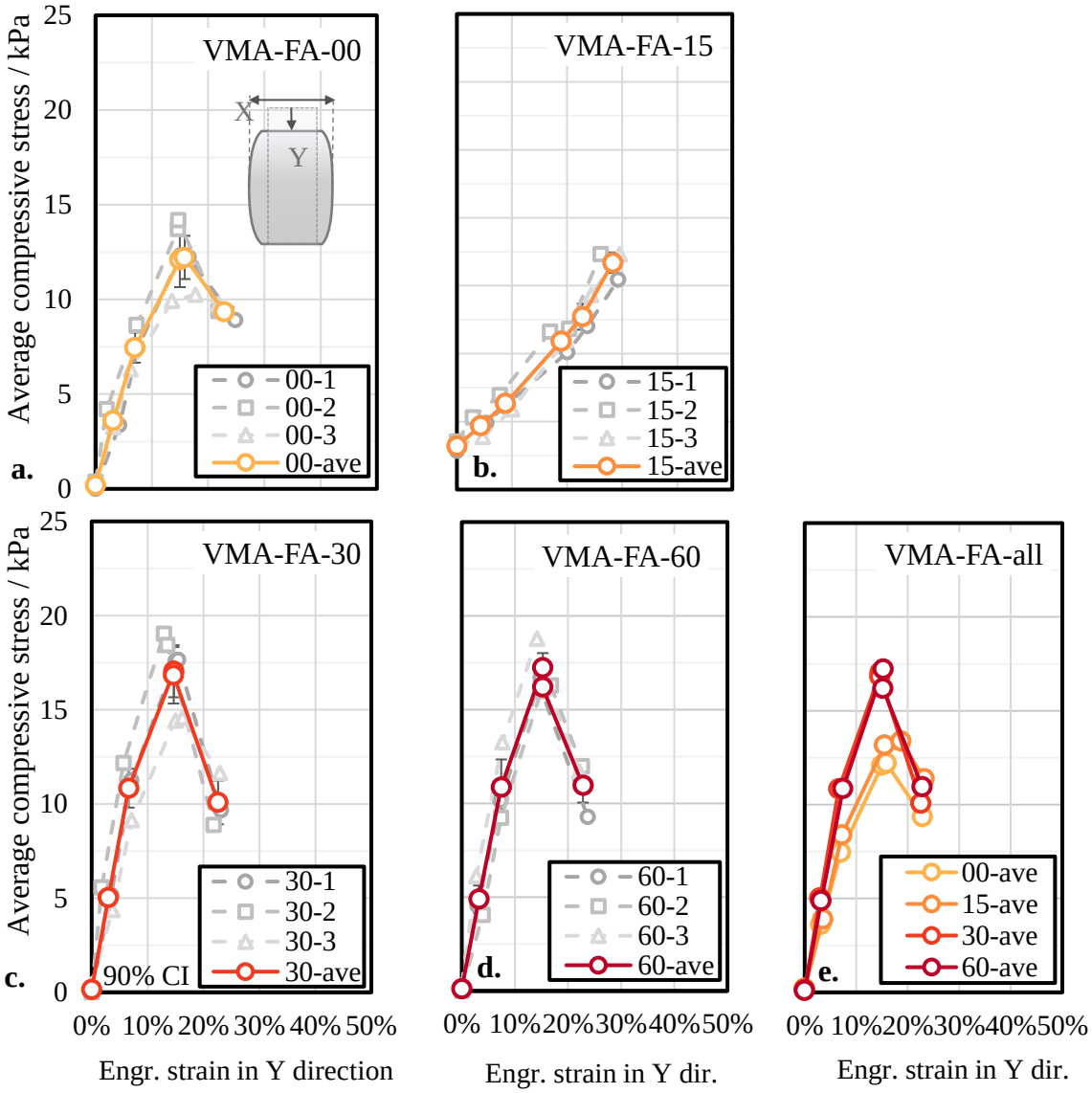

Figure A.13. Average stress of VMA-FA mixture at various material ages. Data gathered via green strength tests.

Results for the mix NM0.5

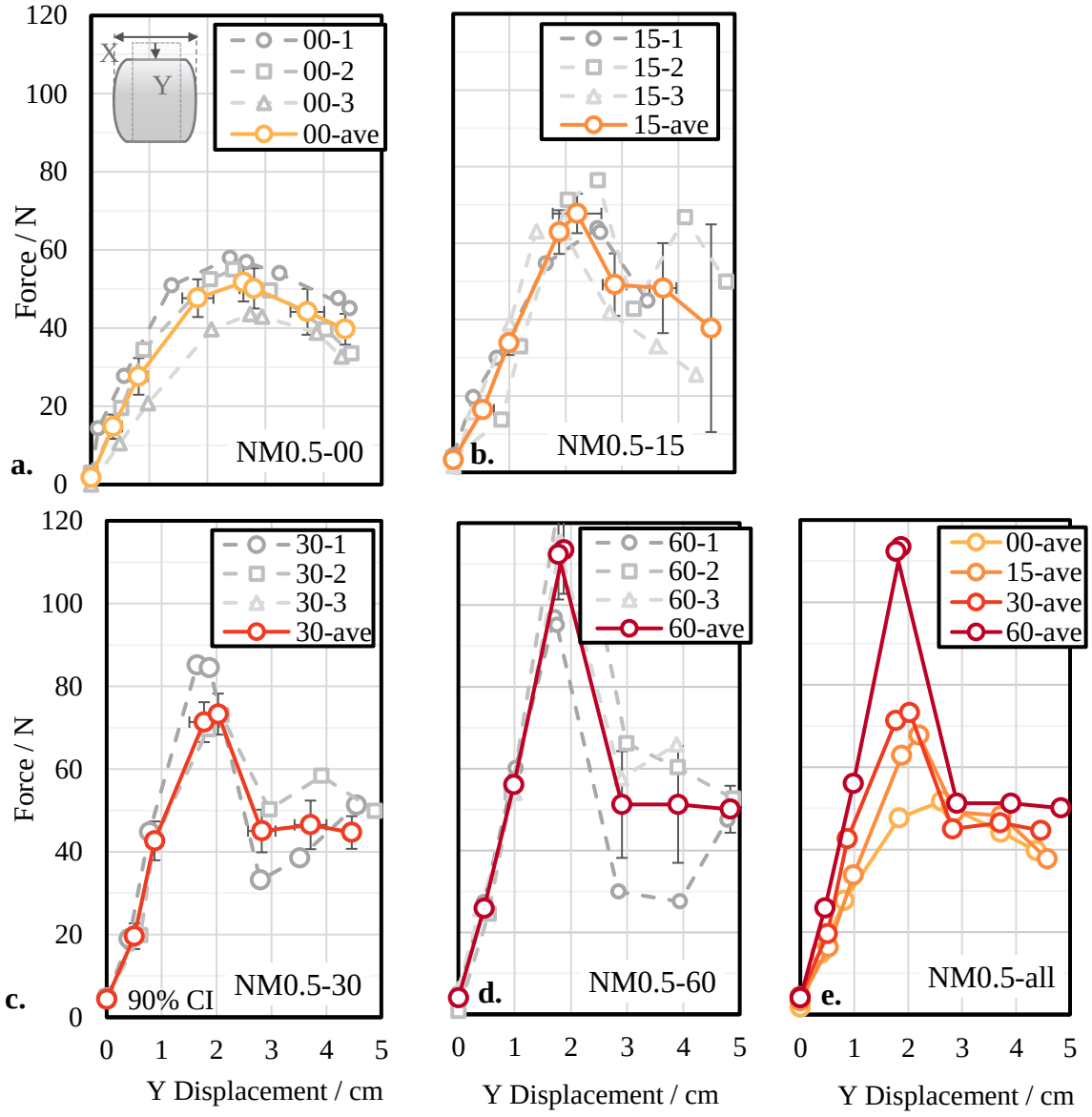

Figure A.14. Force response of NM0.5 mixture at various material ages. Data gathered via green strength tests.

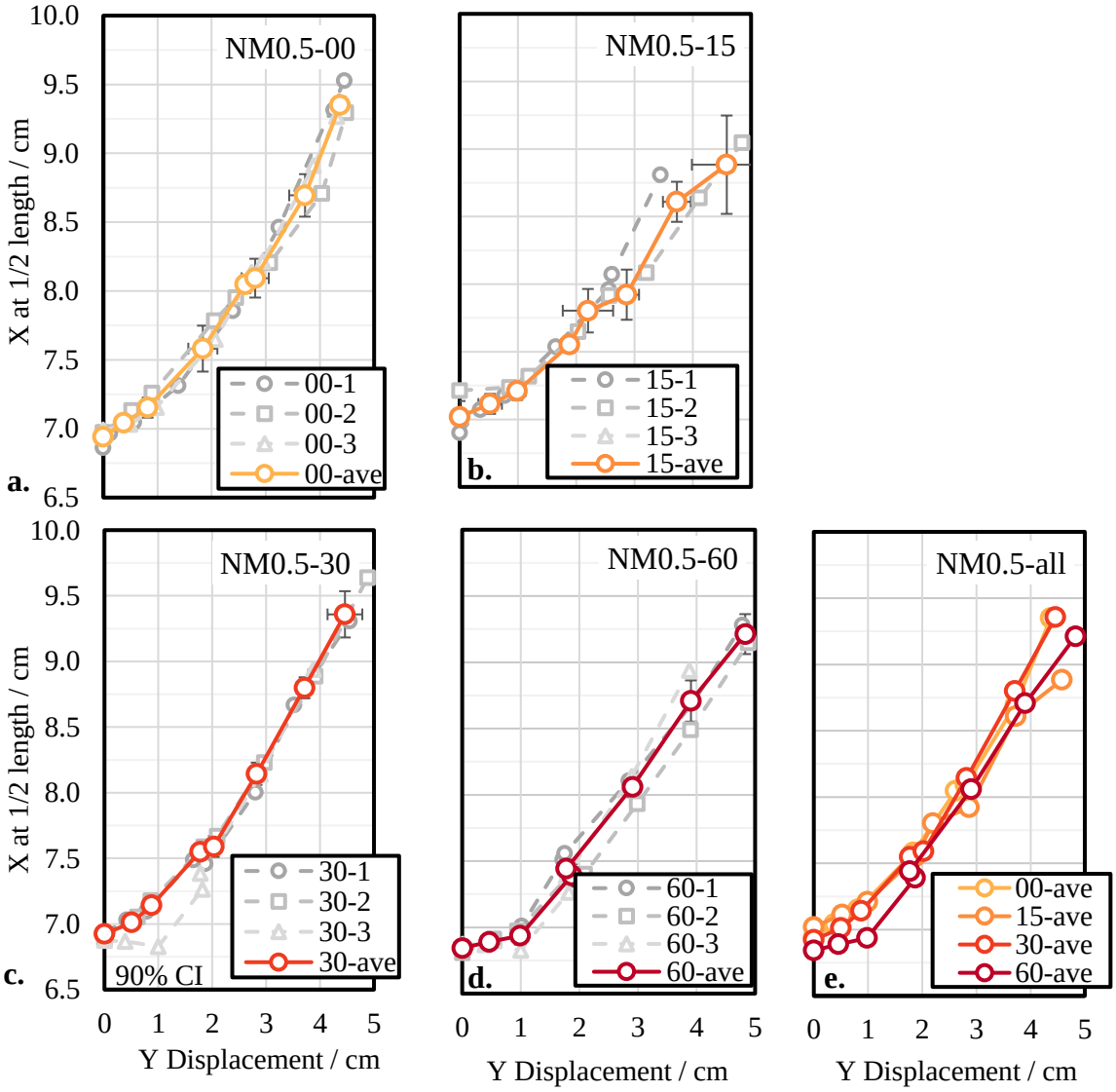

Figure A.15. Lateral displacement of NM0.5 mixture at various material ages. Data gathered via green strength tests.

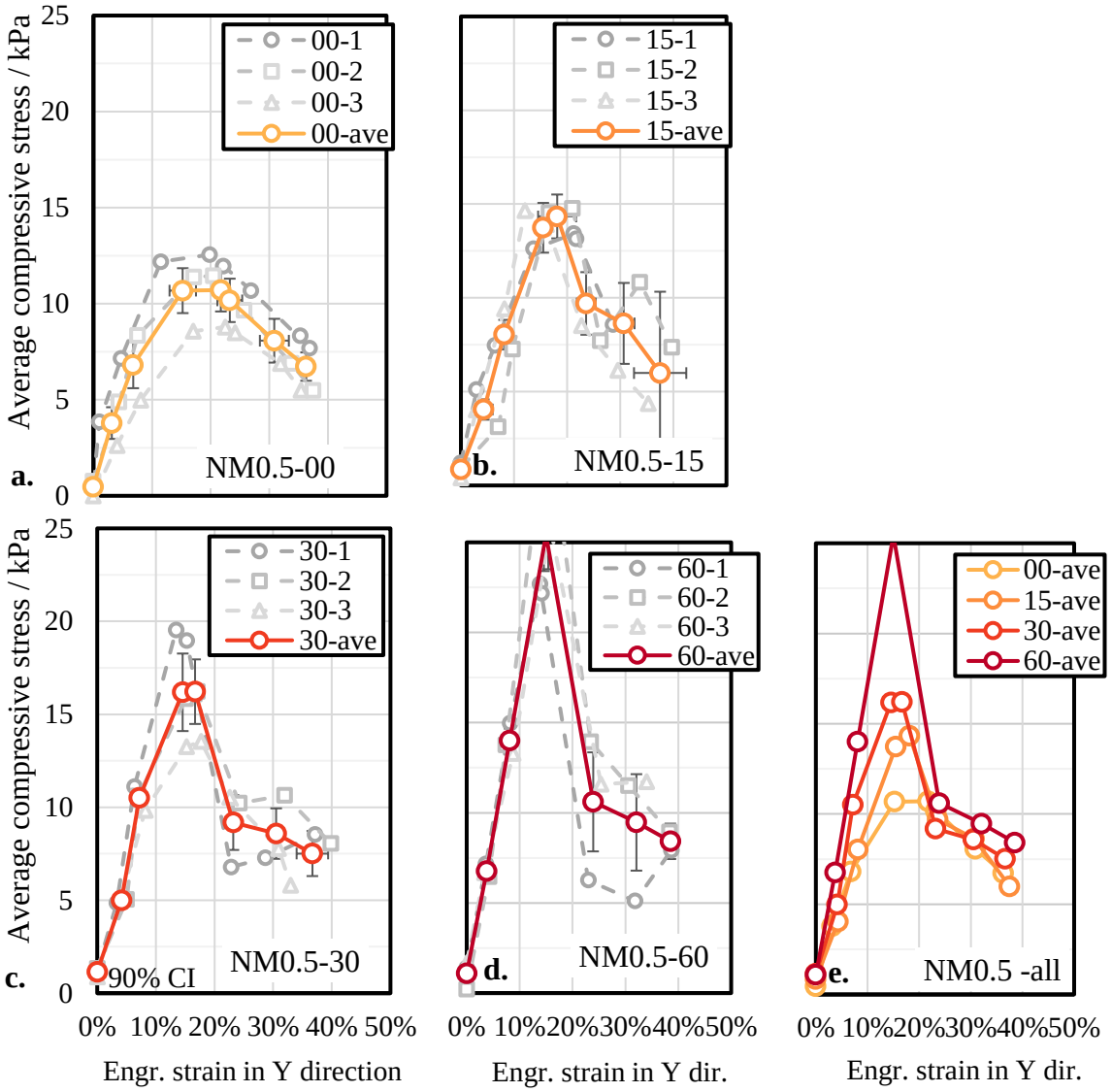

Figure A.16. Average stress of NM0.5-FA mixture at various material ages. Data gathered via green strength tests.

Results for the mix NM0.5-FA

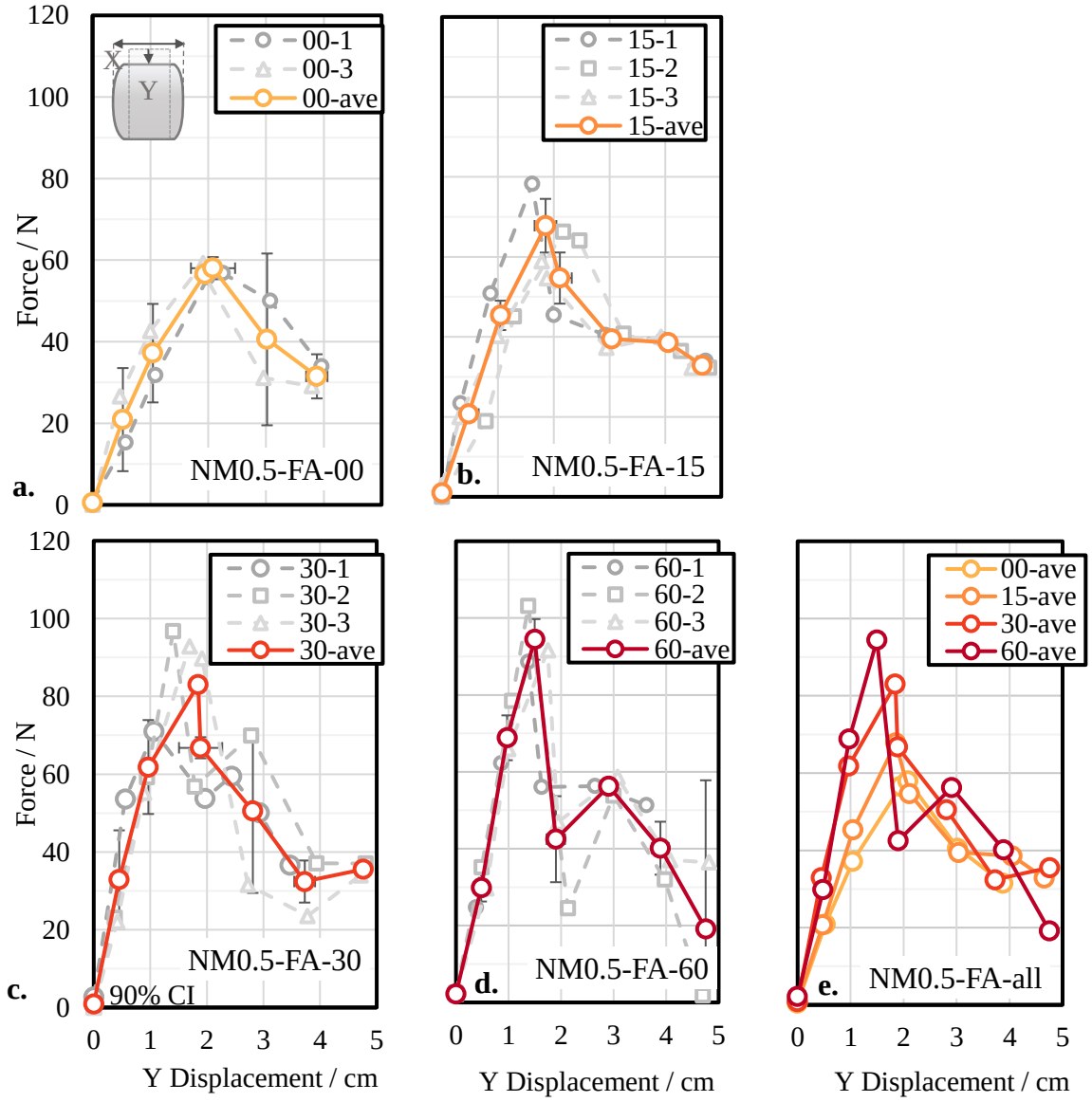

Figure A.17. Force response of NM0.5-FA mixture at various material ages. Data gathered via green strength tests.

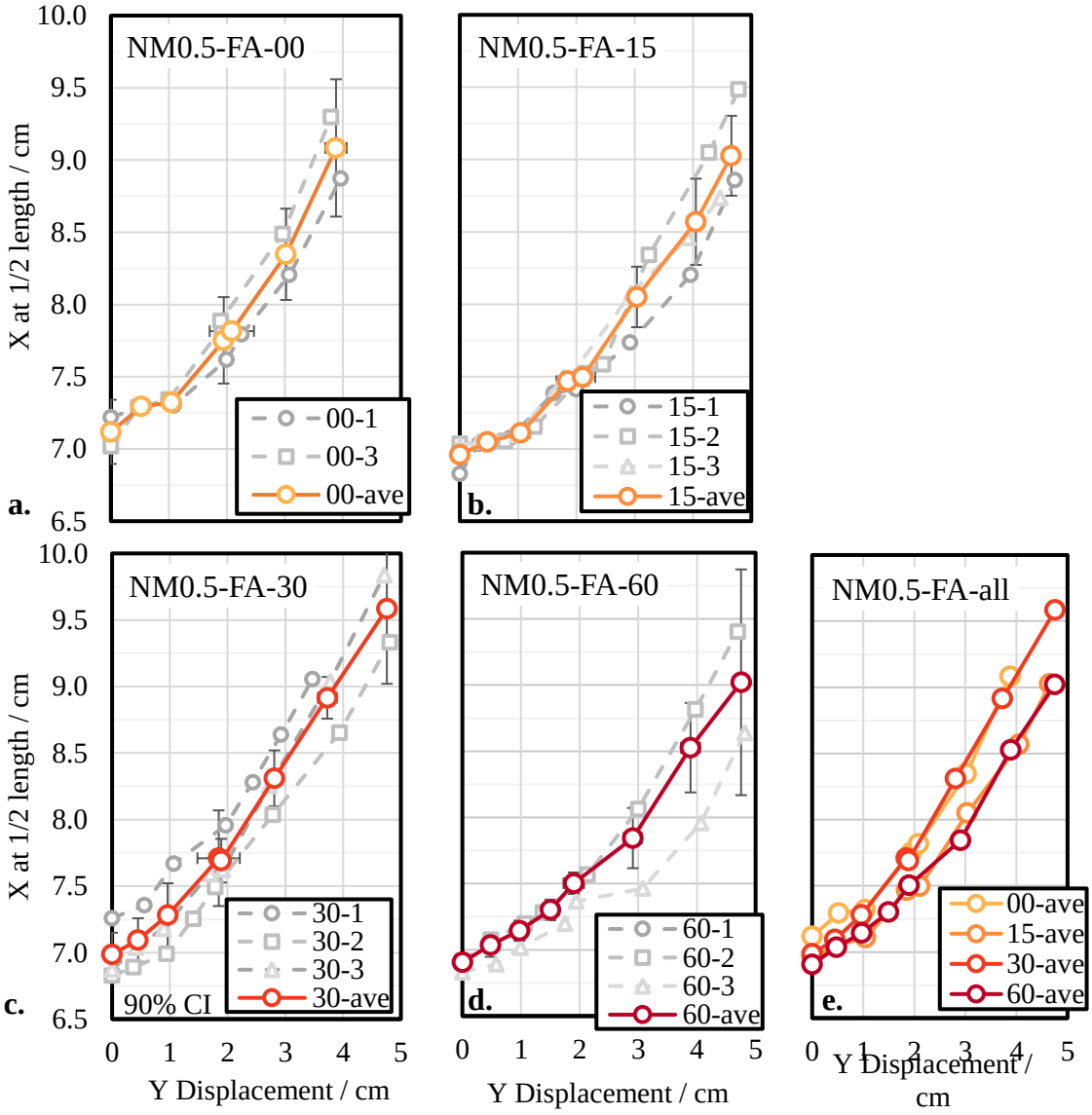

Figure A.18. Lateral displacement of NM0.5-FA mixture at various material ages. Data gathered via green strength tests.

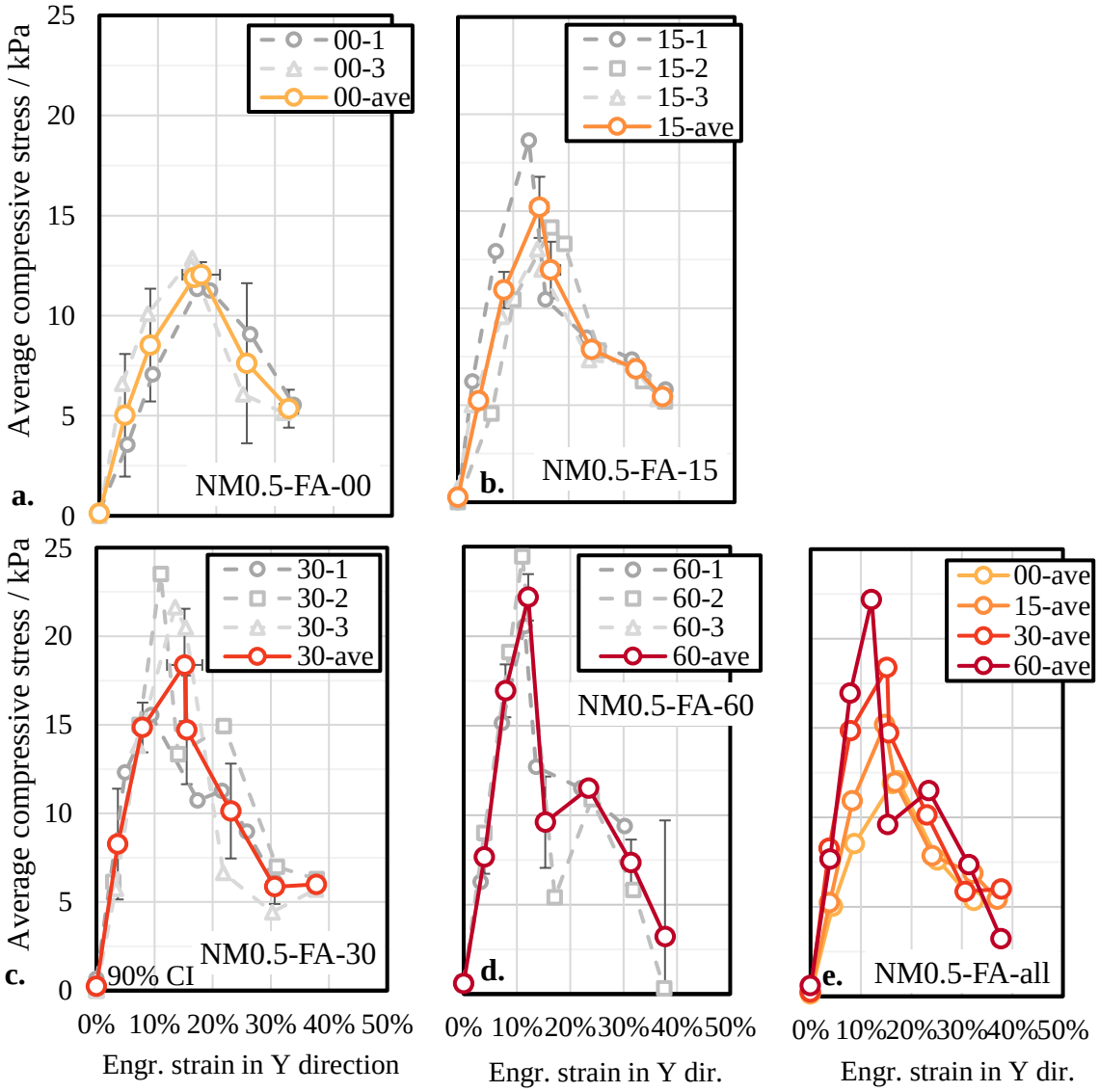

Figure A.19. Average stress of NM0.5-FA mixture at various material ages. Data gathered via green strength tests.

Results for the mix NM1

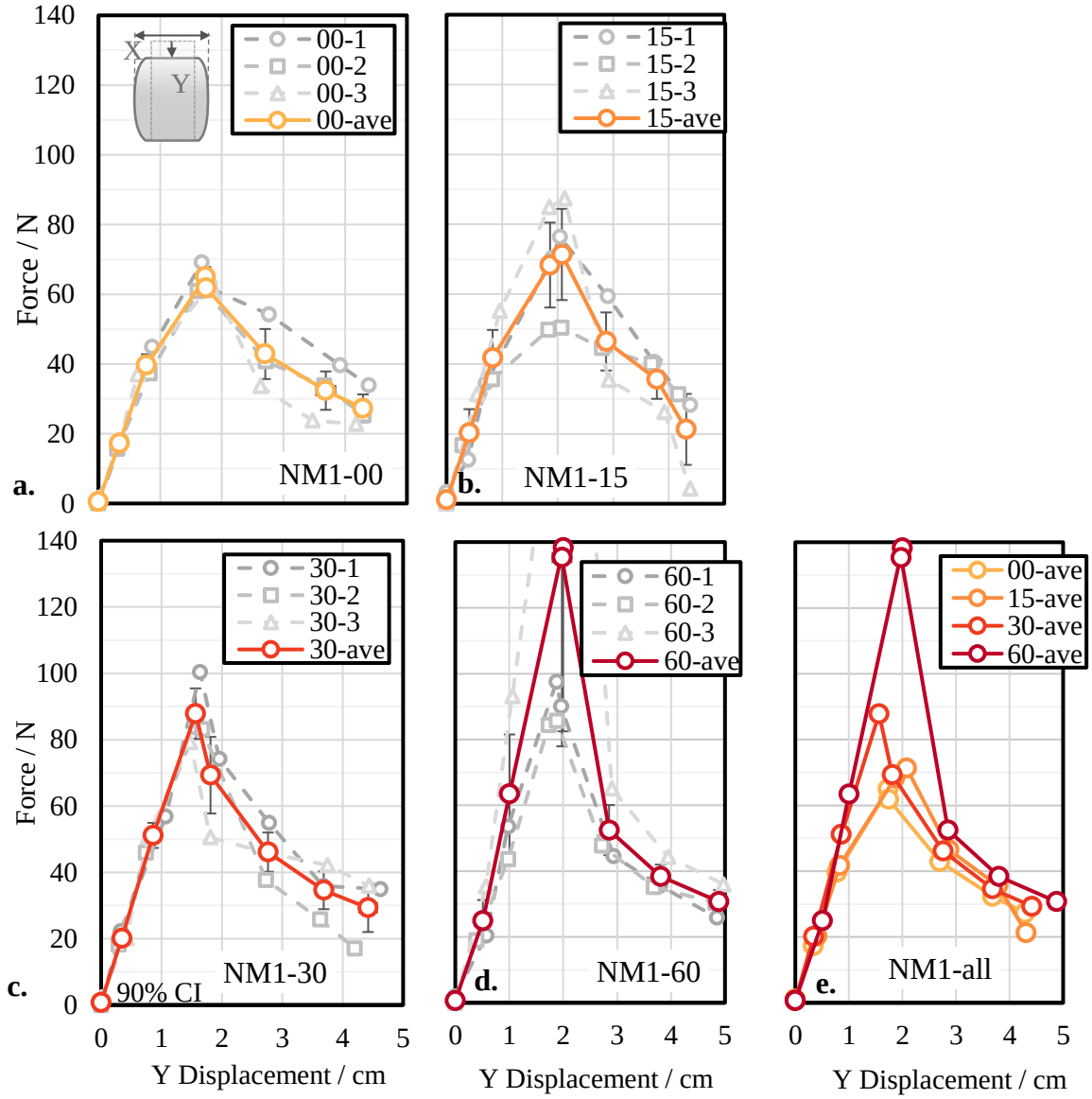

Figure A.20. Force response of NM1 mixture at various material ages . Data gathered via green strength tests.

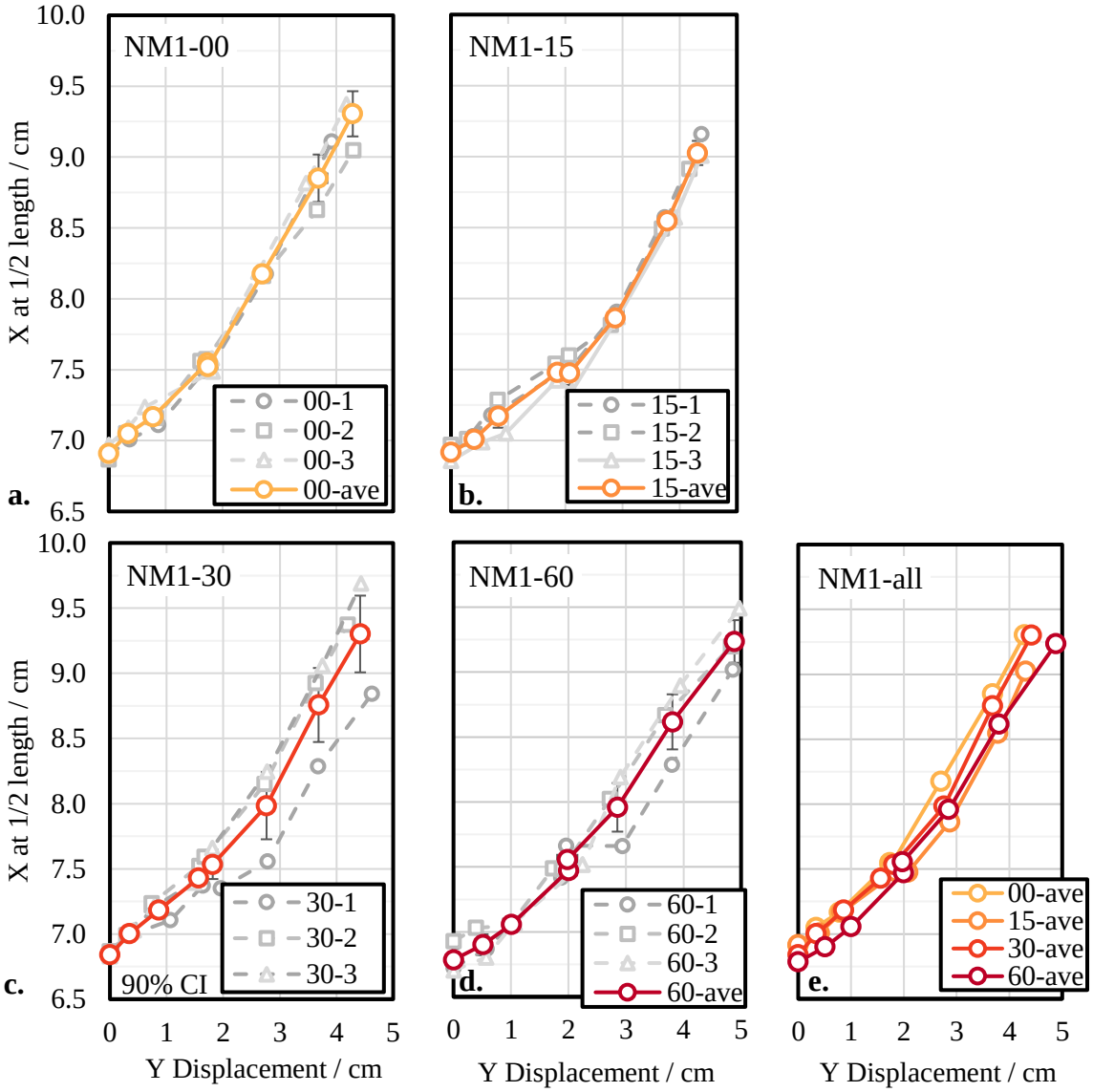

Figure A.21. Lateral displacement of NM1 mixture at various material ages. Data gathered via green strength tests.

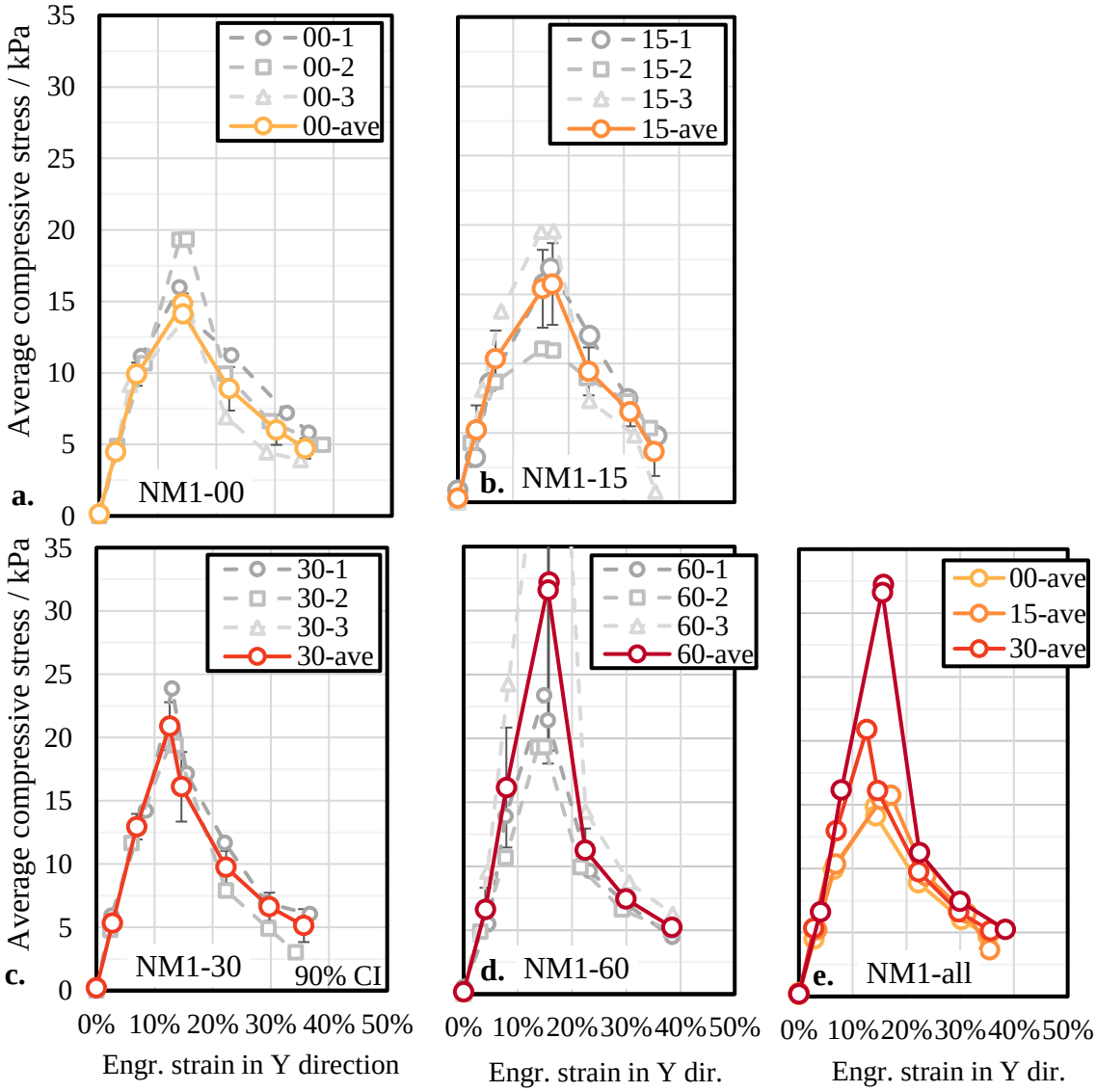

Figure A.22. Average stress of NM1 mixture at various material ages. Data gathered via green strength tests.

Results for the mix NM1-FA

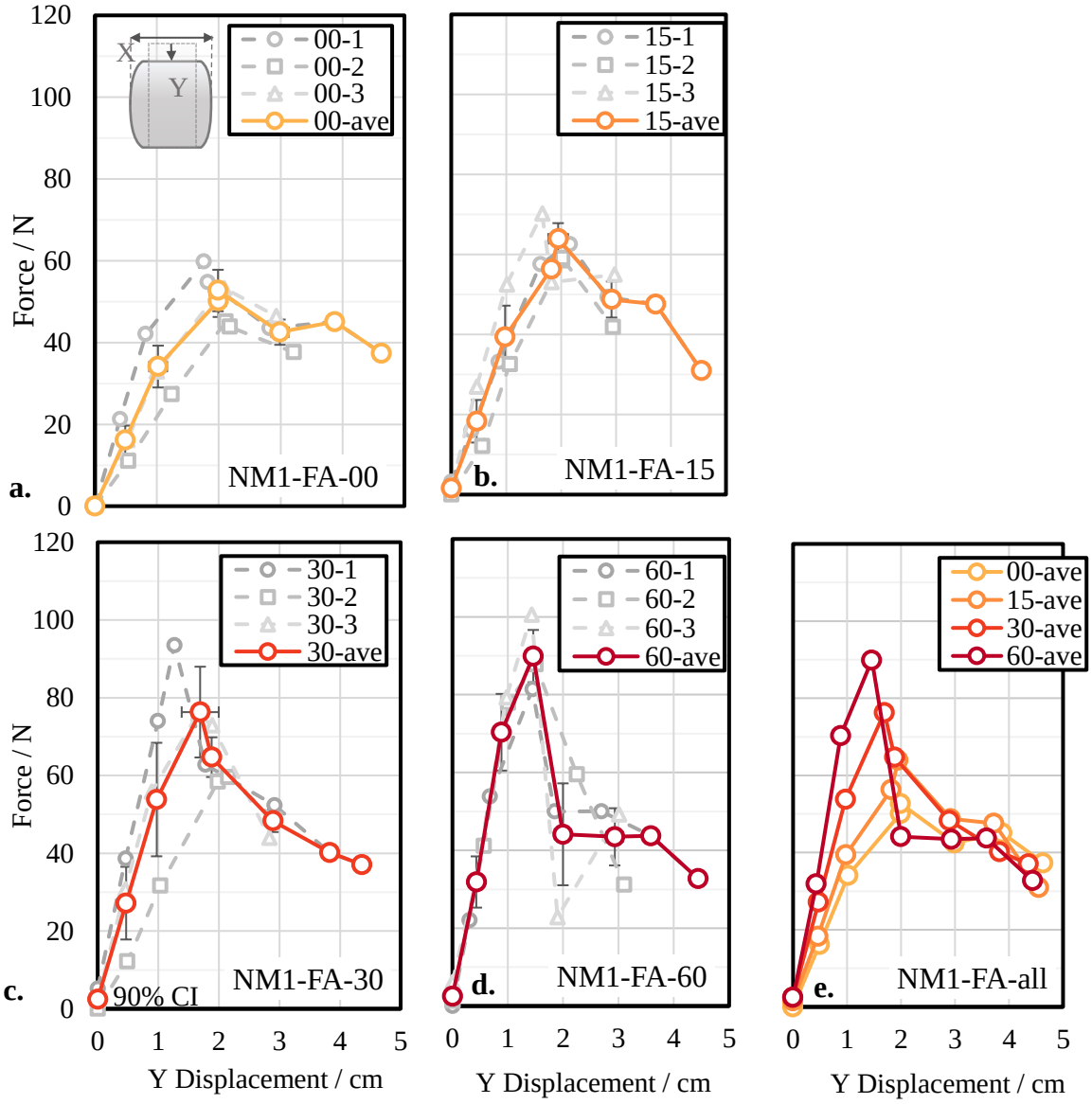

Figure A.23. Lateral displacement of NM1-FA mixture at various material ages. Data gathered via green strength tests.

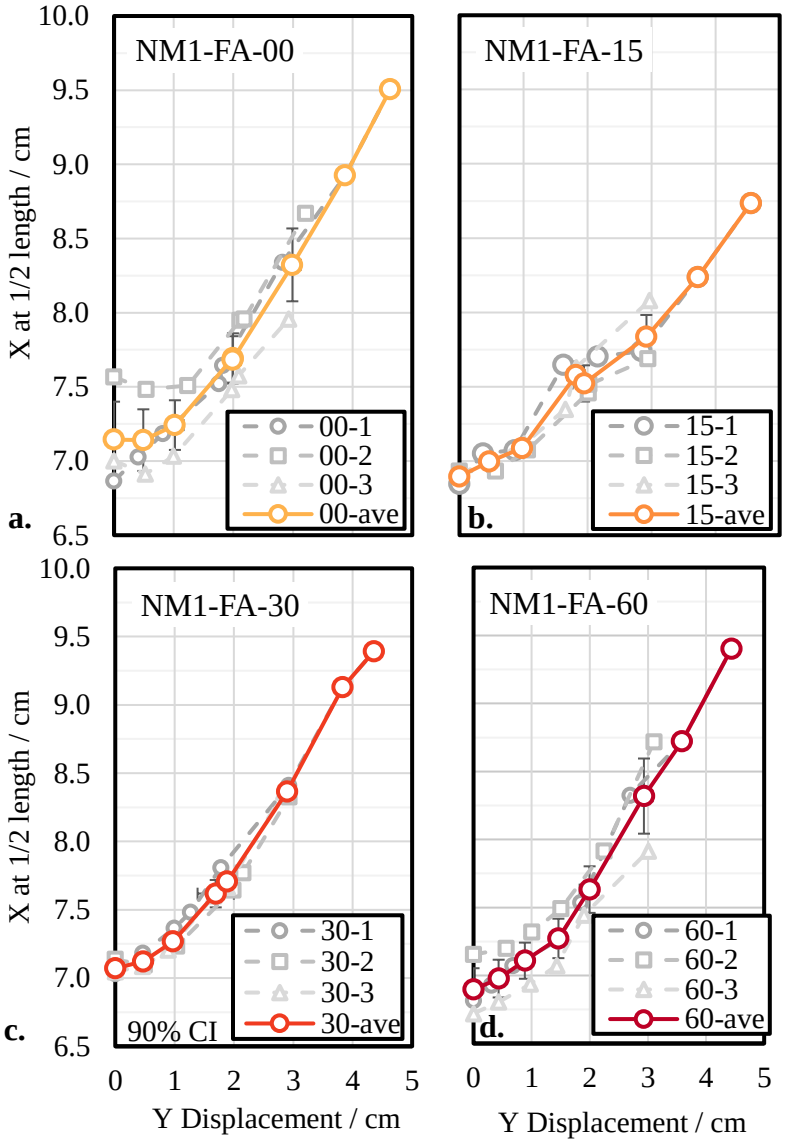

Figure A.24. Lateral displacement of NM1-FA mixture at various material ages. Data gathered via green strength tests.

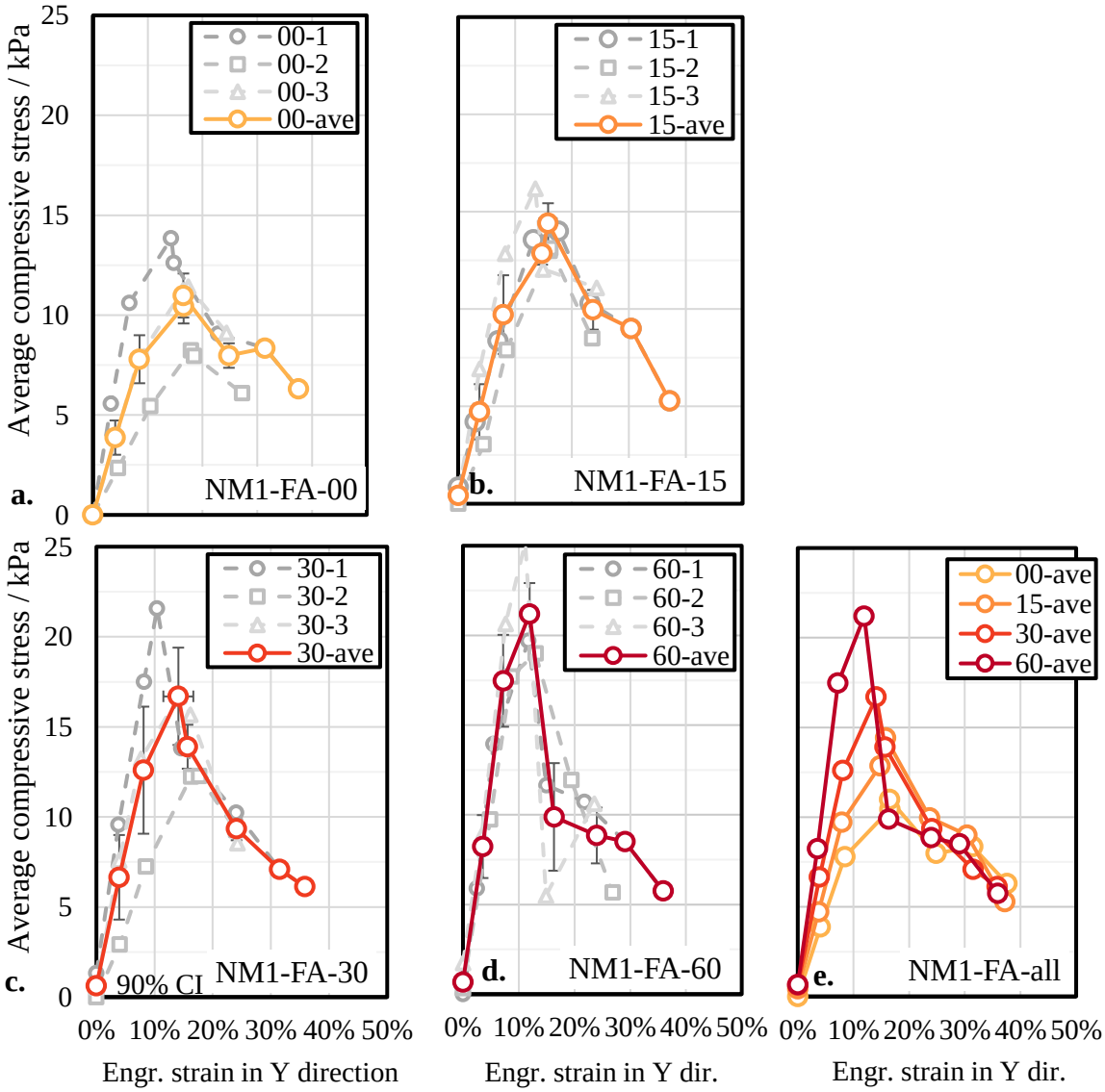

Figure A.25. Average stress of NM1-FA mixture at various material ages. Data gathered via green strength tests.

Results for the mix SEP0.5

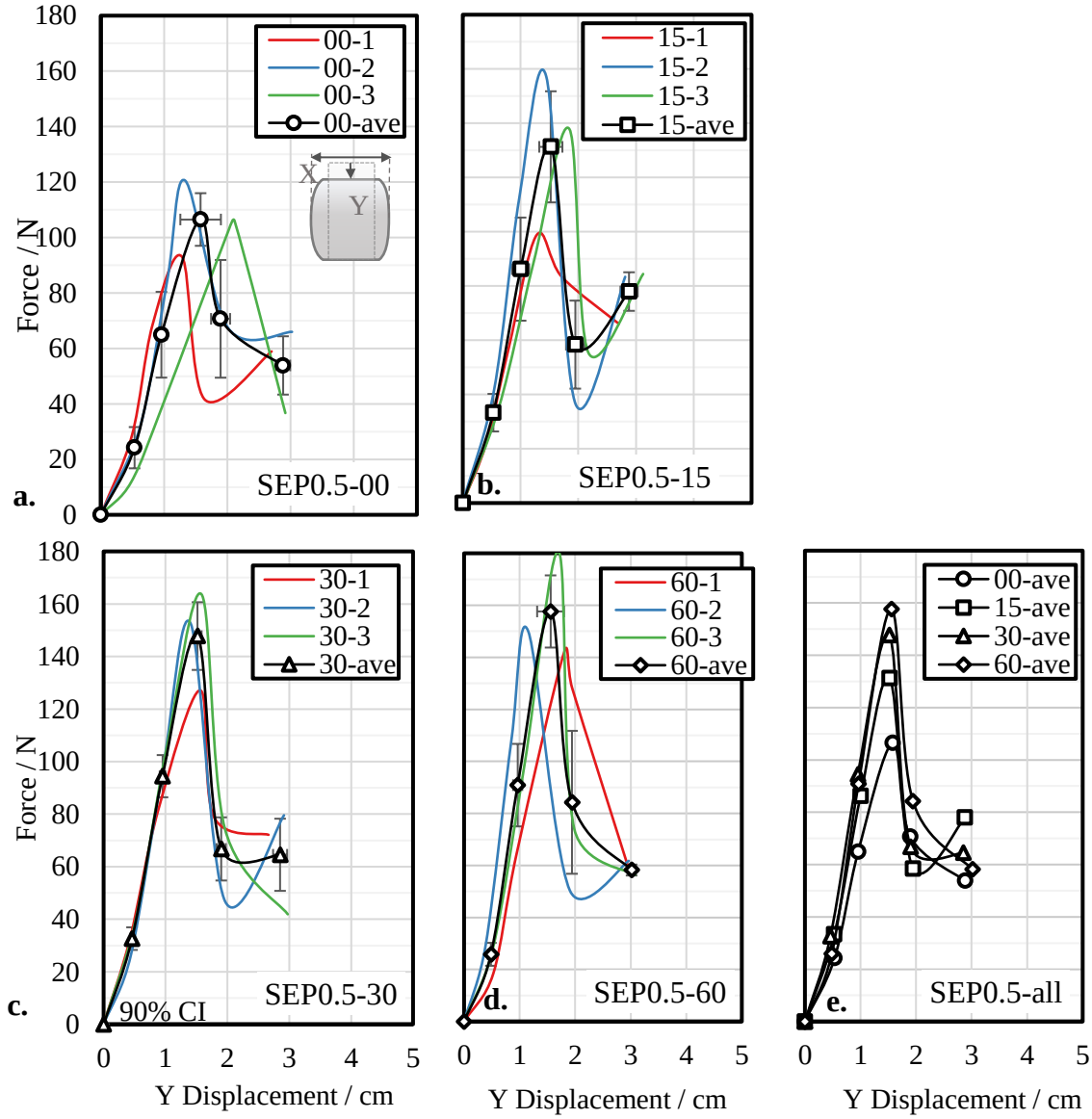

Figure A.26. Force response of SEP0.5 mixture at various material ages. Data gathered via green strength tests.

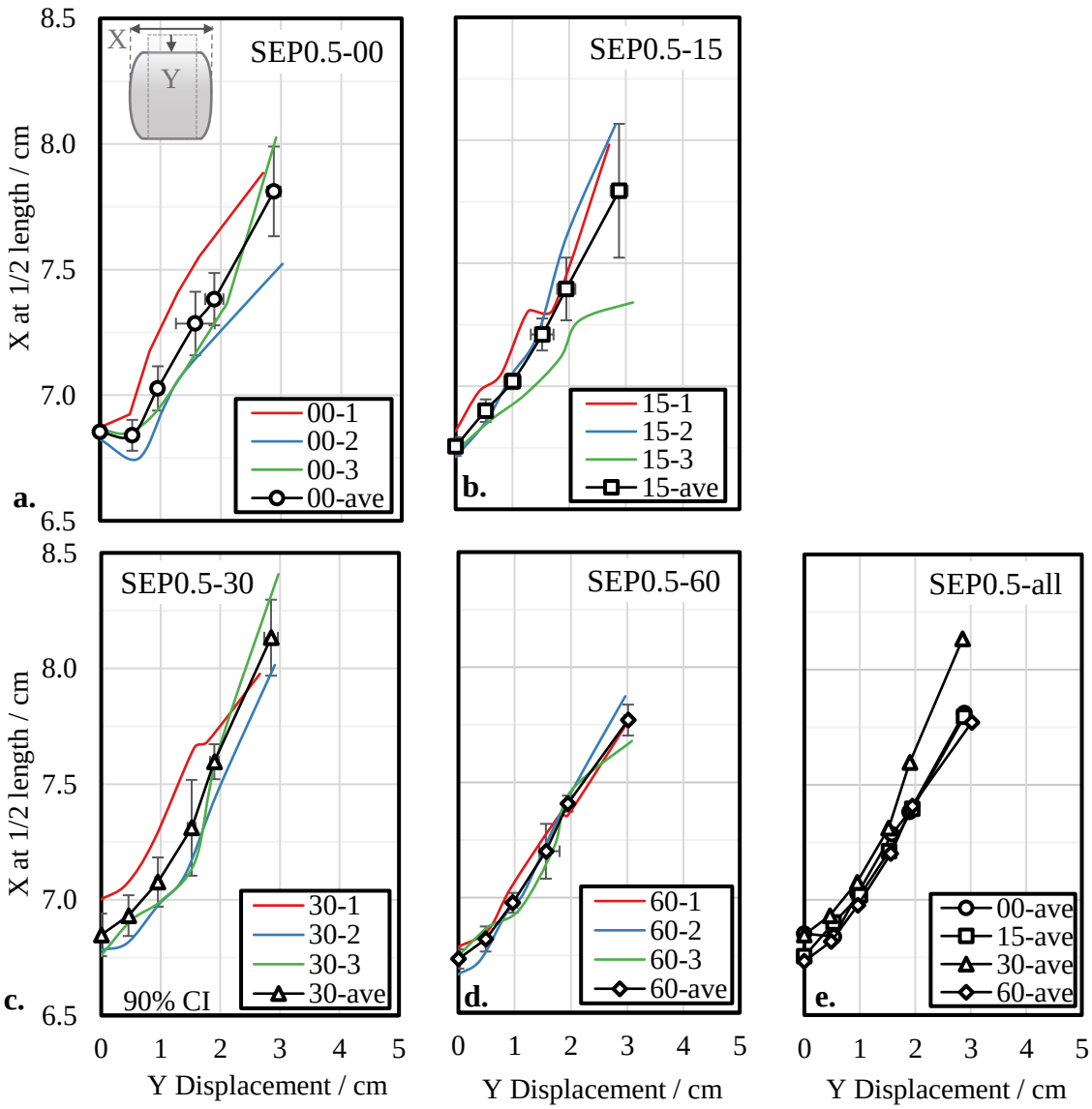

Figure A.27. Lateral displacement of SEP0.5 mixture at various material ages. Data gathered via green strength tests.

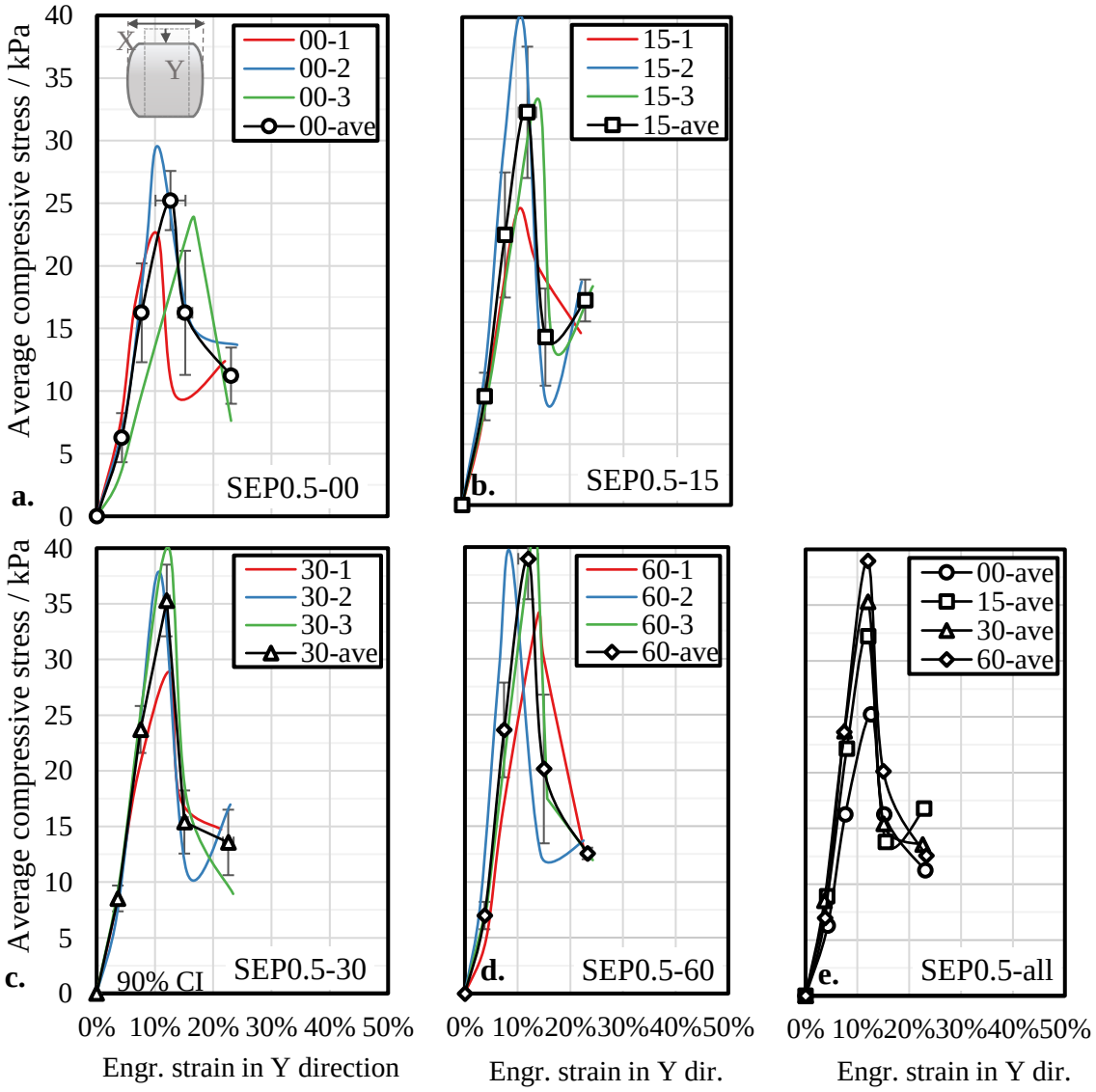

Figure A.28. Average stress of SEP0.5 mixture at various material ages. Data gathered via green strength tests.

Green strength and ageing time

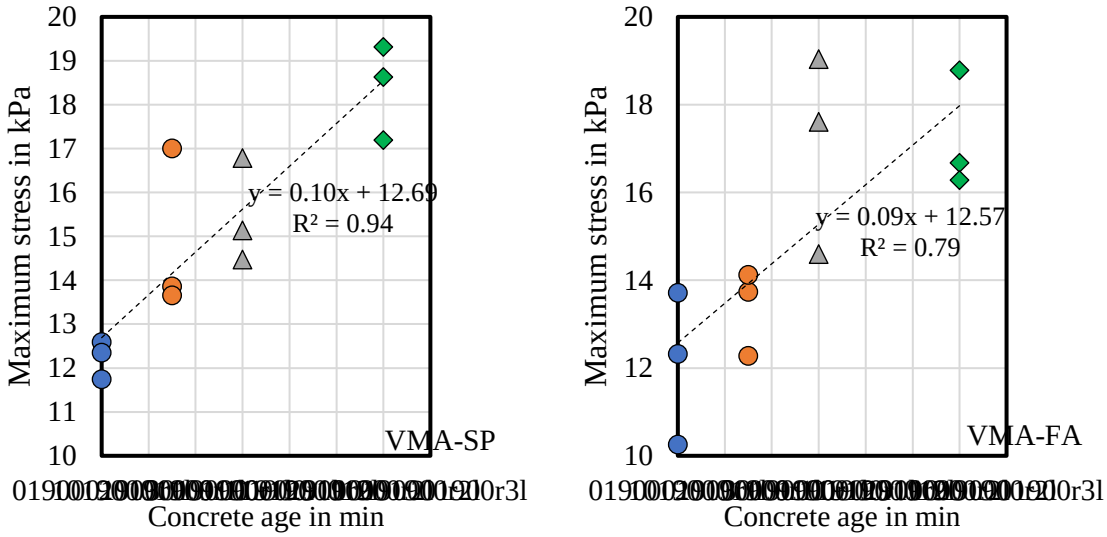

Figure A.29. Concrete aging time vs. maximum strength for VMA-SP and VMA-FA. Mixture left: VMA-SP, mixture right: VMA-FA.

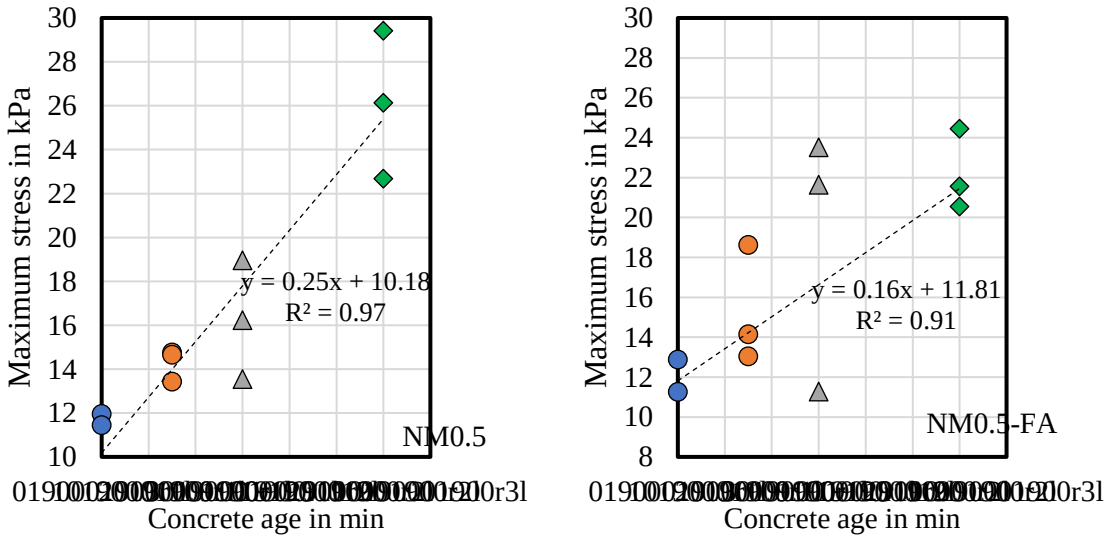

Figure A.30. Concrete aging time vs. maximum strength for NM0.5 and NM0.5-FA. Mixture left: NM0.5, mixture right: NM0.5-FA.

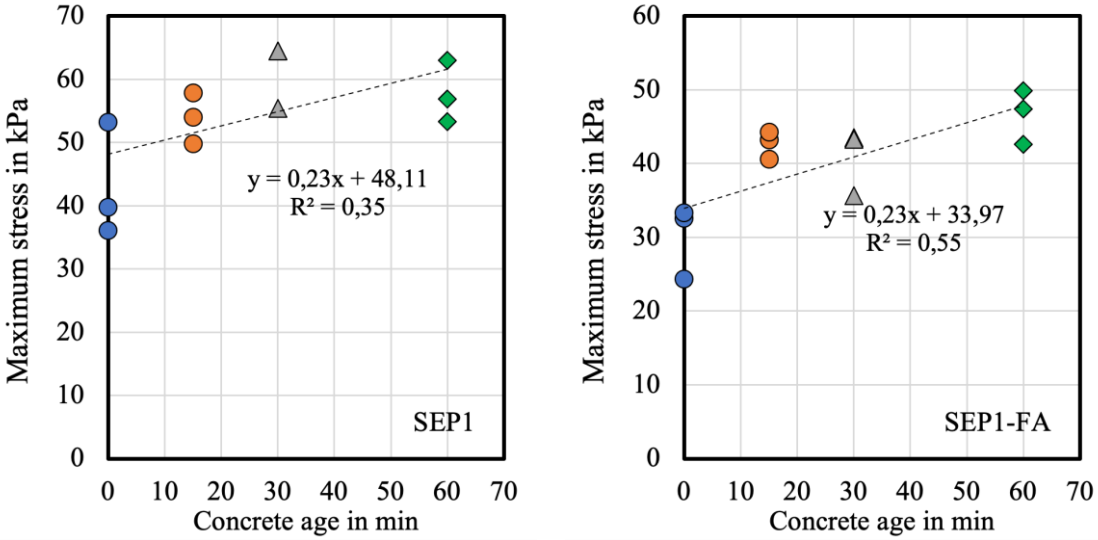

Figure A.31. Concrete aging time vs. maximum strength for SEP1 and SEP1-FA. Mixture left: SEP1, mixture right: SEP1-FA.

APPENDIX B: ERROR ANALYSIS

This section describes the followed methodology for the determination of the 90% confidence intervals (CI) of the calculated quantities based on the green strength measurements. Figure B.1 shows the independent and dependent variables related to the test kinematics.

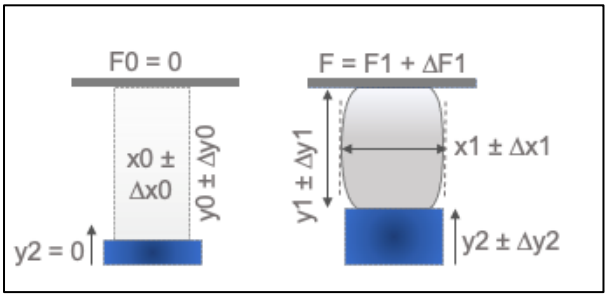

Figure B.1. The independent and dependent variables of the green strength test.

For the analysis, we assume the initial displacement y_2, and the initial force F_0 are zero. Here, the independent variables are the initial specimen height y_0, the initial diameter x_0, the current specimen height y_1, the current specimen diameter x_1, and the current reaction force against deformation F_1. Their 90% CIs are designated as Δy_0, Δx_0, Δy_1, Δx_1, and ΔF_1 respectively. These CIs are determined by independent measurements five times for each variable for each test. The 90% CI values are calculated assuming a Student-t distribution for the measurements. In MS Excel, ST.DEV and CONFIDENCE.T functions are used.

To calculate the 90% CI of the compressive displacement Δy_2, the tolerance stack-up is determined via equation:

$$y_2 \pm \Delta y_2 = (y_0 \pm \Delta y_0) - (y_1 \pm \Delta y_1) = (y_0 - y_1) \pm (\Delta y_0 + \Delta y_1). \quad \text{(B.1)}$$

Similarly initial planar cross-section of the specimen A_0 and its respective confidence interval ΔA_0 can be calculated as:

$$A_0 \pm \Delta A_0 = \frac{\pi}{4}(x_0 \pm \Delta x_0)^2 = \frac{\pi}{4}x_0^2 \pm \left[\frac{2\Delta x_0}{x_0}\right]\%. \quad \text{(B.2)}$$

In (B.2), the notation [.]% denotes relative CI. Same relationship is also applied to the calculation of the 90% CI of average stress during deformation σ_y. We define σ_y as an average uniform stress along y-direction if no-barreling or shear sliding takes place as represented in Figure B.2.

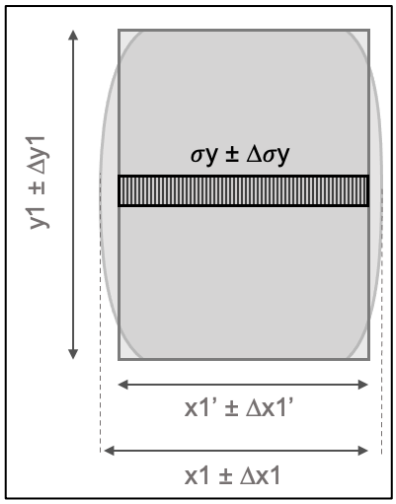

Figure B.2. Specimen deformation under an average uniform stress assumption.

Here x_1' and $\Delta x_1'$ denote the average diameter without barreling and its respective 90% CI respectively, these values are related to the measured variables according to:

$$(y_1 \pm \Delta y_1)\frac{\pi}{4}(x_1' \pm \Delta x_1')^2 = (y_1 \pm \Delta y_1)(A_1' \pm \Delta A_1') = (y_0 \pm \Delta y_0)(A_0 \pm \Delta A_0). \quad \text{(B.3)}$$

In (B.3), A_1' and $\Delta A_1'$ denote the average uniform cross-sectional area and its 90% CI subjected to the average normal stress $\sigma_y \pm \Delta\sigma_y$. Similarly, σ_y is related to F_1 and A_1' with the equation $\sigma_y = F_1 / A_1'$.

Combined, these relationships allow for determining $\sigma_y \pm \Delta\sigma_y$ in terms of measured variables and their 90% CI as shown:

$$\sigma_y \pm \Delta\sigma_y = \frac{F \pm \Delta F}{A_1' \pm \Delta A_1'} = \frac{F \pm \Delta F}{A_0 \pm \Delta A_0 \frac{y_0 \pm \Delta y_0}{y_1 \pm \Delta y_1}}$$

$$= \frac{F \pm \Delta F}{\frac{\pi}{4}(x_0^2 \pm \Delta x_0)^2 \frac{y_0 \pm [\Delta y_0 / y_0]\%}{y_1 \pm [\Delta y_1 / y_1]\%}}$$

$$= \frac{F \pm [\Delta F / F]\%}{\frac{\pi}{4}(x_0^2 \pm [2\Delta x_0 / x_0]\%) \frac{y_0 \pm [\Delta y_0 / y_0]\%}{y_1 \pm [\Delta y_1 / y_1]\%}}$$

$$= \frac{F \pm [\Delta F / F]\%}{\left(\frac{\pi}{4} x_0^2 \pm \left[2\frac{\Delta x_0}{x_0}\right]\%\right)\left(\frac{y_0}{y_1} \pm \left[\frac{\Delta y_0}{y_0} + \frac{\Delta y_1}{y_1}\right]\%\right)} \tag{B.4}$$

$$= \frac{F}{\frac{\pi}{4} x_0^2 \frac{y_0}{y_1}} \pm \left[\frac{\Delta F}{F} + 2\frac{\Delta x_0}{x_0} + \frac{\Delta y_0}{y_0} + \frac{\Delta y_1}{y_1}\right]\%$$

$$= \underbrace{\frac{F}{\frac{\pi}{4} x_0^2 \frac{y_0}{y_1}}}_{\sigma_y} \pm \underbrace{\left[\frac{\Delta F}{F} + 2\frac{\Delta x_0}{x_0} + \frac{\Delta y_0}{y_0} + \frac{\Delta y_1}{y_1}\right] \frac{F}{\frac{\pi}{4} x_0^2 \frac{y_0}{y_1}}}_{\Delta\sigma_y}.$$